NUREG/CR-2269
RG, XA

Probabilistic Models for the Behavior of Compartment Fires

Manuscript Completed: November 1980
Date Published: August 1981

Prepared by
N.O. Siu

School of Engineering and Applied Science
University of California
Los Angeles, CA 90024

Prepared for
Division of Risk Analysis
Office of Nuclear Regulatory Research
U.S. Nuclear Regulatory Commission
Washington, D.C. 20555
NRC FIN B6284

-1-a

ACKNOWLEDGMENTS

The author gratefully acknowledges the aid and guidance provided by Professor G. Apostolakis in this work. A special acknowledgment goes to Dr. M. Kazarians for his helpful comments and constructive criticism. Finally, the author thanks Pickard, Lowe, and Garrick, Inc. for the useful information provided for the nuclear power plant compartment fire analyses presented in Chapter 5 of this report.

ABSTRACT

Physical models which predict the thermal hazards (including temperatures and heat fluxes) during a compartment fire as functions of space and time are developed. Since large uncertainties are inherent to the analysis, the models are probabilistic.

General models are constructed for the periods of fire growth and fully-developed burning. These models are used in sample analyses to estimate the fire hazard in particular compartments.

The overall methodology requires the synthesis of a deterministic physical model from information available in the literature. Uncertainties in the input parameters required by the deterministic model are assessed and are incorporated with the uncertainties in the model itself, to form state of knowledge distributions for the thermal hazards.

TABLE OF CONTENTS

TABLE OF CONTENTS (continued)

TABLE OF CONTENTS (continued)

TABLE OF CONTENTS (continued)

Appendices

LIST OF TABLES

LIST OF FIGURES

LIST OF FIGURES (continued)

LIST OF FIGURES (continued)

LIST OF VARIABLES

Variable	Definition
A	Area (m^2)
B	Height of doorway (m)
C_O	Orifice coefficient for opening
C_S	Surface controlled burning rate constant (kg/J)
C_V	Ventilation controlled burning rate constant
D	Diameter (m)
E	Error factor for quantifying modeling uncertainties
F_{1-2}	Shape factor from object 1 to object 2
H_f	Heating value of fuel (J/kg)
M	Mass (kg)
Q_p	Heat content of pilot fuel (J)
$\dot{Q}$	Rate of heat production (W)
T	Temperature (°K)
T^*	Ignition temperature (°K)
V	Volumetric flow rate (m^3/s)
W	Rate of air flow (kg/s)
Z	Height (m)
a	Absorption coefficient (m^{-1})
b	Wood crib stick width (m)
c_p	Specific heat (J/kg°K)
f_c	Conditional frequency of fire involving two cable trays
f_p	Porosity factor
g	Gravitational constant (9.8 m/s^2)

LIST OF VARIABLES (continued)

h	Heat transfer coefficient ($W/m^2{}^\circ K$)
k	Thermal conductivity ($W/m^\circ K$)
$\dot{m}$	Burning rate of fuel (kg/s)
$\dot{m}''$	Specific burning rate (kg/m^2s)
$\dot{m}''_0$	Specific burning rate constant (kg/m^2s)
$\dot{q}''$	Heat flux (W/m^2)
$\dot{q}''_{fl,r}$	Radiative heat flux from flame to fuel bed (W/m^2)
s	Wood crib stick spacing (m)
t	Time (s)
t^*	Time to ignition (s)
$\bar{v}$	Flame front average velocity (m/s)
α	Thermal diffusivity (m^2/s)
β	Plume entrainment coefficient (Eq. 4.9)
χ	Fraction of Q radiated away from fire
ε	Emissivity
η	Combustion efficiency
θ	Characteristic dimensionless parameter for fire growth
ℓ	Length (m)
ν	Kinematic viscosity (m^2/s)
ρ	Density (kg/m^3)
σ	Stefan-Boltzmann constant (5.6697×10^{-8} $W/m^2{}^\circ K^4$)
τ	Characteristic time (s)
ψ	Dimensionless parameter for fire growth
ω	Plume entrainment coefficient (Eq. 4.9)

LIST OF VARIABLES (continued)

Subscripts	Definition
A	Ambient
d	Neutral plane at doorway (see "n" below)
DRM	Result of deterministic reference model calculation
e	Environment
ext	External to fuel bed
fl	Flame
f	Fuel, fuel bed
FV	Forced ventilation
G	Gas
n	Neutral plane (divides hot gas layer from cold air beneath)
O	Opening (e.g. window)
o	Object, or property evaluated at level of fuel bed
p	Pilot
W	Wall

Chapter 1

INTRODUCTION AND SUMMARY

Fire can represent a threat to the safe operation of nuclear power plants, not only because it can damage machinery in the immediate vicinity of the flames, but also because it can damage control and power cables passing nearby. Since power plants rely heavily upon these cables to link their various systems, a fire can cause the failure of many components well removed from the blaze.

In order to proceed with a quantitative analysis of the fire risk to nuclear power plants, the frequency that a given component will fail due to fire is needed. The determination of this frequency in turn requires models for the frequency of fire occurrence within a power plant, the distribution of the magnitude of fire severity given that a fire occurs, and the probability of component failure upon exposure to fire of a given severity.

In this work, we concentrate on developing the second model of these three, i.e. the probabilistic model for the time-dependent thermal hazard a component is exposed to during a nuclear power plant compartment fire. Our approach requires the construction of a physical model for the fire scenario of interest. We call this model our deterministic reference model (DRM). The uncertainties in the input parameters used by the DRM are propagated through the DRM, and are then combined with a probability distribution quantifying our uncertainty in the accuracy of

the DRM, to form a probability distribution for the frequency that a component is exposed to a specified thermal hazard (e.g. high temperature). Relevant data to aid our construction of the parameter and modeling uncertainty distributions are often unavailable, and so subjective judgment is an important input in this process.

To assist the fire hazard analysis, we develop general models for two different phases of a compartment fire: the fire growth period and the period of fully-developed burning.

In Chapter 2, we outline the time history of an enclosure fire, and review some of the models available in the literature. We observe that the majority of work on compartment fire models has been devoted to the period of fully-developed burning, where the fire essentially involves the entire compartment, and that there are few models available to describe the period of fire growth preceding fully-developed burning. We further note that the methods of approach used are generally deterministic.

In Chapter 3, we argue that any analysis of a freely burning fire must deal with large uncertainties, and that a probabilistic approach is appropriate for this problem. We identify the various classes of uncertainties which arise in our models, and formulate the methodology (briefly outlined above) employed to handle them.

In Chapter 4, we apply our general approach to the period of fire growth. The reference model is synthesized from a number of separate correlations and models for individual fire phenomena. The uncertainties in the reference model's predictions are discussed, and the model is used to simulate a number of experiments documented in the literature, in order to test its validity.

Unless the fuel geometry is particularly simple, a large amount of bookeeping is required during the fire growth computations. The reference model, therefore, is in the form of a computer program, called COMPBRN, and is described in more detail in Reference (1).

In Chapter 5, we consider fire hazards in two specific cases. The first scenario concerns the exposure of an electrical component housed in a metal cabinet to high temperatures induced by an external fire. We construct a simple model to predict the air temperature within the cabinet, and show that moderately sized oil-fueled fires may be of some concern. In the second case, we utilize our complete probabilistic methodology in assessing the frequency that two cable trays in the cable spreading room, each in a different electrical division, are involved in a fire.. We incorporate models not only for the growth of fire but also for the elapsed time before suppression.

Although a great deal of emphasis has been placed on the modeling of the fully-developed period in the compartment fire literature, we do not consider it to be of as great importance to nuclear power plant fires, not only due to the relatively low concentrations of highly flammable material in the power plants and the large size of the rooms, but also because many accident sequences may be initiated and well in progress during the growth period. We treat the fully-developed burning period model in Chapter 6, and conduct an analysis of a hypothetical fire in the cable spreading room which has reached the fully-developed stage.

We remark that our models are primarily thermal in nature, that fluid flow and chemical kinetics effects have been either neglected or treated extremely roughly. Our approach appears to be reasonable during the

early portion of fire growth and during the fully-developed burning period, but is considerably weaker in between these two regimes. A notable deficiency is our lack of a model for the transition between growth and fully-developed burning, called flashover, other than a simple thermal model involving a positive feedback term in the equations for fuel burning rates.

Chapter 2

OVERVIEW OF THERMAL HAZARD MODELS

During a fire a given component may suffer damage by absorbing a critical amount of heat. Our models for the thermal hazard within a burning compartment must therefore predict the amount of heat the component absorbs which in turn requires knowledge of the amount of heat the component is exposed to. In this work we concentrate on the latter quantity; components are modeled crudely, although more detailed models can be developed for specific problems.

The two primary modes of heat transfer considered are convection and radiation. The convective heat flux to the object is given by

$$\dot{q}''_{o,c} = h [T_e - T_o] \qquad (2.1)$$

If the radiative heat flux impinging on the object is $\dot{q}''_r$, the absorbed heat flux is given by

$$\dot{q}''_{o,r} = \varepsilon \dot{q}''_r \qquad (2.2)$$

If the heat flux at the source is $\dot{q}''_s$, we can re-write Equation (2.2) as

$$\dot{q}''_{o,r} = \varepsilon F_{o-s} \dot{q}''_s \qquad (2.3)$$

F_{o-s} represents the fractional solid angle of the object's surroundings that the source occupies. We note that the object also re-radiates a heat flux $\dot{q}''_{rr}$ given by

$$\dot{q}''_{rr} = \varepsilon \sigma T_o^4 \tag{2.4}$$

In keeping with our simple modeling, we generally fix T_o at room temperature and ε at unity. Thus, our models calculate the "cold wall heat fluxes" to black bodies; the resulting quantities are conservative estimates of the actual values.

The models in the literature which estimate $\dot{q}''_o$, the sum of $\dot{q}''_{o,c}$ and $\dot{q}''_{o,r}$, can be divided into two categories: the static models and the dynamic models. Although we describe the static models in the following section, the remainder of this work shall concentrate on the dynamic models, since these form a more general set which includes the static models.

2.1 STATIC MODELS

The static models for predicting the thermal hazard from a fire are generally derived for fires in the open, or at least where enclosure effects are negligible. A representative example is presented in Reference (2), where a fire over a fixed diameter pool of fuel is assumed, and the thermal hazard as a function of distance is calculated. Since convection is only important in regions of elevated temperature (i.e. in or above the flames), only radiative heat fluxes are calculated. Other similar analyses are presented in References (3) and (4).

In each case, the source heat flux $\dot{q}''_s$ and the shape factor F_{o-s}, which contains the problem geometry, must be calculated. Typically, an average flame temperature T_{fl} is assumed. If we further assume blackbody behavior, there results

$$\dot{q}''_s = \sigma T_{fl}^4 \tag{2.5}$$

This equation shall be discussed in more detail in Chapter 4, where an alternate formulation of $\dot{q}''_s$ is employed. As for F_{o-s}, numerous analytical formulae have been derived for a variety of geometries [5,6]. If the flame is modeled as a cylinder, the height may be computed immediately (with knowledge of the fuel burning rate) from Thomas' correlation [7], and used in the shape factor computation. Thomas' flame height correlation is discussed briefly in Chapter 3, and shape factors for some representative geometries are presented in Appendix A.

2.2 DYNAMIC MODELS

If the exposure fire is allowed to grow, neither the source term $\dot{q}''_s$ nor the shape factor F_{o-s} is constant any longer. Furthermore, if the fire is located within a room, the heating room boundaries and the accumulating layer of hot gases near the ceiling become increasingly important heat sources as time progresses. Thus, we must review the available dynamic models for compartment fires.

2.2.1 Compartment Fire Development

Conceptually, the time history of a compartment fire (a fire which is contained within a room) can be resolved into four stages or periods: initiation, growth, fully-developed burning, and decay (see Fig. 2.1).

The initiation phase involves the ignition of a small fuel element in the room of interest. If the primary fuel bed is cable insulation, which is generally difficult to ignite, additional pilot fuels such as paper, oil, cleaning fluid, or plastic foam may be important. The last fuel was a major contributor to the initiation of the Browns Ferry Fire

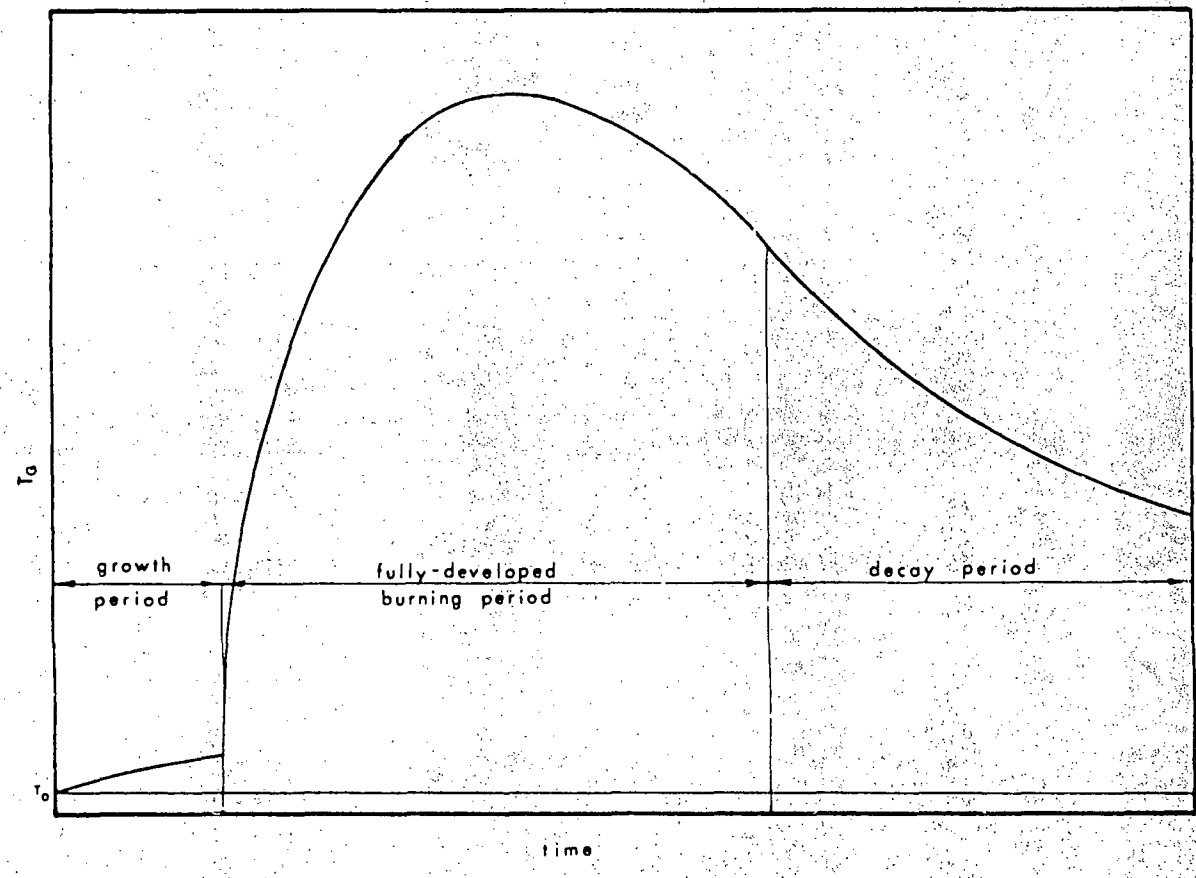

Fig. 2.1 - Compartment Fire Behavior

[8]. At this stage of fire development, the only hazard to plant components is in the immediate vicinity of the fire.

In the following period of fire growth, the fire spreads over the fuel bed by continuous flame front movement, by radiative and convective heating of non-contiguous fuel elements, and sometimes by direct transport of burning fuel, spread by firebrands being a good example of the latter process. The growing fire also heats up the compartment walls and ceiling, and creates a layer of hot gases next to the ceiling. These bodies in turn act as heat sources which radiate and reflect heat back to both the burning and non-burning portions of the fuel bed, increasing the volatilization of the fuel, and thus increasing the rate of fuel feed within the flames and enhancing the ease of ignition of the fuel outside the flames. This positive feedback loop leads to an accelerating fire growth rate, which may become so large that the entire compartment becomes involved in the fire during an almost instantaneous period called flashover.

The period of fully-developed burning which follows flashover, if it occurs at all, is characterized by burning rates which are limited only by the available ventilation or free fuel surface area. During this period, the temperature and heat flux levels tend to be fairly uniform. This can be contrasted with the behavior during the period of fire growth, where the heat flux and temperature levels are strongly peaked near the fire.

The period of fire decay occurs when the majority of combustible fuel within the room has been consumed. During this period, the intensity of the fire dies down and the fuel often smolders rather than burns in an open flame.

It should be noted that the progress of a compartment fire can be slowed down and halted at any moment by suppression efforts. Furthermore, even if such efforts are delayed or totally lacking, the achievement of fully-developed burning is not assured, since a fire over a small fuel bed may not generate enough heat to ignite distant fuel elements. A crude suppression model is described in the application of our model to a nuclear power plant cable tray fire in Chapter 5.

2.2.2 Fully-Developed Burning Period Models

Of all the work done on compartment fires, the greatest amount has been done on fires which have reached the fully-developed stage of burning. This emphasis is due to the relative simplicity of the analysis, and the fully-developed burning regime's great importance to general fire safety engineering.

A fully-developed compartment fire is a fire which is burning all available fuel in the room and is limited only by the total amount of fuel surface area or by the total amount of ventilating air flowing into the room. There is essentially no concern with the spatial growth of the fire within the enclosure since at least most of the fuel is already involved in the blaze. Furthermore, strong turbulent mixing of the hot room gases and relatively uniform fuel distribution allow the analyst to at least initially ignore spatial variations in the temperature and heat flux fields. The room can thus be modeled as a point in space, and the complex set of equations which govern the fire reduces to a simple heat balance equating the heat generated to the heat lost to the environment.

Although a detailed formulation of this model is provided in Chapter 6, the general scheme is as follows:

- All of the fuel in the room is assumed to burn at a rate (in kilograms per second) determined by the amount of available fresh air or fuel surface area. The rate of heat liberation within the compartment is directly proportional to this mass burning rate.
- Heat is lost from the compartment by radiation and convection to the room walls, by radiation out the room windows and doors, and by the physical removal of hot gases by the room ventilation. The heat loss to the walls is a function of the wall temperature, which is obtained by solving the transient heat conduction equation for the wall.
- The heat gained by the compartment air is equated to the heat lost, and the air temperature is solved for. Time is incremented and Steps 1-3 are repeated until most of the fuel (typically 70% of the original mass is consumed.

The solution resulting from this procedure can be expressed as a plot of the average room temperature as a function of time. The maximum temperature achieved and the time it is reached are only functions of the fuel loading, the fuel type, the fuel surface area, and the ventilation level of the compartment, the fuel loading being the amount of fuel per unit area of compartment.

This is the basic approach adopted by a fair number of researchers, including Odeen [9], Kawagoe and Sekine [10], Harmathy [11], and Tsuchiya and Sumi [12], although each researcher incorporates varying degrees of sophistication into his model. Some time-temperature curves from Reference

(10) are shown in Figure 2.2, as well as actual data from the fires simulated.

The functional relationship between time and temperature derived in this fashion forms the basis for the most widely recognized design codes [13]. In fact, many nations employ some form of a standardized time-temperature curve to determine the stress a material should be exposed to during flammability tests. This curve is considered to characterize a standard exposure fire and leads to descriptions of fire severity in terms of the equivalent duration of the standard fire. For instance, a fire of relatively low severity which burns for three hours may be described as being equivalent to a fire following the standard time-temperature curve for one hour. This equivalence can be related to the concept of a critical amount of absorbed heat leading to component damage, and to the integration of Equation (2.1) over time. The time-temperature curves for these two fires are shown in Figure 2.3.

2.2.3 Fire Growth Models

During the period of fire growth, the heat fluxes $\dot{q}''_{o,c}$ and $\dot{q}''_{o,r}$ are highly non-uniform functions of space. $\dot{q}''_{o,c}$ is essentially zero except for objects in the immediate vicinity of the flames, the hot gas plume above the flames, or the hot gas layer near the ceiling. As for $\dot{q}''_{o,r}$, F_{o-s} is a purely geometric factor and will vary strongly with location. The prediction of fire growth with time is thus extremely important, since this governs the behavior of $\dot{q}''_{o,c}(\vec{r},t)$ and $\dot{q}''_{o,r}(\vec{r},t)$.

A reasonable method for handling growth period fires is to use a quasistatic approach, an approach based on the static calculations dis-

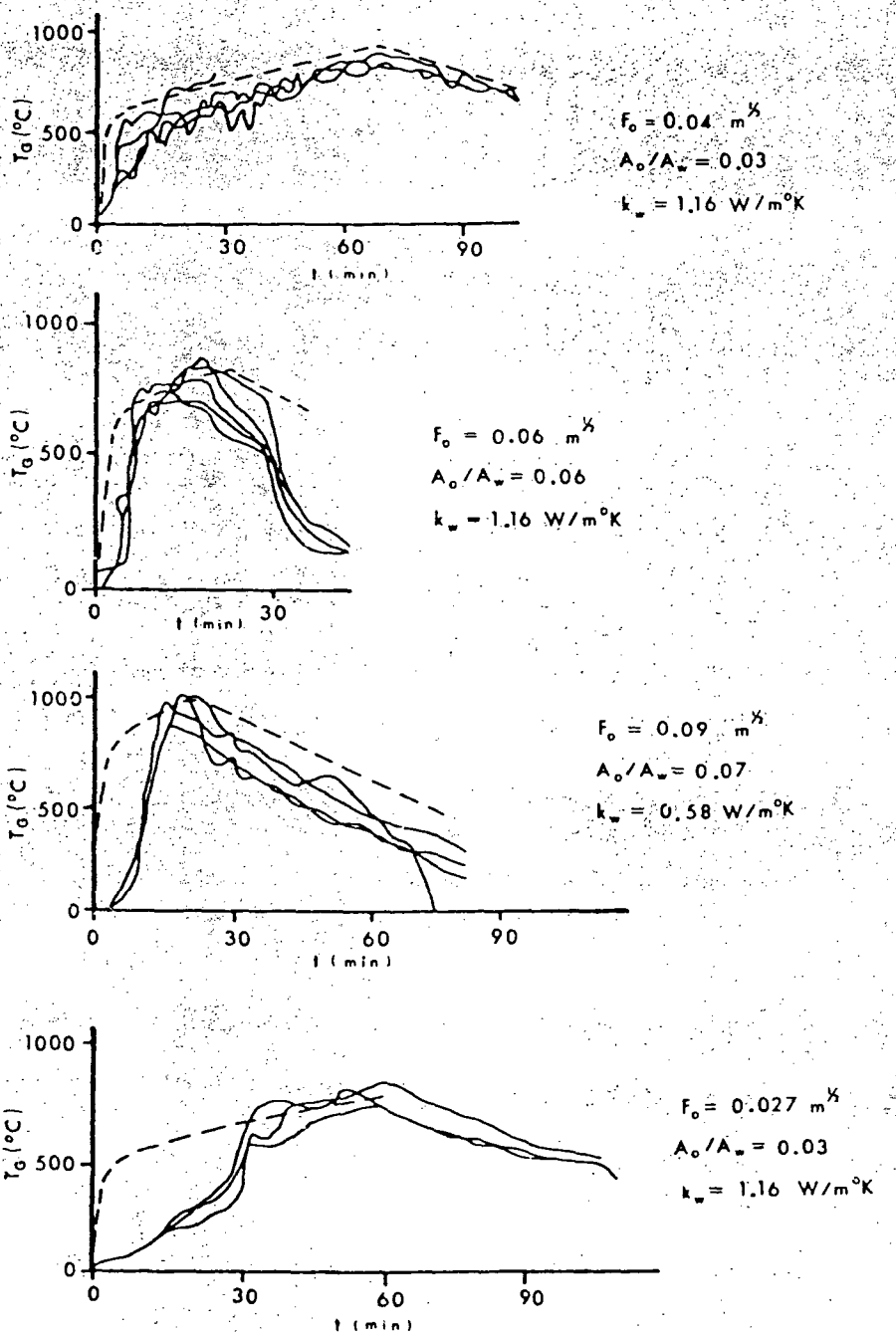

Fig. 2.2 - Experimental Verification of Model [10]

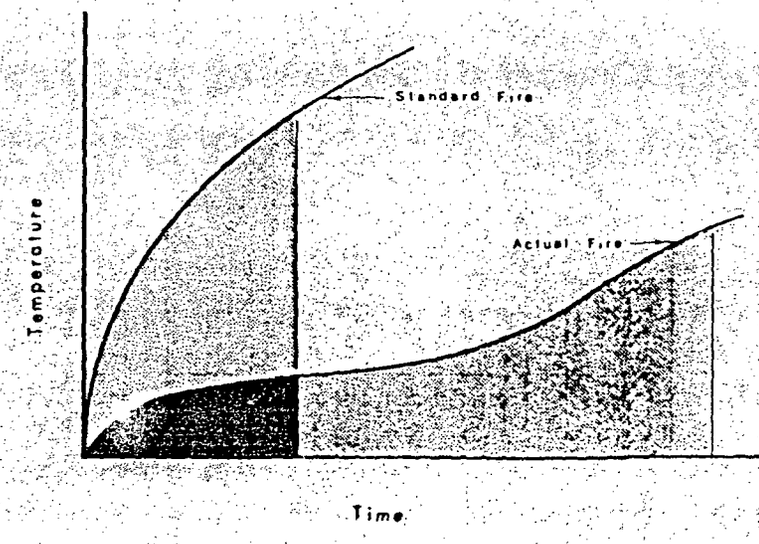

Fig. 2.3 - Time-Temperature Curves for Two "Equivalent" Fires

cussed earlier but extended to account for fuel element ignition and thus fire growth. Essentially, at each point in time, time-independent calculations for flame size, burning rates, heat release rates, shape factors, and heat absorption are done, fuel elements are ignited if they have absorbed enough heat, time is incremented, and the process repeated. Further models are also required to account for the presence of compartment boundaries, since the above static calculations are constructed either to analyze fires in the open or fires which are considered too small to be affected by the surrounding room.

These needed refinements are outlined by Quintiere [14], who not only describes the calculations required to proceed with a compartment fire growth analysis, but also presents a simple model for a fire spreading continuously over the floor of a room.

The essential differences in behavior between a fire in an enclosure and a fire in the open are caused by the restriction of air flow about the fire as well as the physical presence of the room boundaries. This restriction not only limits the amount of fresh air which can reach the fire but also inhibits the movement of hot gases away from the flames. A layer of these gases accumulates in the compartment and adds its radiative heat fluxes to the heat reflecting from the room boundaries back to the burning and unburnt portions of the fuel bed. Under the influence of this feedback, the fuel bed releases volatile gases more rapidly; hence the burning rates increase and the unburnt fuel ignites more readily.

The refinements suggested by Quintiere are simply relations needed to determine the airflow into the compartment, the size and temperature of

the gas layer, the wall temperature, and the radiative heat fluxes from the gases and walls back to the fuel bed. Except for the fluid flow model, which is developed by Rockett [15], most of the relations are derived from heat balances over the fire plume, the hot gas layer, and the room walls and ceiling. Unfortunately, Quintiere does not advance his model beyond the general formulation stage, save for the simple spread model mentioned, and this model is not really directly applicable to nuclear power plants where fire spread over discontinuous fuel beds must be considered.

A more complete formulation of the same basic model is presented by Pape and his co-workers [16,17]. Their model is in the form of a computer code, which upon input of the appropriate room geometry and fuel characteristic parameters, deterministically yields a certain output (e.g. the heat flux as a function of the distance from the fire). An interesting twist in their model results from recognition that the fuel burning rates will vary strongly as a function of the configuration and composition of the fuel bed. Since these burning rates are difficult to model for all but the most simplified of fuel beds, subjective probability distributions are employed.

A major drawback of Pape's model is the neglect of burning rate enhancement due to heat feedback to the burning fuel bed (Quintiere references experimental results which show increases in the burning rate of up to 60 per cent for wood cribs and 300 per cent for plastic slabs due to this effect). We also note that their model is not completely probabilistic, since no uncertainties other than those in the burning rates are explicitly addressed.

One of the important problems arising with the general approach outlined is that of completeness. Since the overall model is only a synthesis of component models, which describe burning rates, heat release rates, flame heights, ignition times, etc., it cannot deal with phenomena not included in the component models. For example, Glassman, in his comments appended to Ref. (14), states that flashover might not just be simply the result of an accelerating growth process caused by positive feedback to the fire, but may also be caused by the sudden availability of a source of energy (such as a flame) near the compartment ceiling where large quantities of unburnt gas may reside. The energy source ignites the gases and the resulting flame spreads almost instantaneously through the entire hot gas layer; the huge increase in the room heat fluxes caused by such a process leads to the ignition of the remaining unburnt portions of fuel in the compartment. Clearly, although such a flashover mechanism might be very difficult to model, its neglect could lead to overly simplistic predictions of the fire hazard for a given room.

An alternative approach to the growth problem is presented by Fitzgerald [18]. This probabilistic analysis views the compartment of interest as a group of fuel packets separated by spatial barriers. Fire propagation is treated with an event tree type analysis, similar to that used in nuclear plant accident analyses, with the frequencies of "barrier failure" to be derived from the heat transfer considerations.

For instance, suppose there are three fuel packets in the compartment of interest, which if burning, can only transmit heat to each other by convection or radiation (this defines a "fuel packet"). Assume in our

scenario that packet 1 is burning and that packet 2 will ignite before packet 3 does. Packet 1 will either self-extinguish before packet 2 ignites or it will not, and there are frequencies associated with each of these events which theoretically can be derived from heat transfer considerations. Similarly, the frequency that the fire propagates from packet 2 to packet 3 can be found, and so the frequency of total room involvement can be computed. An event tree for this scenario is shown in Figure 2.4.

An important advantage of this procedure is that the exceedingly complicated problem of fire growth can be resolved into smaller and simpler calculations. However, since the growth rate of a fire is strongly dependent on the current size and shape of the fire, as will be discussed in greater detail in Chapter 4, the barrier failure frequencies are functions of the fire configuration. If the room contains four fuel packets, the frequency of propagation from packet 1 to packet 2 will depend on whether packet 3, packet 4, neither, or both are already burning. Thus the number of barrier failure frequencies which must be computed increases geometrically with the number of fuel packets. Adding to these difficulties, the failure frequencies also depend on time, since the temperature and extent of the hot gas layer as well as the fuel burning rates increase as the fire continues to burn.

Thus, although the explicit separation of the probabilistic framework from the heat transfer calculations in Fitzgerald's model shows promise, its advantages over the synthesis approach seem small when analyzing complex fire configurations.

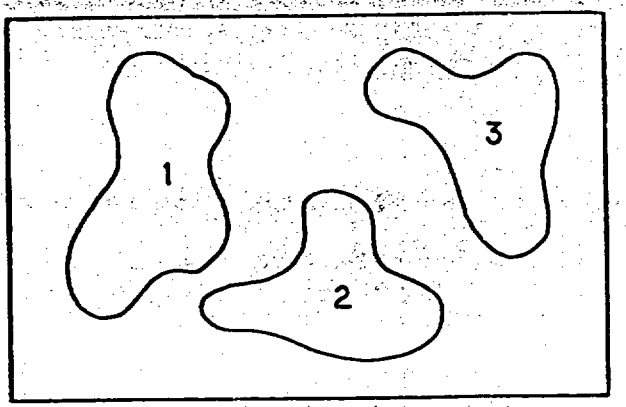

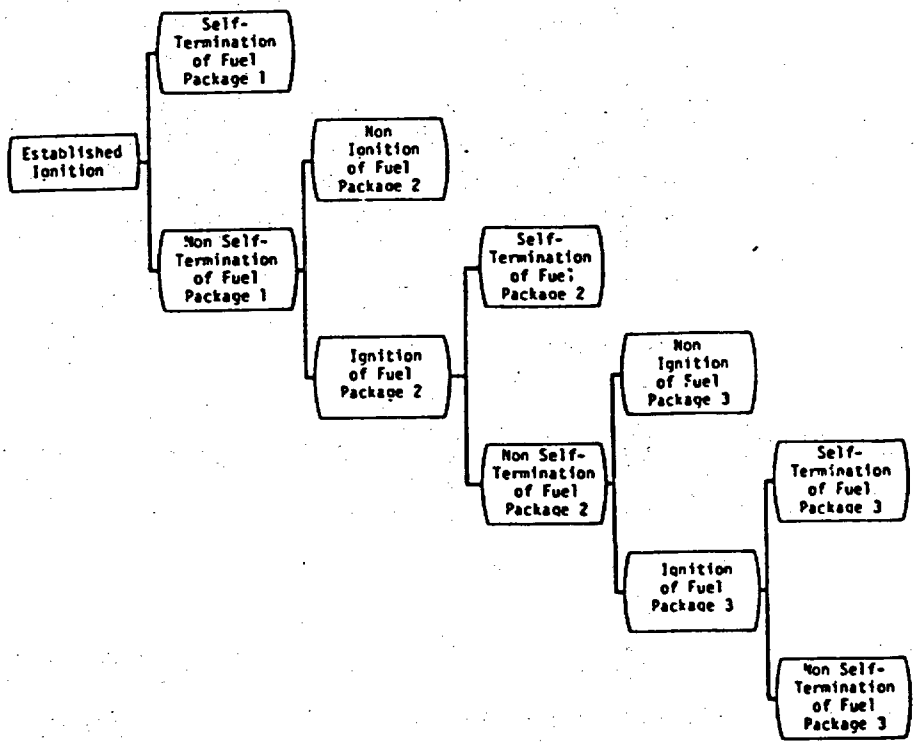

Fig. 2.4 - Fire Growth Event Tree Model [18]

Chapter 3

GENERAL METHODOLOGY

A complete model of the thermal hazards caused by a compartment fire in a nuclear power plant should incorporate sections to handle each of the four phases (initiation, growth, fully-developed burning, and extinction) in a fire's history. We note that the first is important primarily because it determines the frequency at which components will be exposed to fires of any magnitude. In this report however, we shall neglect both the period of ignition and that of extinction. The period of ignition shall be ignored because the results of researchers [19,20] indicate that the frequency of fires within nuclear power plants can be estimated to a good degree from the available data. In the remainder of the report it shall be assumed that a small fire already exists in the compartment of interest. As for the extinction period, it can be seen that the heat-induced stresses on any component during fire decay will be at most equal to the stresses experienced during growth and fully-developed burning. Furthermore, a fire in a nuclear power plant compartment probably will not be allowed to burn to completion; suppression efforts are expected to be finished before all of the available fuel is consumed. Since there are a number of simple models in the literature which will give reasonable order-of-magnitude estimates for stress level decay as a function of time [9,10], we shall not emphasize analysis of this phase either.

The overall model proposed therefore has two parts. The first deals with the growth period, while the second part concerns the fully-developed burning phase. In both parts, the approach shall be probabilistic (i.e. our state of knowledge shall be expressed in terms of probability distributions), an approach which requires that we identify and quantify the uncertainties in our analysis. In the remainder of this chapter, we shall discuss the various types of uncertainties encountered in our problem and the the methods used to incorporate these uncertainties into the analysis.

3.1 IDENTIFICATION OF UNCERTAINTIES

Ideally, any physical situation can be modeled using the basic laws of mass, momentum, and energy conservation. The solution of the resulting equations, plus any necessary auxiliary equations modeling, for example, the chemical reactions involved, would in principle describe fully the situation we wish to examine. However, a freely burning fire is an extremely complex phenomenon, involving turbulent transport of heat, mass, and momentum, radiative heat transfer, and a multitude of chemical reactions. Its governing equations are sufficiently numerous and involved that analytical or numerical solutions are presently impossible to find for all but the most simplified configurations. Since the presence of room walls will add even more complexity to the equations, an accurate description of the progress of a compartment fire presently cannot be derived purely from first principles.

Owing to the lack of a rigorous overall model for fire, much of the information incorporated in our fire model is empirical. This informa-

tion may be in the form of correlations of experimental data, using correlating variables obtained from dimensional analysis of the governing equations, it may be in the form of uncorrelated data obtained from highly specific tests, or it may be in the form of engineering judgment and experience. Such knowledge can tell us how the burning rate of a given wood crib in a given experimental enclosure will vary with stick spacing, or if a given electrical cable on a given tray and exposed to a given heat flux will ignite, at least within certain degrees of accuracy. However, it is not immediately clear how accurate this information is if the test conditions are changed slightly, and more importantly how useful it is in the field where conditions are anything but standardized. An interesting picture of our empirical state of knowledge is given by Emmons [21], who looks at the flammability ratings of twenty-four different wall materials. The results of standardized flammability tests for six European countries are shown in Figure 3.1, and the correlation of the results is rather weak. As an extreme example, one material was rated the least flammable by one country's test, and the most flammable in another's.

The uncertainties in our knowledge of fire which contribute to the confusion mentioned above can be broadly classified into one of two types: statistical uncertainties due to the random nature of fire, and state-of-knowledge uncertainties in our modeling of fire.

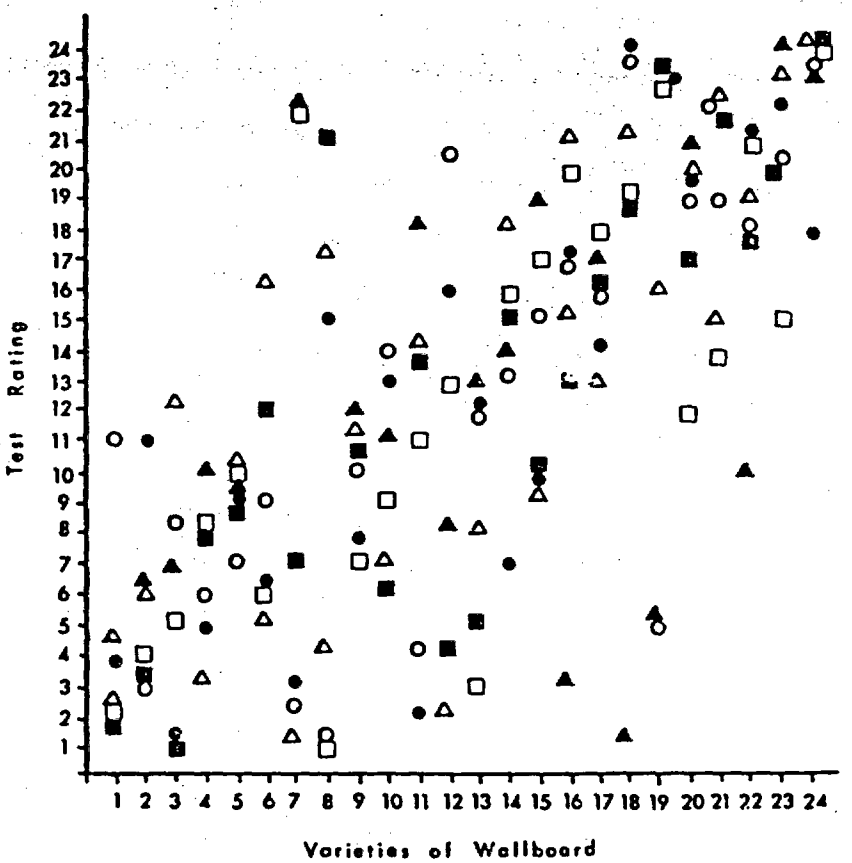

Fig. 3.1 - Flammability Ratings of Wallboard [21]

3.1.1 Statistical Uncertainties

Fire is a random phenomenon. The behavior of a flame at a given time is strongly dependent on the surrounding environment as well as its own current configuration. Random fluctuations in the air flow field around the fire and in the fuel bed beneath it act as randomly varying boundary conditions for the flame. Since the burning rate of a fire is partially dependent on the heat flux from the flame back to the fuel bed, and this feedback depends on the flame's current shape, these fluctuations can lead to different burning and growth patterns for nominally identical rooms.

The behavior of the heat fluxes and temperatures in a compartment are direct functions of the fire's behavior; it therefore follows that these fire-induced stresses are also random variables. This variation caused by the randomness of fire is termed statistical uncertainty; if we perform a particular experiment a large number of times under "identical" conditions and measure a specific variable, e.g., the temperature at a particular point in space, we will obtain a frequency distribution for that variable.

3.1.2 State of Knowledge Uncertainties

The statistical uncertainties described above are inherent in the nature of fire. Even if our knowledge of fire were to increase dramatically, we would not be able to reduce these uncertainties significantly. Such an increase in knowledge, however, would markedly reduce our modeling uncertainties. These uncertainties arise when we attempt to predict the frequency distribution for the parameter of interest, applying a "sim-

ple" model (simple in the sense that it is solvable) to a complex problem [22].

Our uncertainties in the modeling of the given fire can be further categorized as being uncertainties in the fundamental physical modeling, in the additional modeling required to allow reasonable computation times, and in the values of the parameters to be used when the model is applied toward a real compartment fire. To illustrate these different sources of uncertainty, we consider the growth period model presented in Chapter 4.

The growth period model is a synthesized model; its components are the many models available in the literature which describe various physical phenomena, including models for the burning rate as a function of ventilation, flame height as a function of burning rate, radiated heat flux as a function of flame height, etc. In general, each of these models was developed independently. Our uncertainty in the modeling of the basic physics of fire therefore is due not only to our uncertainty in how good each model's predictions are under the conditions it was developed for, but also to our uncertainty in the synthesis of these independent models. One of our primary concerns is whether or not the synthesis contains enough component models (i.e. if all important phenomena have been modeled).

The second type of modeling uncertainty arises because we usually cannot implement the synthesized growth period model directly. Analytical formulae can only be used for the simplest configurations; for more general cases, we must resort to the computer. The translation of our model into a working computer code requires additional modeling of the

given problem, including the discretization of all space, angle, and time dependent variables. This additional modeling leads to a number of changes in the physical situation depicted by the model. Some of the more important ones include the separation of a single flame over a long fuel bed into a number of smaller separate flames, the realignment of an arbitrarily oriented object parallel to one of the room boundaries, and the modeling of a three-dimensional fuel element as a two-dimensional slab. The uncertainties due to fuel bed discretization are discussed in greater detail in Chapter 4. While this additional modeling is generally not required from a theoretical standpoint, it is useful practically speaking, if a solution is to be obtained within reasonable time and expense limits.

Finally, we note that we cannot specify the dimensions, thermodynamic characteristics, and geometry of a fuel bed within an arbitrary compartment to the degree of detail required by our models. A single slab of wood may have strong non-uniformities in density, water content, and structure, all of which will lead to variations in the burning rate of the slab. In the application of our model to a fire in a nuclear power plant compartment therefore, we can only specify representative but not exact fuel bed characteristics. If we are describing a fire in a class of rooms (e.g. cable spreading rooms), the fuel bed characteristics will be even more uncertain, due to plant-to-plant variability. The variations of the parameters specified from those which actually describe the room under consideration clearly lead to additional uncertainties in our modeling.

3.2 FREQUENCY-MAGNITUDE RELATION FOR FIRE SEVERITY

3.2.1 A Statistical Approach

In principle, a frequency distribution for the fire severity could be constructed directly from examination of data from fires in experiments and in the field. Such an approach is used by Fleming et al. [23], who utilize data estimates from fires in both nuclear and non-nuclear installations. An important feature of their analysis is their use of the volume of the room directly involved in the burning as a measure of fire severity. Since they assume that the burning volume may be roughly characterized as a cylinder whose height is the height of the compartment, their measure of severity reduces to the effective diameter of that cylinder. A plot of the data and their fitted regression line is shown in Figure 3.2; a frequency distribution for the actual fire severity and the suppression time can be easily derived.

While this measure for fire severity has some advantages, being certainly related to the maximum severity of the fire, and being easily measurable after extinguishment, we recognize that a component may be damaged even if it is not directly involved in the flames. Although the "volume of involvement" can be redefined to include areas damaged but not necessarily burnt, a more direct approach is to use additional measures of severity more fundamental to the physics of the fire, namely the spatially dependent temeperature and heat flux distributions. Unfortunately, there is little data for the temperature and heat flux levels achieved during compartment fires, either from experiments or from real fires.

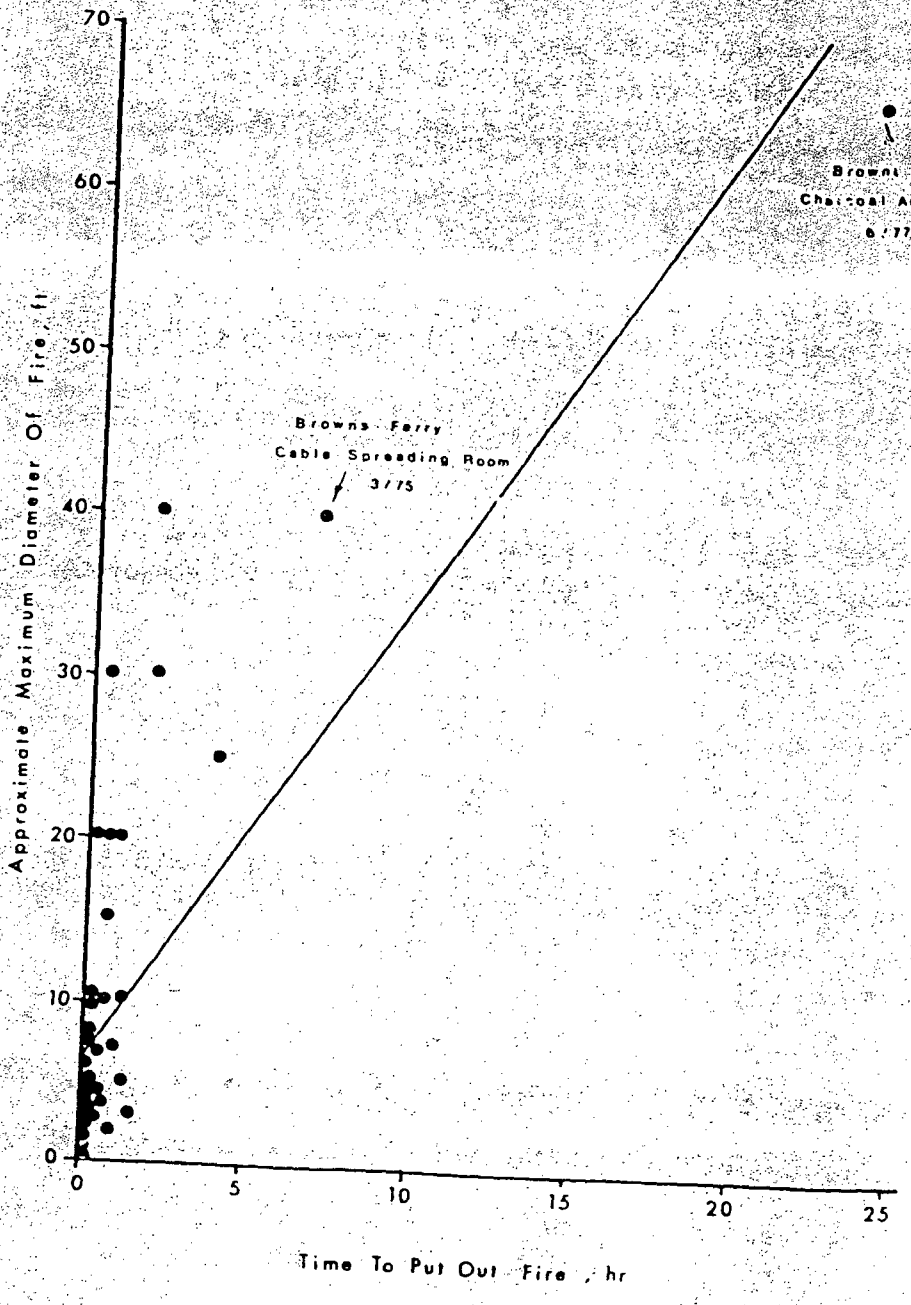

Fig. 3.2 - Data for Compartment Fire Severity [23]

3.2.2 The Reference Model Approach

Aside from the fact that there is relatively little physical data available for full-scale compartment fires, another difficulty which arises if we attempt to construct a statistical model for fire severity is that the data is not usually directly applicable to nuclear power plant rooms. As we have emphasized earlier, a fire's environment plays a crucial role in the development of the fire. Extrapolation of test results for a wood-fueled fire in a well ventilated small room to a large, electrical insulation fueled, poorly ventilated cable spreading room is a difficult procedure.

In order to handle fires in situations for which we have little or no experimental data, we utilize a deterministic model of fire which provides us with predictions of fire severity which incorporate the physical characteristics of the fire. These predictions serve as reference points for our uncertainty analysis.

3.2.2.1 Simplifications Due to Diffuse State-of-Knowledge

Before we describe the reference model approach in detail, we first assert that our state-of-knowledge uncertainties in the behavior of fire are much larger than the statistical uncertainty. The result of this assertion is that we need only predict the "average" value of any given fire severity measure, rather than its entire frequency distribution.

As was discussed earlier in this chapter, the randomness of fire ensures that even if we are given a specific fire, any measure of thermal hazard we consider will have a frequency distribution. Thus, in general we must predict not a single value of fire stress (at any particular

point in time) but rather a frequency distribution for fire stress. However, because our modeling uncertainties are non-zero, our predicted distribution will probably differ from the actual distribution. Rather than making a single prediction, therefore, we produce a series of estimating distributions and subjectively assess the likelihood (i.e. the probability) that each estimator is the true distribution. In Figure 3.3, we illustrate the approach with a simple example, where we believe the left-most curve is the actual frequency distribution with probability p_1, the central curve is the actual distribution with probability p_2, etc.

The general "probability of frequency" methodology [24,25] outlined above is simplified if our state of knowledge is relatively weak (see Figure 3.4). In this case, the statistical uncertainties (indicated by the width of the three frequency distributions) are overwhelmed by the state of knowledge uncertainties (indicated by the distance between the curves), even if the statistical uncertainties are not small in an absolute sense. We therefore may treat the frequency distributions as highly peaked curves located at some representative parameter of central tendency (i.e. the mean, median, or mode), and so our problem reduces to the task of predicting this parameter, rather than the entire frequency distribution.

To make our following discussion of the reference model approach concrete, let us assume that we wish to predict T_e, the temperature of the air surrounding the component of interest. From the above discussion, we decide to construct a probability distribution for the median $\hat{T}_e$ of the frequency distribution for T_e. The distribution of $\hat{T}_e$ will be com-

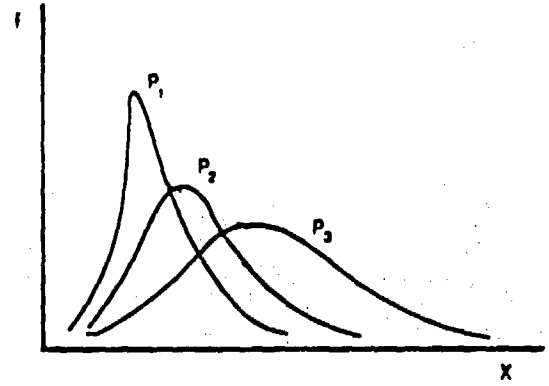

Fig. 3.3 - Uncertainty in Frequency Distribution of X

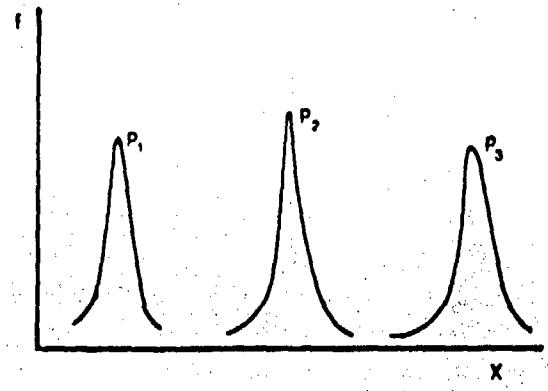

Fig. 3.4 - Uncertainty in Frequency Distribution of X (small statistical uncertainty)

posed of three elements: a deterministic reference model (DRM), a set of probability distributions for each input parameter required by the DRM, and a probability distribution which measures our confidence in the accuracy of the DRM.

3.2.2.2 The Deterministic Reference Model

The deterministic reference model is a model which explicitly incorporates the physics of the problem. Given a set of input parameters, the DRM will yield point estimates of each of the physical variables (e.g. temperature, heat flux, fire size, etc.) used to measure fire severity. We treat the DRM's prediction as an "expert's opinion"; when we later quantify the uncertainties in the DRM, we are expressing our belief in the credibility of the expert in a spirit similar to the approach used by Apostolakis and Mosleh [26] and Apostolakis et al. [27].

It should be noted that the DRM does not necessarily provide a "best-estimate" output, although efforts are usually made to ensure that it does; if there are competing models available, simplicity and usability are also important factors in the choice of the reference model. A good example of this last point is illustrated by the choice of flame height models.

The model for the flame height above a horizontal pool used in this work is that given by Thomas [7]. His semi-empirical correlation is

$$Z_{fl} = 42\, D_f \left[\dot{m}''/\rho_A\sqrt{gD_f} \right]^{.61} \qquad (3.1)$$

However, a better correlation for flame heights is given by Steward [28]:

$$\log_{10}(2Z_{fl}/D_f) = 0.20 \log_{10} N_{CO} + 1.21 \qquad (3.2)$$

where

$$N_{CO} = \frac{\dot{Q}^2 (r + \omega \rho_A / \rho_o)^2}{g \rho_A^2 H_f^2 (D_f/2)^5 (1 - \omega)^5}$$

$$\omega = \frac{V_A}{V - V_o}$$

r = stoichiometric air-to-fuel ratio (kg air/kg fuel)

and the subscript o stands for the fuel properties at the flame base.

The results of the two correlations are shown in Figure 3.5, and Steward's predictions seem to be better for a wider range of fires. However, full advantage cannot be taken of Steward's correlation unless N_{CO} is known, and this requires a thorough characterization of the burning fuel. Such detail is not easily found for the various fuels within nuclear power plants, there being a myriad of varieties of electrical insulation alone. Furthermore, Thomas' results are quite adequate for the type and sizes of fires expected (solid or liquid fueled, and moderately sized).

3.2.2.3 Incorporating Parameter Uncertainties

Once the DRM is constructed, the uncertainties in the input parameters are propagated through the DRM to obtain distributions for the output variables. Suppose our reference model, which may be a single equation or a computer program, operates on n input parameters

$$X_1, X_2, \ldots, X_n .$$

The DRM processes these parameters and yields a single estimate T_{DRM}. The relation between T_{DRM} and $\hat{T}_e$ shall be described later. If we input two different sets of values,

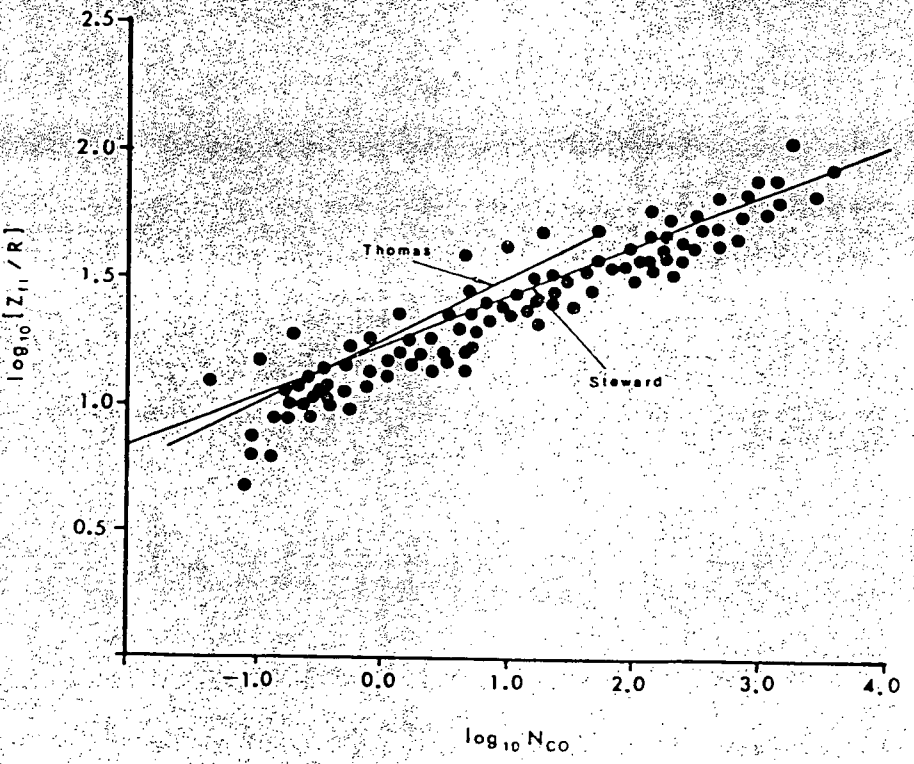

Fig. 3.5 - Comparison of Thomas' and Steward's Flame Height Correlations [28]

$$\vec{x}_1 = (x_{11}, \ldots, x_{1n})$$

and

$$\vec{x}_2 = (x_{21}, \ldots, x_{2n}),$$

the DRM will give us two different output values: $T_{DRM,1}$ and $T_{DRM,2}$, respectively. Clearly, if we input m input vectors

$$\vec{x}_1, \vec{x}_2, \ldots, \vec{x}_m,$$

m values for T_{DRM} will result. If we construct the ith element of each of the m input vectors by random sampling from the probablility distribution for X_i (assuming that the parameters are independent), the m values of T_{DRM} calculated will also have a distribution (see Figure 3.6).

If our reference model is actually a simple function, this propagation of the parameter uncertainties may be accomplished by analytical methods, e.g. the method of moment propagation [29]. As the model becomes more complex, we resort to numerical methods.

A simple but brutal numerical approach is the Monte Carlo simulation technique, where the input vectors are propagated through the actual reference model. A major drawback of this method is that very large numbers of samples are required to obtain good results, and if the model is in the form of a complex code rather than a single equation, the simulation costs can be prohibitive.

A similar but slightly more refined approach utilizes response surfaces [30,31]. The main difference between this method and the Monte Carlo approach is that in the former, the reference model is replaced by a response surface, an approximating function for the model. Since this reponse surface is typically a sum of polynomials of each of the input

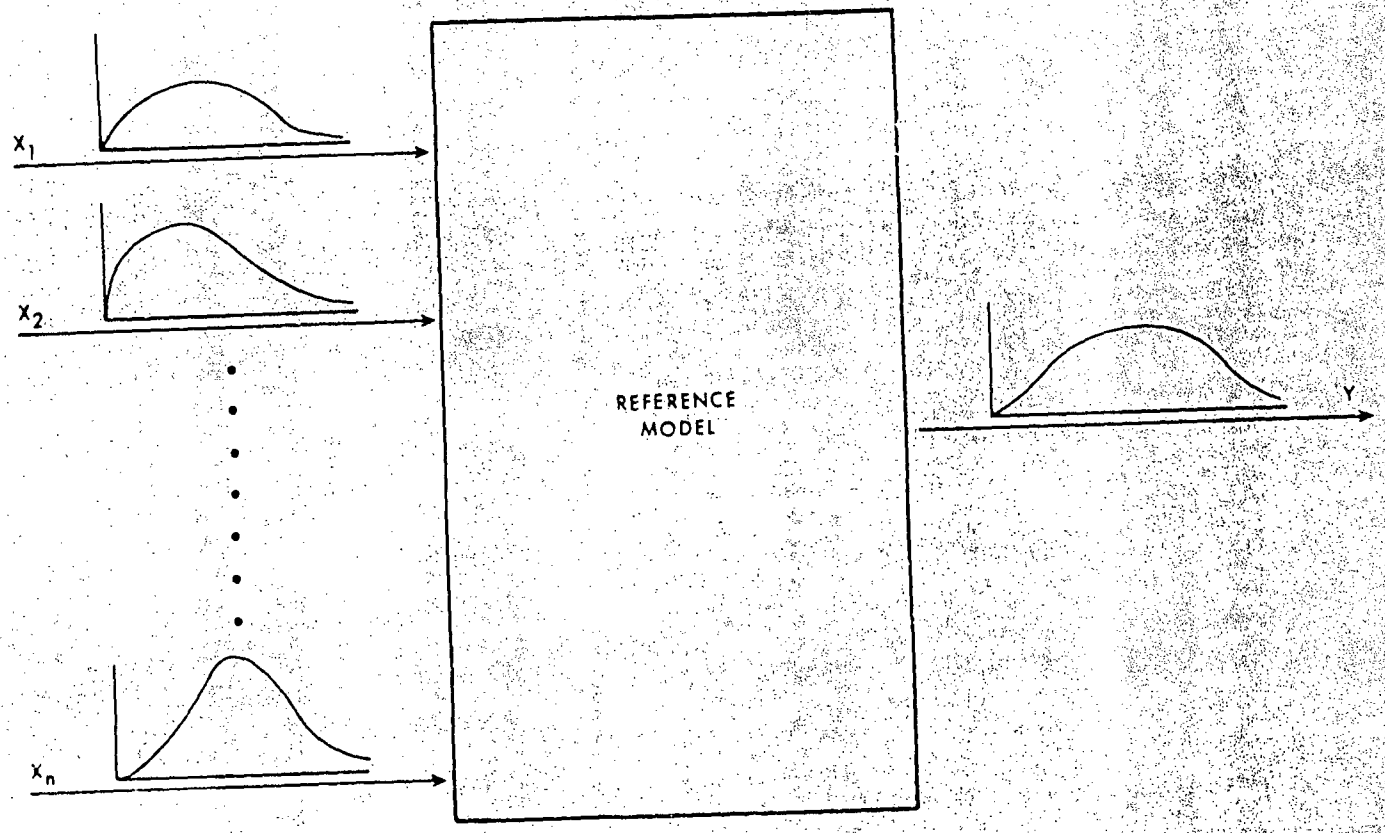

Fig. 3.6 - Schematic for Propagation of Uncertainties Through the Reference Model

independent variables, the time spent performing calculations can be reduced tremendously, this being of great importance if the number of random input vectors is large. Further, if the response surface is constructed using the Latin Hypercube Sampling technique [31] (see Appendix B), the number of trials which must be conducted is much less than the number needed for a Monte Carlo simulation of comparable accuracy.

3.2.2.4 Incorporating Uncertainties in the DRM

The two remaining types of modeling uncertainty to be handled are the uncertainty in the basic physical modeling and the uncertainty in the numerical implementation of the physical modeling. Although they come from somewhat different sources, we consider both collectively.

We recall that we wish to construct our probability distribution for the median external temperature $\hat{T}_e$, and that so far we possess a probability distribution for T_{DRM} which incorporates our uncertainties in the problem parameters. We now define an error function E_T such that

$$\hat{T}_e = E_T \, T_{DRM} \tag{3.3}$$

E_T may be thought of as a factor which measures our confidence in the prediction of the DRM.

Since even if we were absolutely certain of the actual values of the problem parameters, we would not know the exact factor by which the DRM's prediction varies from the actual value of $\hat{T}_e$, we must construct a distribution for E_T which incorporates our state of knowledge uncertainties. A distribution weighted to the right of the point E_T equals unity indicates that we believe that our DRM tends to underpredict the

actual value of $\hat{T}_e$, while a distribution weighted to the left will indicate the opposite. The distribution for E_T may be in the form of a histogram; one possible procedure for construction of the histogram (in the absence of strong data) is as follows.

1. Choose the upper and lower bounds for the histogram. These are the absolute values above and below which the assessor does not realistically expect to see any occurrences given his present state of knowledge. Any such occurrence would be classified as an extremely rare event.
2. Roughly quantify the degree to which the model overpredicts the actual stress. This percentage will show what fraction of the histogram area is to the left of the point $E_T = 1.0$.
3. Roughly quantify the accuracy of the reference model; decide how often the real value will be within a certain factor of the predicted value. This will indicate the peakedness of the distribution about the point $E_T = 1.0$.
4. Select histogram divisions. These divisions should be selected in such a way that they are meaningful to the assessor. Thus the probability that the error factor will be between 1/3 and 2/3 is easier to understand and judge than the probability that it is between 0.42 and 0.71, for example. The number of histogram divisions should be low enough that the assignment of probabilities to each histogram block in step 5 need not be extremely precise.

5. Assign probabilities to each histogram block, subject to the above constraints. The assessed probabilities should reflect the analyst's state of knowledge. Too precise values generally do not accurately reflect the assessor's uncertainties. Finally, the sum of the probabilities should clearly equal unity.

6. Check the resulting histogram and adjust if necessary for consistency. The analyst should ensure that the histogram not only complies with the above restrictions but also that he agrees with the statements made by the histogram. A good test of the histogram is to calculate its various percentiles and verify if these values do agree with the assessor's beliefs.

7. The analyst may use one of a number of techniques to fit a continuous distribution to the histogram. In this case, he should check and see if the percentiles of the fitted distribution conform with his beliefs.

In assessing the histogram block probabilities, a variety of different forms of evidence may be used. Thus, we may consider not only data from experiments and real fires but also predictions of their reference models predictions by experts in the field, qualitative information from the literature and critical assessments of the limitations and assumptions in the DRM used. Even if data is available, it should be mentioned that a subjective weighting of the applicability of the data to the fire situation considered must often be made.

It is important to note that the distribution for the error factor strongly depends on the measure of stress considered. For example, we expect that the error factor for the DRM's prediction of spatially dependent heat fluxes will exhibit different behavior from the error factor for the predicted fire plume temperature. We further note that E_T is dependent on the problem parameters: our assurance in the DRM's predictions will change, according to the particular fire modeled. As an example, we will show in Chapter 4 that our model does a fairly good job for small wood-fueled fires. On the other hand, we have less confidence in our simulations of larger fires, or fires fueled by less flammable materials such as electrical insulation.

Chapter 4

THE GROWTH PERIOD MODEL

The emphasis of our model for the fire hazards during the fire growth period is on the description of fire growth, since the temperature and heat flux fields which control fire growth also determine component damage. In other words, the thermal stresses imposed on a component are available as intermediate quantities in our fire growth model, and so no additional models are needed.

The model for fire growth is constructed as described in Chapter 3. A reference model which deterministically predicts the progress of a compartment fire is derived in Section 4.1 from the physical considerations of the problem. The input parameter uncertainties to be propagated through the reference model are described in Section 4.2, and the modeling uncertainties which contribute to the DRM's error factor for each output variable are treated in Section 4.3. In Section 4.4, we briefly outline some DRM simulations of actual experiments, and in Chapter 5, we analyze two different nuclear power plant compartment fire scenarios.

4.1 THE REFERENCE MODEL

As was seen earlier in Chapter 2, there currently is no overall model capable of dealing with the dynamic process of fire growth. While progress has been made towards detailed modeling of a growing compartment fire starting from first principles [32], the practical application of such a model to real fire situations may not be possible for some time.

An alternative approach, used in this work, is to model the growing fire using a quasi-steady framework which incorporates the large number of steady-state models available in the literature for the different aspects of a fire's behavior. Thus, the reference model computations proceed as follows.

At each point in time, the steady state burning rate of an ignited fuel element is computed with the aid of an appropriate model (the choice of model depends on the nature of the fuel and whether or not the fire is ventilation controlled). The heat release rate is computed from the burning rate and the effective heating value for the fuel; this quantity in turn is used to compute the heat transferred to the surroundings by radiation and to the accumulating layer of hot gases near the ceiling by convection. Upon determining the average temperature and thickness of the ceiling gas layer, the heat fluxes to any non-burning fuel element in the room are calculated, and the element is considered ignited if various ignition criteria are met. The size and intensity of the fire are thereby updated and the process continues, marching forward in time. A flow diagram for the basic computational scheme is shown in Figure 4.1.

In the following reference model, it will be assumed that the primary mode of heat transfer from the flame to an object will be thermal radiation. Radiation is important during the growth period for a number of reasons, the most important being that the hot gases from the fire are initially restricted to the buoyant plume immediately above the fire and a thin layer next to the ceiling, leaving most of the room essentially at ambient temperature where convective heat transfer is small. These

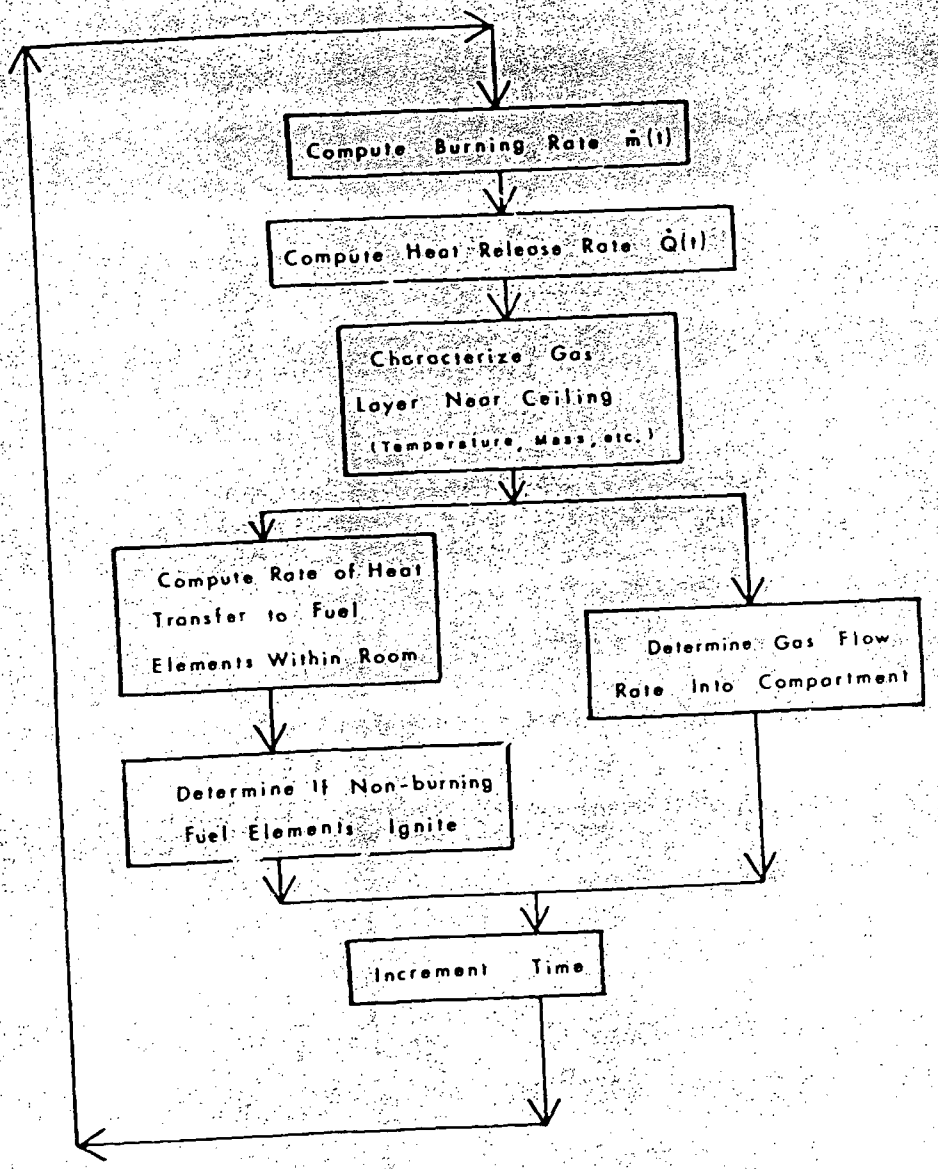

Fig. 4.1 - Flow Chart for Growth Model Calculations

effects will be accentuated in nuclear power plant rooms, since these rooms tend to be large (and thus possess large amounts of thermal inertia), and the combustible fuels tend to be widely separated.

Of course, the quasi-steady and the radiative dominance assumptions may become weaker as the fire growth accelerates towards fully-developed burning. Smaller time steps and more detailed fluid flow models can be used to alleviate these respective problems, but our knowledge of the burning conditions during the period immediately preceding flashover is so weak that these improvements may not be of much help.

In the remainder of this section, the various component models diagrammed in Figure 4.1, which are needed to synthesize the reference model, are described broadly. The computer program COMPBRN which actually implements the reference model calculations is described in Reference (1).

4.1.1 Heat Release Rate

The heat release rate of a fire is the central variable for any computation of the fire's behavior, whether inside or outside an enclosure. The total rate of heat released is given by

$$\dot{Q} = \eta \dot{m} H_f \qquad (4.1)$$

$\dot{m}$, the burning rate, depends on the available ventilation, surface area of the fuel, and the nature of the fuel. A fire is termed "ventilation controlled" if the rate of burning is limited by the amount of oxygen available, one cubic meter of air being capable of combusting approximately 113 Btu of organic fuel [33]. If the fire is not ventilation

controlled, its instantaneous burning rate is limited by the current fuel surface area.

For ventilation controlled fires,

$$\dot{m} = C_V W_{in} \tag{4.2}$$

For fuel surface controlled fires, the burning rate per unit area of fuel surface is given by

$$\dot{m}/A_f = \dot{m}''_0 + C_S \dot{q}''_{ext} \tag{4.3}$$

Equation (4.3) is a simplified version of a gross heat balance performed at the surface of the fuel. As explained in [34], the rate at which heat must be supplied to volatilize the fuel bed equals the total rate that heat is supplied to the fuel bed minus the rate of heat loss from the fuel bed, i.e.

$$\dot{m}'' H_f = \dot{q}''_{fl,r} + \dot{q}''_{ext} - \dot{q}''_{loss} \tag{4.4}$$

or

$$\dot{m}'' = (\dot{q}''_{fl,r} - \dot{q}''_{loss})/H_f + (1/H_f)\dot{q}''_{ext}$$

Clearly, $\dot{q}''_{fl,r}$ and $\dot{q}''_{loss}$ can vary from fire to fire. We introduce a constant $\dot{m}''_0$ to model this heat balance, but if experimental evidence is not available, the actual value to be used in calculations may not be easy to find. Table 4.1 provides some representative values for C_S for a variety of materials, Figure 4.2 provides empirical verification of Equation (4.3), Figure 4.3 displays the behavior of $\dot{m}''_0$ for liquid pool fires, and Figures 4.4 and 4.5 respectively provide correlations for $\dot{m}''_0$ for fires over wood cribs (assemblies of wood sticks or beams stacked in evenly spaced layers of alternating directions) and liquid pools.

Table 4.1 - Best Estimates for C_S

C_S (kg/J)	Fuel	Reference
5.53×10^{-7}	Wood	[34]
1.93×10^{-6}	Heptane	[34]
6.21×10^{-7}	PMMA	[34,35]

Table 4.2 - Best Estimates for H_f

H_f (J/kg)	Fuel	Reference
1.86×10^7	Wood	[11]
4.30×10^7	Oil	[44]
1.85×10^7 - 2.70×10^7	Cable Insulation	[45]

Table 4.3 - Various Estimates for χ

χ	Fuel	Reference	Notes
.35 - .36	Benzene	[36]	7.6 cm < D < 122 cm
.30 - .40	Gasoline	[36]	D = 122 cm
.20 - .27	Butane	[36]	30.5 cm < D < 76 cm
.16 - .17	Methanol	[36]	7.6 cm < D < 122 cm
.17	Fir	[42]	D = 7.3 cm *
.177	PMMA	[42]	"
.215	Polyethylene	[42]	"
.42	PMMA	[40]	23 cm < ℓ < 122 cm

* Small-scale experiments at high pressure

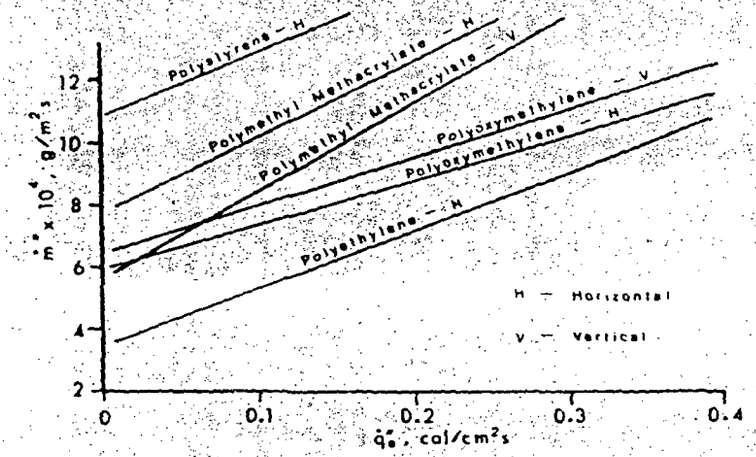

Fig. 4.2 - Burning Rate vs. External Heat Flux [35]

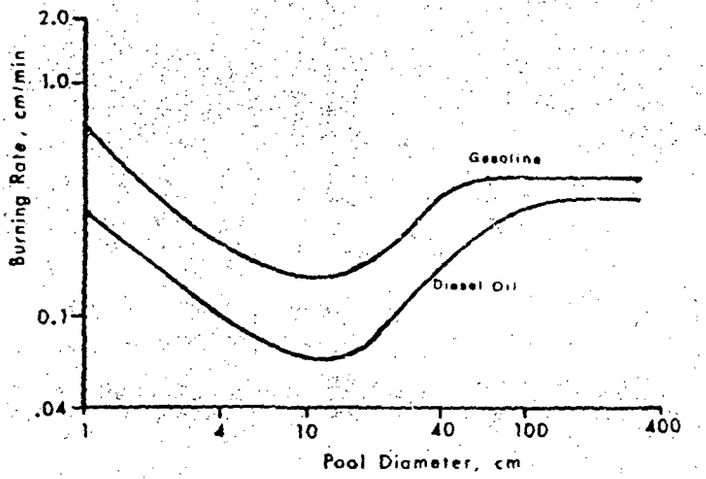

Fig. 4.3 - Surface Regression Rate for Liquid Fires [36]

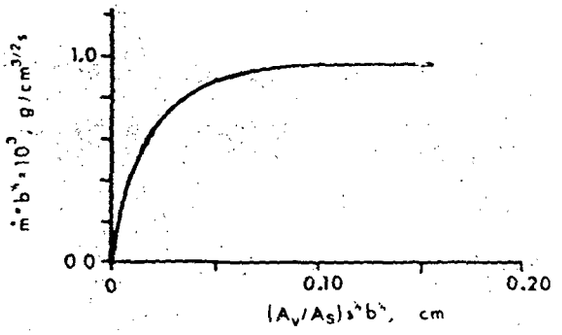

Fig. 4.4 - Burning Rate Correlation for Wood Cribs [37]

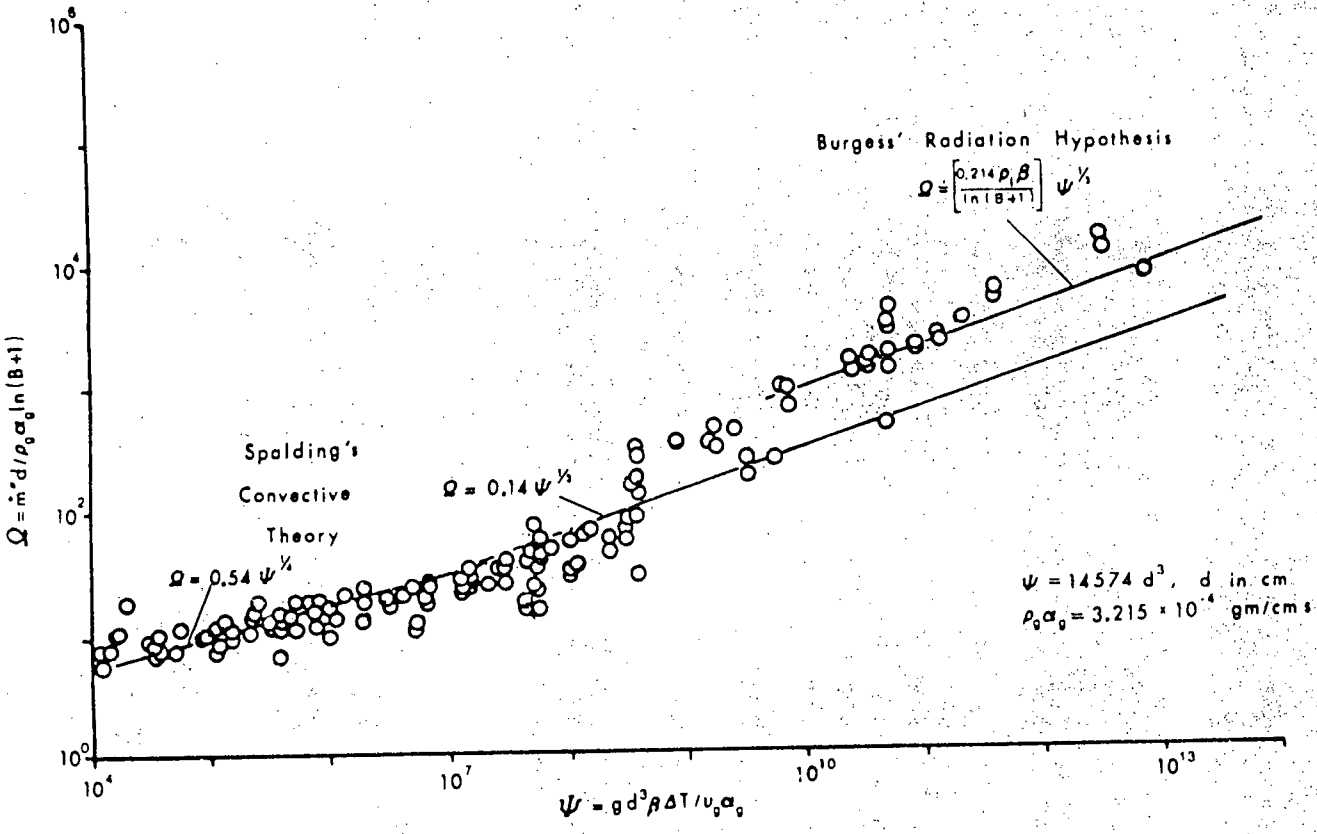

Fig. 4.5 - Correlation for Burning Rate [38]

4.1.2 The Ceiling Gas Layer

The layer of hot gases near the ceiling which accumulate during a compartment fire may play a significant part in the growth rate of the fire. Heat fluxes from this layer preheat non-burning fuel elements, reducing the time to ignition of these elements.

In order to characterize this layer, we need to know both its depth and its average temperature. Although some work has been done on the gas layer created by a small fire under a high ceiling [39], we adopt a simpler model, employed by Pape et al [16], which allows for more general situations.

In this approach, we perform a gross heat balance on the gas layer in a manner very similar to that used for the entire room in the fully-developed burning period analysis described in Chapter 6.

The gas layer gains sensible heat by the transport of hot gases from the various fire plumes in the room; it loses heat by the flow of hot gases out of the compartment (either by the forced ventilation system or by flow through any doors or windows), and by convection to the ceiling. Although radiation exchange with the remainder of the compartment also occurs, the net effect of this mechanism on the heat content of the gas layer is fairly small during much of the growth period, and shall be neglected.

Equating the heat losses to the heat gains in a manner consistent with our quasi-static approach to the growth problem, we obtain (assuming a single fire for simplicity)

$$(1-\gamma)\,\dot{Q} = W_{out}\, c_p\, (T_G - T_A) + h\, A_{ceil}\, (T_G - T_{ceil}) \qquad (4.5)$$

In the fully-developed burning period model, we assume that the hot gases occupied the entire compartment volume, and so the expression for W_{out} is very simple. When the hot gases gather in a layer, as seen in Figure 4.6, the computations are somewhat more difficult.

Assuming that the stratification between the hot upper layer and the cold lower layer is strong, the rate of gas flow out of the compartment opening is given by [15]

$$W_{out} = .67\ C_O\ A_O\ \rho_A \sqrt{2gB(T_A/T_G)(1 - T_A/T_G)}\ (1 - Z_n/B)^{3/2} + W_{FV} \tag{4.6}$$

and the rate fresh air flows into the compartment is, neglecting friction losses within the room,

$$W_{in} = .67\ C_O\ A_O \rho_A \sqrt{2gB(1 - T_A/T_G)}\ (Z_n/B - Z_d/B) \times (Z_n/B + .5Z_d/B)^2 + W_{FV} \tag{4.7}$$

If the fuel mass burning rate is much smaller than either of these mass flow rates, as is usually the case, a mass balance on the entire compartment yields

$$W_{out} = W_{in}$$

or

$$(T_A/T_G)\ (B - Z_n)^{3/2} = (Z_n - Z_d)\ (Z_n + .5Z_d)^2 \tag{4.8}$$

To find another relation between T_G, Z_n, and Z_d, we note that the fire pumps hot gases into the upper layer at a rate given by

$$W_{pl} = \dot{m}\ \omega\ \left[\beta \frac{Z_d - Z_o}{D_f/2} + 1\right]^{5/3} + \dot{m}\ (1 - \omega) \tag{4.9}$$

where

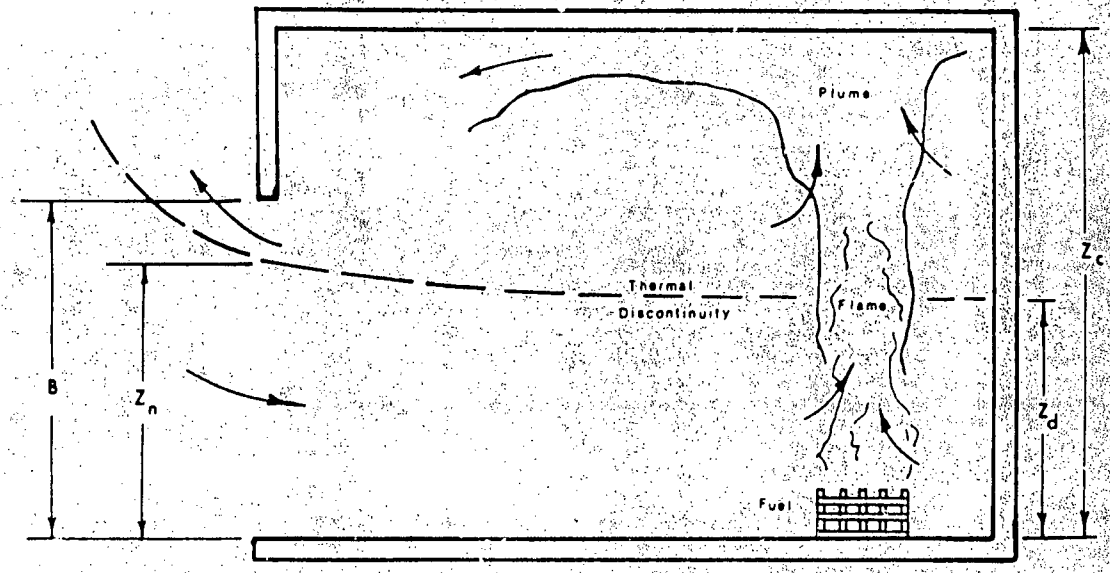

Fig. 4.6 - Fire Scenario Assumed for Ceiling Gas Model [15]

Z = height of flame base above floor (m)

$\beta \sim 1.0$

$\omega \sim 0.5$

The values of β and ω are somewhat dependent on the particular fuel burnt.

Performing a mass balance on the hot gas layer,

$$W_{pl} = W_{out}$$

and so

$$\dot{m}\omega[\beta\frac{Z_d - Z_o}{D_f/2} + 1]^{5/3} + \dot{m}(1-\omega) = .67C_o A_o \rho_A \sqrt{2gB(T_A/T_G)(1-T_A/T_G)}(1-Z_n/B)^{3/2} + W_{FV} \quad (4.10)$$

Equations (4.5), (4.8), and (4.10) form a coupled system of non-linear algebraic equations which can be solved iteratively for T_G, Z_n, and Z_d, using a variety of approaches (e.g. a Newton-Raphson iteration scheme).

4.1.3 Heat Transfer to Fuel Elements

For the medium to large fires of interest to safety engineers, radiation and convection are the dominant mechanisms for transferring the heat released by combustion from the flame to the surroundings.

4.1.3.1 Radiative Heat Transfer from Flame

It has been shown experimentally that the total amount of heat radiated away by a fire of moderate to large size (greater than 20 cm in diameter) is a constant fraction of the total heat released by the fire [40,41,42], although there is some disagreement as to the actual value of this fraction. There is presently no model derived from theory which

accounts for this empirical observation, but some justifications for the constancy of the radiant output fraction have been advanced [41]. Thus,

$$\dot{Q}_r = \chi \dot{Q} \qquad (4.11)$$

As mentioned in Chapter 2, most formulations for $\dot{Q}_r$ are of the form

$$\dot{Q}_r \sim T_{fl}^4 \qquad (4.12)$$

since the black-body radiative output of a differential hot gas volume element is proportional to the local T^4 product. However, determination of the average flame temperature in practice is usually accomplished by measuring the radiative output of the flame and then back calculating for T_{fl}. Therefore, there seems to be little practical advantage for this latter approach over the one adopted.

Once the amount of heat radiated away from a flame is known, the amount received by any object in the flame's vicinity can be calculated using the standard methods of radiation heat transfer analysis. Using Equation (2.3), and assuming all incoming radiation is absorbed ($\varepsilon = 1.0$), we have

$$\dot{q}''_{o,r} = F_{o-fl} \dot{Q}_r / A_{fl} \qquad (4.13)$$

4.1.3.2 Radiative Heat Transfer from Hot Gas Layer

To calculate the radiative transfer from the hot gas layer to an object outside the layer, we assume that the layer acts as a uniform source at the ceiling height. In a manner analogous to our computation for radiative heat transfer from a flame, we then have

$$\dot{q}''_{o,ceil} = F_{o-ceil} \dot{q}''_{ceil} \qquad (4.14)$$

The shape factor formulae necessary to compute F_{o-ceil} are given in Appendix A.

If we model the ceiling gas layer as a homogeneous isothermal infinite slab of thickness D with wavelength independent properties, it can be shown that with a few other assumptions (see Appendix D),

$$\dot{q}''_{ceil} = \varepsilon\sigma T_{ceil}^4 X+(1-\varepsilon)\dot{q}''_D X^2+\sigma T_G^4(1-X)[1+(1-\varepsilon)X] \qquad (4.15)$$

where

$X = \exp(-1.5aD)$

$\dot{q}''_D$ = incoming heat flux impinging on gas layer free surface

4.1.3.3 Heat Transfer Within the Flame

Since it is likely that any object in direct contact with a flame will be severely damaged in a short period of time, an extremely detailed model for the heat transferred is not necessary. We therefore conservatively assume that for objects touched by the flame,

$$\dot{q}''_o = \dot{Q}/A_{fl} \qquad (4.16)$$

In other words, the object is subjected to an average heat flux level within the flame, where attenuation is ignored.

4.1.3.4 Convective Heat Transfer

The convective heat transfer to an object is governed by Equation (2.1):

$$\dot{q}''_{o,c} = h\,[\,T_e - T_o\,] \qquad (4.17)$$

For the fire scenario postulated, where the hot gases released by the fire stratify near the ceiling, we generally neglect convective heat

transfer outside of the gas layer and the buoyant plume above the fire, since T_e is essentially the ambient room temperature outside of these zones. To compute convective transfer within these zones, we require values for h and for T_e. A number of correlations and models for both of these quantities are described in Appendix C. As for T_o, we neglect the object's rising heat content, and calculate the cold wall heat fluxes by maintaining T_o at ambient levels.

4.1.3.5 Heat Reflected and Emitted from the Walls

The boundaries of an enclosure reflect heat from a fire back into the enclosure, and also radiate increasingly larger amounts of heat as they warm up. An accurate description of these heat fluxes would require detailed shape factor calculations of the type outlined in Appendix A. However, since these fluxes tend to be small, only an order-of-magnitude assessment is necessary.

In order to account for wall reflection, the enclosure boundaries can be assumed to be uniform sources of heat fluxes of strength

$$\dot{q}''_W = (1 - \varepsilon_W) \sum_i \dot{Q}_i / A_W \qquad (4.18)$$

The heat flux to an object from wall reflections can then be found using the shape factor from a rectangular surface to a differential surface, as seen in the ceiling gas layer computation.

As for the emission of heat from the walls, the wall temperatures are generally low enough that this effect can be neglected, at least until the fire becomes quite large in size.

4.1.4 Fuel Bed Ignition and Fire Spread

Once the heat fluxes received by a fuel element are computed, the question of whether or not that element ignites and contributes to the fire growth must be answered.

As is generally the case in this model, we present a simplistic description of a rather complicated phenomenon. In this particular instance, a fuel element is considered ignited simply if its surface temperature exceeds a critical ignition temperature.

The concept of an ignition temperature is a somewhat imprecise one, since the temperature at which the volatile gases above the fuel surface will ignite is dependent upon a number of variables. These variables include the concentration of oxygen in the vapor-air mixture, the time history of the heat input into the fuel, and rate of heat losses to the fuel and environment. We shall discuss the uncertainties resulting from this simplistic model in a later portion of this chapter.

For additional simplification, we further model all fuel elements as semi-infinite slabs, and neglect heat losses to the environment via radiation and convection. The solution of the heat conduction equation, assuming a constant input heat flux $\dot{q}''_o$ at the slab surface, then yields an ignition time t^* given by

$$t^* = (\pi/4\alpha)\,[k(T^* - T_o)/\dot{q}''_o]^2 \qquad (4.19)$$

4.2 PARAMETER UNCERTAINTIES

The input parameters X_i required by the reference model described in the previous section include not only the fuel bed physical properties (e.g. burning rate, heat of combustion, density, etc.), but also the dimensions and geometry of the fuel bed and its location and orientation within the compartment. In most problems, we assume that our only input parameter uncertainties are in the fuel bed properties, that the geometry of the problem is well-known.

Although the number of fuel bed descriptors required by our DRM is quite large (see Reference (1)), we consider the uncertainties only in a limited number of them. The parameters considered are those which govern the burning rate in Equations (4.2) and (4.3), i.e. C_V, $\dot{m}''_0$, and C_S, those which govern the heat release per unit fuel volatilized, i.e. η, H_f, and γ, and the piloted and spontaneous ignition temperatures, T^*_p and T^*_s respectively, which govern the spread rate of the fire. The remaining parameters are assumed either to be well-known or have a lesser impact on the calculations; the treatment can be generalized to include these additional factors with little difficulty.

4.2.1 Burning Rate Parameters

The parameters C_V, $\dot{m}''$, and C_S are important because they determine the rate at which flammable vapors are made available for combustion. Of the three, C_S has perhaps the least uncertainty, being essentially the inverse of the fuel's heat of vaporization. Figure 4.2 shows that C_S, the slope of the burning rate lines, varies little for a number of different plastics.

The remaining two factors exhibit a greater degree of variability because we are modeling the complex burning process with constants. In Equation (4.2), we propose a direct proportionality between the burning rate and the compartment ventilation rate, although the former involves detailed phenomena at the fuel bed surface and the latter is a result of grosser fluid movements at the compartment level. In Figure 4.7, we present a frequency diagram for C_V obtained from Gross and Robertson's experiments with scaled down wood-fueled enclosure fires [43]. To allow for fires which burn other fuels, we can argue that since the combustion of enough fuel to release 113 Btu requires approximately 1 cubic foot of air, regardless of the actual amount of fuel vaporized, that the burning rate should be inversely proportional to the fuel heating value, i.e.

$$\dot{m} = C_V W_{in} [H_{f,wood}/H_{f,other}] \qquad (4.20)$$

As for $\dot{m}''_0$, we have already discussed reasons for its variability from fire to fire, and correlations have been presented in Figures 4 4 and 4.5. The largest uncertainties in $\dot{m}''_0$ arise when we consider cable insulation fires, there being little experimental data for this quantity. In fact, for fire-resistant insulation, it may be argued that $\dot{m}''_0$ may be negative, since in some cases it has been observed that an external heat flux must be applied before the cable will burn, and that if the external heat source is removed, these insulation fires will self-extinguish.

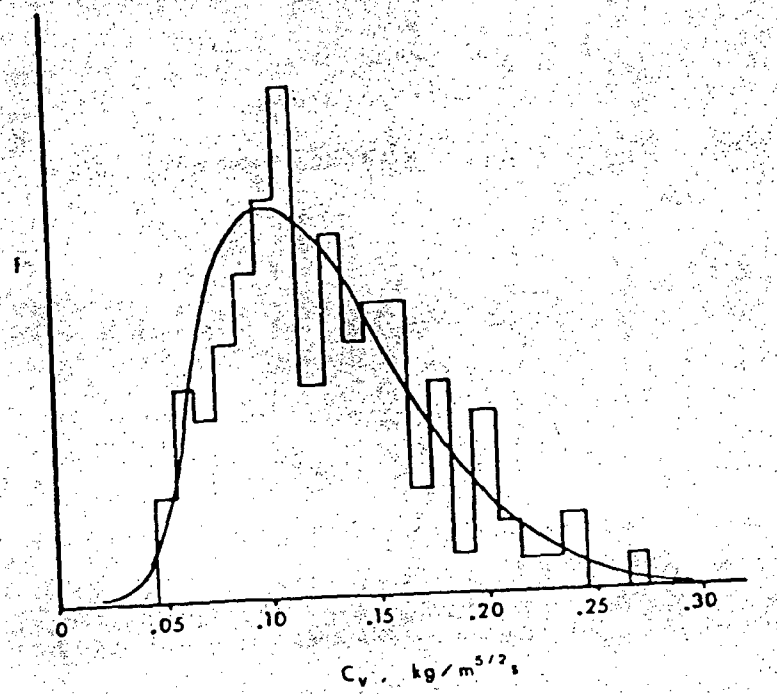

Fig. 4.7 - Histogram and Fitted Lognormal for C_v (Data from [43])

4.2.2 Heat Release Parameters

Of the three parameters mentioned in this group, η and H_f control the total amount of heat released per unit mass of fuel volatilized, while χ determines the fraction of this heat which is radiated from the flame. H_f is usually quite well-known for a variety of fuels; some typical values are given in Table 4.2. The combustion efficiency is not as well-known, but is expected to be fairly close to unity for fires which have access to large amounts of fresh air. χ has been measured to be in the range 0.20 to 0.40, and some typical estimates are given in Table 4.3. Throughout this work, we conservatively assume that χ equals 0.40.

From the above discussion, we see that the only uncertainties considered arising from this group of parameters are uncertainties in the types and amounts of fuels in the fuel bed studied. If the fuel bed is well specified, these uncertainties will be negligible.

4.2.3 Ignition Temperatures

The ignition temperature T^* is defined to be the threshold surface temperature of the fuel such that the fuel ignites when this value is exceeded. However, it was noted earlier that the concept of a threshold ignition temperature is somewhat imprecise; while we postpone a detailed discussion until the next section, we note that the values quoted in the literature for both piloted and spontaneous ignition generally exhibit significant variations (see Table 4.4). Further uncertainties result if the fuel bed is not well-specified (e.g. an uncertain mixture of cable insulations). We choose only to incorporate this latter source of uncertainty at the parameter level, leaving the uncertainty in the ignition

Table 4.4 - Ignition Temperatures (°C)

Material	Piloted		Spontaneous		Reference
	Average	Range	Average	Range	
3/4" Pine Wood	408	345 - 570	490	415 - 565	[46]
1/2" Pine Dowel	341	300 - 380	660	455 - 735	[46]
1/4" Oak Dowel	351	285 - 405	-	-	[46]
Box Cardboard	323	300 - 365	635	540 - 750	[46]
Newspaper	283	235 - 340	295	270 - 365	[46]
White Canvas	335	300 - 370	-	-	[46]
Green Cotton Cloth	328	265 - 415	440	390 - 545	[46]
Black Rubber	421	315 - 500	665	640 - 690	[46]
Polyurethane Foam	294	155 - 415	380	360 - 400	[46]

Table 4.5 - Properties of Wood Crib in [37]

b (stick thickness)	3.17 cm
ℓ (stick length)	22.7 cm
n (no. of sticks per layer)	4
N (no. of layers)	6
h (height of crib)	19.8 cm
s (spacing between sticks)	3.16 cm
$P\ (\frac{\text{vent area} \times \sqrt{sb}}{\text{exposed surface area}})$	0.04 cm

temperature for each particular material to be treated with the remaining modeling uncertainties.

4.3 MODELING UNCERTAINTIES

We distinguish two basic classes of modeling uncertainties: uncertainties in our basic physical modeling, and uncertainties in the numerical implementation of our reference model.

4.3.1 Uncertainties in Basic Modeling

Our uncertainties in the deterministic model for fire growth result primarily from uncertainties in the various component models used to construct the DRM (see Section 4.1), although there is some uncertainty in the synthesis of the component models. As discussed in Chapter 3, we treat all modeling uncertainties with a single error factor E_T in actual simulations; however, we could easily define error factors for each component model and propagate these uncertainties through the DRM in a manner identical to that used to propagate parameter uncertainties.

4.3.1.1 Heat Release Rate Modeling Uncertainties

The burning rate equations (4.2) and (4.3) are the most important sources of uncertainty in our heat generation model. Equation (4.3) is of special interest, since it introduces non-linearities into the analysis.

Although the forms of both equations are appropriate in a variety of situations (see Appendix E for two tests of Equation (4.3)), we are not certain that they are accurate for the wide spectrum of fires which may be observed in nuclear power plant compartments.

The burning rate equations used were developed for the combustion of relatively flammable materials in compartments with medium to high levels of ventilation. If the ventilation levels are very low, the fuel may smolder rather than burn, and what open flaming exists may oscillate in intensity and extent [48].

If the fuel bed is of low flammability, as is typically the case when cable insulation is the main substrate, our modeling of the burning process must be examined more carefully.

As an example, we consider a cable insulated with polyvinylchloride (PVC). The decomposition of PVC is a highly endothermic reaction. Further, HCl forms nearly 60% of the products of decomposition, HCl being a non-combustible gas. The result is that PVC is extremely difficult to burn; as soon as the external source of heat used to pilot the flame is removed, the fire tends to self-extinguish. On the other hand, for strength and rigidity considerations, PVC is usually impregnated with various other polymers before it is used as insulation. These plasticizers often increase the flammability of the insulating material. In order to accurately model the burning of the cable, we must determine the heat required to decompose the PVC-plasticizer mixture, the composition of the resulting vapors (a composition which usually changes as a function of temperature and heating rates), and the heat released by the burning of the combustible fraction of these vapors. Such a detailed model involving the fuel chemistry is well beyond the scope of this work, but we must recognize the uncertainty resulting from our simplistic modeling of the problem.

Another source of uncertainty in our modeling of burning rates is our neglect of physical movement of the fuel bed. This neglect is reasonable when dealing with wood-fueled fires. However, when plastics (e.g. cable insulation) are involved, melting and dripping of the plastic often alters the behavior of the fire, because this movement carries heat away from the fire. Since heat losses decrease the rate of burning, this neglect clearly is conservative.

4.3.1.2 Ceiling Gas Layer Modeling Uncertainties

Our uncertainty in the model for the ceiling gas layer is a direct result of the crudeness of the analysis used. More specifically, we have assumed that the layer will be strongly separated from the colder air below. While such a flow configuration is often observed, especially for smaller fires, alternative flow patterns are also possible, as demonstrated by the detailed numerical calculations presented in Reference (32). Another of our modeling assumptions leading to uncertainties is our assumption of a uniform gas temperature throughout the layer. In his work on ceiling gas temperature profiles, Alpert [39] reports not only variations as a function of radial distance from the plume axis but also with distance from the ceilng. In fact, the correlation given in Appendix C is actually derived for the maximum gas temperature in the layer at a particular radius. Alpert mentions that the axial temperature profile falls from this maximum (usually a few inches away from the ceiling) to essentially room temperature within a distance of 5.5 to 12.5% of the ceiling height. While strong mixing and plume interactions may tend to reduce these variations, nevertheless, our constant tempera-

ture model will lead to optimistic calculations of fire stress on a component in some situations, and conservative calculations in others.

4.3.1.3 Heat Transfer Modeling Uncertainties

Our basic formulation of the heat transfer from a heat source to a fuel element neglects the partial reflection of the impinging radiative heat fluxes, as well as the re-radiation, convection, and other losses from the element. The conservative modeling error introduced by this neglect increases with time, since these mechanisms become more important as the fuel element heats up.

4.3.1.4 Fuel Element Ignition Modeling Uncertainties

Although we have modeled all fuel elements as semi-infinite slabs in the derivation of Equation (4.19), this assumption does not lead to large errors, especially for materials with low thermal diffusivities, such as electrical insulation. A more fundamental source of uncertainty in our modeling is the use of a threshold temperature ignition criteria.

The process of thermal decomposition (which leads to burning) generally begins at temperatures well below the levels associated with combustion. Figure 4.8 shows a thermal decomposition curve for polystyrene. While rapid volatilization occurs at around 350°C, the fuel is acually producing combustible vapors at temperatures around 250°C and above. Combustion of these gases only requires oxygen and a suitable heat source. Thus, while ignition is far more likely at higher surface temperatures, it cannot be ruled out at lower levels. We can see that the crucial issue is not whether the fuel surface reaches a certain

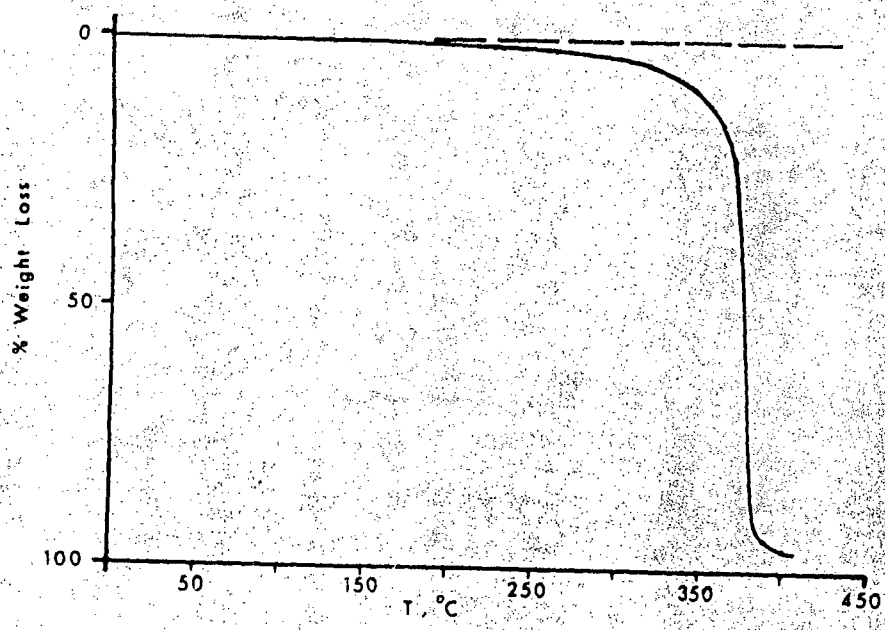

Fig. 4.8 - Thermal Decomposition Curve for Polystyrene [49]

temperature level, but rather if the heat gains by the gses are great enough to overcome the losses and trigger the combustion reactions, and if the resulting heat of combustion is great enough to sustain the reaction. Indeed, the fact that two different ignition temperatures are specified for fuels, depending on whether or not a flame is in contact with the fuel surface and pilots the flame, indicates that the ignition temperature is a function of the environment.

4.3.2 Uncertainties in Numerical Implementation of DRM

In Section 4.1, a deterministic reference model for estimating the progress of a compartment fire was outlined. For realistic problem configurations, the calculational scheme needed to implement the DRM requires a large number of computations. In order to arrive at a reasonable computer code which requires limited storage area and execution times, further simplifications and approximations (over those already made in the formulation of the reference model) are required, sometimes at the expense of the physics of the problem. In the following sub-sections, we discuss the uncertainties arising from three of the more important approximations.

4.3.2.1 Fuel Bed Discretization

The division of a continous fuel bed into a set of adjacent but discrete fuel elements directly affects our modeling of fire growth, since it affects the calculations for the mass burning rate and those for the heat radiated to other objects.

The specific mass burning rate, the rate at which solid or liquid fuel is converted into combustible vapors per unit area of fuel bed, is a direct function of the heat flux input into the fuel bed. This heat flux in turn is a function of flame size, a larger flame leading to larger heat fluxes (all other variables being equal). We can see that if a single fire is treated as several separate fires, we artificially increase the feedback to the burning surface above the level implicitly contained in $\dot{m}''_0$, since the fluxes from each of the smaller flames to a given fuel element are now considered as "external heat fluxes". This augmentation can be justified for the partition of a cable tray, since $\dot{m}''_0$ is generally given for a "pool fire" (i.e. a relatively symmetrical fire), and the elongated fire can be visualized as a number of contiguous pools. However, if a pool fire is subdivided into smaller pools, the calculations will be conservative.

The heat flux interchange between fuel elements is also affected by the separation of a single flame into smaller flames, since in general,

$$F_{o-fl}\ \dot{q}''_{fl} \neq \sum_i F_{o-fl,i}\ \dot{q}''_{fl,i} \qquad (4.21)$$

where the left-hand side represents the actual radiative heat flux to the object, while the right-hand side represents the radiative heat flux computed after the flame has been subdivided. It is not clear how this discretization will affect the computed heat flux in general situations.

4.3.2.2 Radiative Heat Flux Attenuation

As is discussed in Reference (5), the heat fluxes passing through a layer of hot gas or smoke attenuate essentially exponentially with dis-

tance. We neglect this attenuation in our model, even though a burning compartment may contain large quantities of these absorbing media. Thus the heat fluxes from a fire on one side of the room are assumed to reach the other side of the room without losses due to the intervening gases. Perhaps more importantly (since in the preceding example, geometric attenuation will probably be large), the heat fluxes from a flame to a neighboring flame will be unaffected by the distance it must travel through either's hot gases and smoke. The effect of this assumption is seen somewhat in the modeling of Huffman's experiment [62] (Appendix E), where the path lengths between elements of flame and the fuel surface change as flame merging and necking effects become prominent.

4.3.2.3 Ignition of Fuel Elements

The exact solution of the heat conduction equation in a semi-infinite homogeneous medium with a time-varying heat flux at the surface yields the following implicit relation for the ignition time t* as a function of the ignition temperature T* [50]:

$$T(0,t) - T_A = \frac{1}{k}\sqrt{\alpha/\pi}\int_0^{t^*} \dot{q}_o''(t^*-\tau)d\tau/\sqrt{\tau} \qquad (4.22)$$

This equation reduces to Equation (4.19) only if the input heat flux is constant. In our model, we define an average square of the input heat flux as

$$\overline{(\dot{q}_o'')^2} = \frac{\int_0^t (\dot{q}_o'')^2 dt'}{\int_0^t dt'} \simeq \frac{\sum (\dot{q}_o'')^2 \Delta t}{t}$$

and use this value in Equation (4.19).

While a more detailed approach would be to model the component using some finite difference or finite element scheme, we nevertheless expect that this more exact approach would still be subject to uncertainties because of the controversial nature of the ignition temperature concept. To demonstrate this last-named source of uncertainty, Figure 4.9 presents a comparison of experimental data for spontaneous ignition with a theoretical prediction when the incoming heat flux is convective, and Figure 4.10 is a plot of the histogram distribution for the random variable

$$\tau = t^*_{experiment} / t^*_{theory}$$

4.4 REFERENCE MODEL VERIFICATION

Since our discussion in the previous sections indicates a large number of uncertainties in our growth period reference model, we wish to test the model to demonstrate that it does reasonably predict the behavior of fire. In this section, we use the DRM constructed to simulate a number of experiments documented in the literature.

4.4.1 Wood Crib Fire

The first calculation is a simulation of one of a series of wood crib fire experiments conducted by Delichatsios [37]. The specifications of the particular crib studied are given in Table 4.5, and a view of the crib is provided in Figure 4.11.

Two alternative models are developed to handle the complex fuel bed geometry. In each case, we compute the mass burning rate as a function

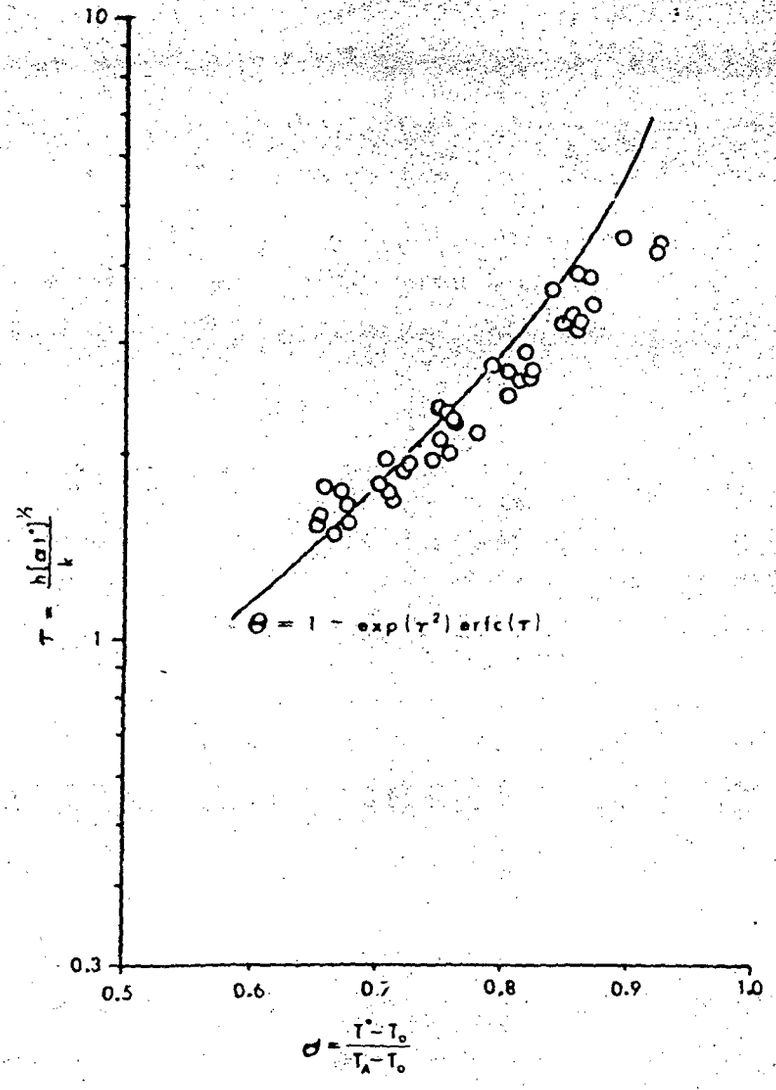

Fig. 4.9 - Spontaneous Ignition Data Versus Theoretical Predictions [38]

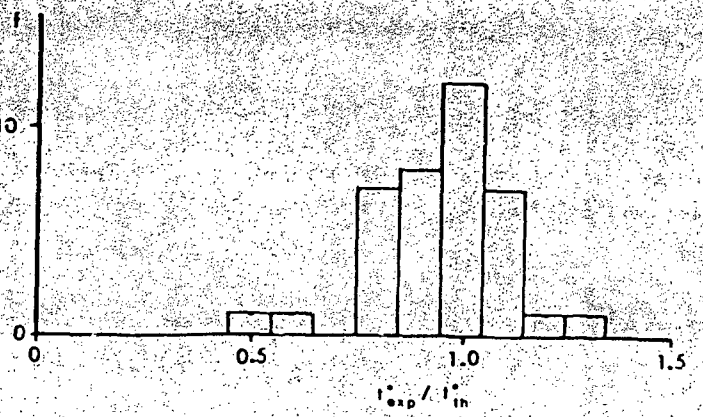

Fig. 4.10 - Variations of Experimental Spontaneous Ignition Times [38]

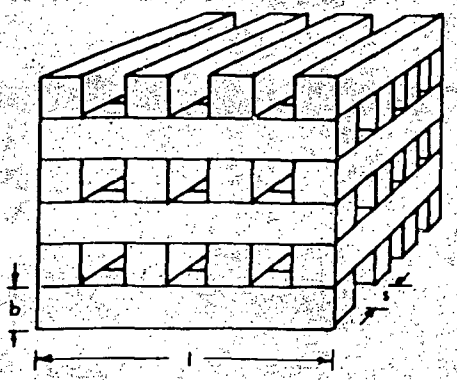

Fig. 4.11 - Diagram of Wood Crib Used in [37]

of time (in kg/s) and the average flame spread velocity over the top of the crib (the effective radius of the square crib divided by the time it takes the fire to cover the crib top entirely).

The first configuration chosen to model the crib is simply a square block of wood, divided into 25 fuel cells. Because our model treats the three dimensional wood sticks of the crib as two dimensional fuel slabs, the fuel slab surface area in the model is enhanced by a "porosity factor", defined as

$$f_p = \frac{A_{\text{fuel surface}}}{A_{\text{fuel base}}}$$

For example, referring to Figure 4.11, the area of the fuel base is approximately ℓ^2. Since the actual surface area of fuel available for burning is about $3Nb\ell$, where N is the total number of sticks, and where we have discounted the bottom face and ends of each stick from the total area, the porosity factor is $3Nb\ell/\ell^2$, or about 13.4 for the crib considered.

The second configuration models each individual crib stick as a separate two-dimensional slab of length ℓ and width b. The porosity factor f_p for each slab is taken to be 3.0 (we once more discount the bottom face of each stick).

Delichatsios does not give any specific information concerning the enclosure surrounding his experiments, and we assume that the enclosure effects are small.

The results of the simulations are shown in Figure 4.12. For each configuration, two trials are made. The first includes a non-zero feedback coefficient C_S for the specific burning rate, while the second does

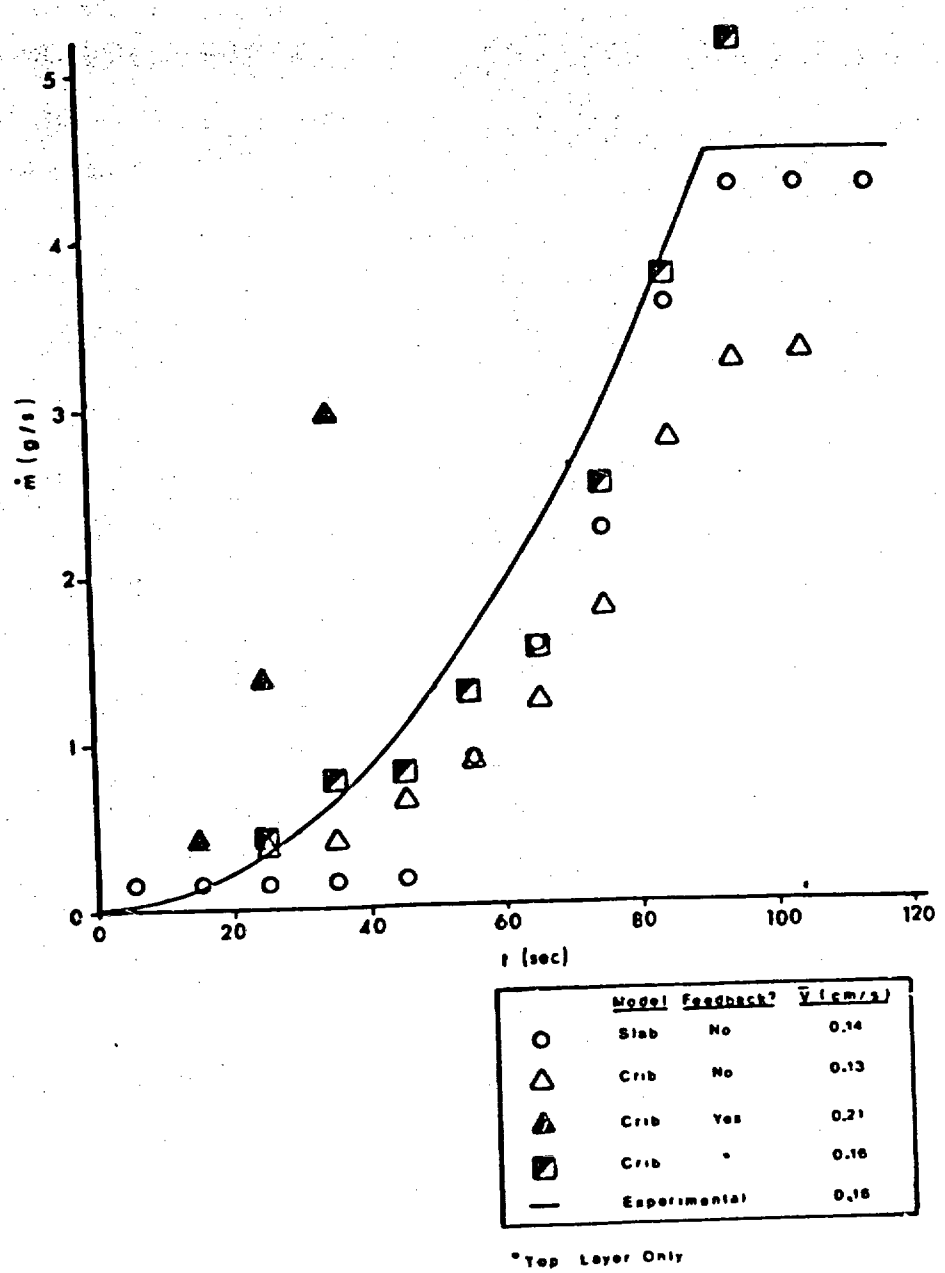

Fig. 4.12 - Reference Model Predictions for Burning Rate of Wood Cribs Versus Experimental Data [37]

not. Note that even though the ventilation level in the room is assumed large enough not to be restricting, the stick spacing of the crib limits the amount of fresh air available to the burning fuel within the crib. Thus, the trials using zero feedback represent the actual experimental data much better than those using non-zero feedback. The best simulation of the experiment is obtained using a synthesis of these two extremes. The top layer of fuel is allowed a non-zero feedback term since it is exposed to the essentially unlimited quantities of fresh air, while the remaining layers are considered to have limited access to air, and so their burning rates may not be enhanced.

Although the agreement between experiment and simulation is encouraging, we must remember that the models we have used in our synthesis have generally been developed for wood-fueled fires. In particular, the value of 0.0062 kg/m^{2}s selected for $\dot{m}''_0$ is a value derived from wood crib data as a best-estimate for surface controlled fires [11]. Thus, the accuracy of the steady-state burning rate prediction of our simple slab model without feedback is not too surprising; we have preserved both the burning rate per unit area ($\dot{m}''_0$) and the actual surface area of the crib (via the porosity factor f_p).

A less expected result is the accuracy of our simulation's handling of the transient burning period of the crib. The predicted burning rate as a function of time and the average velocity of the flame front over the top of the crib agree well with the experimental values, giving us confidence in our simple heat transfer and fuel ignition models.

4.4.2 Vertical PMMA Slab Fire

The simulation described above provides a test for our reference model when the fuel is divided into horizontal strips. To check the validity of the model when the fuel is a long, vertical strip, we refer to the experiment of Orloff et al. [51], where a 1.57 x 0.41 x 0.10 m slab of PMMA was burned. We note that our discussion of a vertical PMMA fire in Appendix E is for verification of the linear feedback model used for the burning rate, and that the model used deals with the fuel as a continuous entity. In this section, we discretize the fuel bed into fifteen separate but contigous fuel cells, in order to apply our reference model.

Comparison of our predictions with the experimental values for the flame propagation velocity up the slab and the steady-state burning rates (see Figure 4.13) shows that as in the previous simulation, our reference model seems to be quite adequate.

4.4.3 Vertical Cable Tray Fires

In both the wood crib and PMMA slab burning experiments, we are dealing with quite flammable fuels. Since we also wish to apply our model to cable tray fires, where the fuel is generally much more difficult to burn, we would like to check the accuracy of our reference model under these different conditions.

In these calculations, we refer to Przybyla and Christian's test burnings of 40% filled cable trays, detailed in [52]. The cables burnt were 0.515 inches in diameter, had a 0.050 inch thick PVC cable jacket, a 0.006 inch nylon conductor jacket, and a 0.22 inch thick PVC insula-

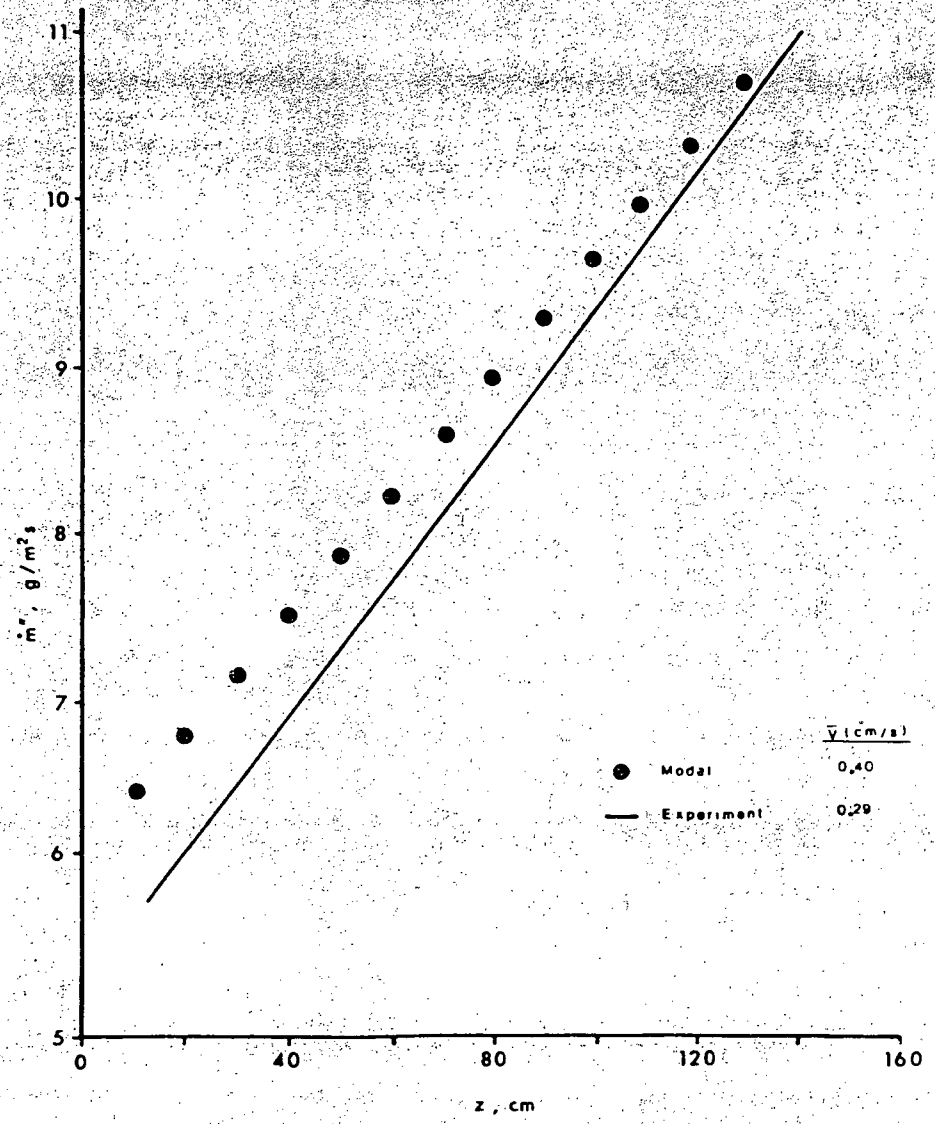

Fig. 4.13 - Reference Model Predictions of Burning Rate of PMMA Vertical Slab Versus Experimental Data [51]

tion layer. The trays were 8 feet long, 12 inches wide, and 3.375 inches deep, and were of open ladder construction. The pilot flame used to initiate and sustain the fire was provided by a 10 inch wide ribbon type propane burner, and was located at varying distances from the cable tray and at varying heights above the cable tray bottom. The test set-up is shown in Figure 4.14.

Before we examine the results of our simulation, we note that the selection of parameter values to be used in the modeling is a major concern. As noted earlier, the primary fuel, PVC, is usually impregnated with a wide variety of substances which may drastically affect the burning characteristics of the main fuel. These effects are generally not quantified, and so many of the parameter values used in the simulation are assumed (see Table 4.6).

In particular, the value for $\dot{m}_0''$ is not known. This quantity may be positive or negative, depending on the flammability of the plasticizers added to the PVC. Since we are only interested in a reasonable reference model simulation of the cable tray experiment, we assume that the threshold takes on a few different values, and then compare the resulting predictions with the experimental data.

We plot the measured heat flux profile along the tray due to the burner only (no cables are burning) in Figure 4.15, to determine the accuracy of our prediction of the external heat flux impinging on the cables, and also compare the predicted average flame front propagation velocity up the tray with the actual range of values in Table 4.7.

We note that in our model, the entire portion of cable tray above the pilot flame eventually becomes involved in the fire. On the other hand,

Table 4.6 - Parameters Used in Cable Tray Fire Simulation

Parameter	Symbol	Value
fuel density	ρ	1715 kg/m^3
fuel specific heat	c_p	1045 J/kg°K
fuel thermal conductivity	k	0.092 W/m°K
fuel heating value	H_f	1.8×10^7 J/kg
fuel piloted ignition temperature	T^*_p	750°K
fuel spontaneous ignition temperature	T^*_s	780°K
fuel specific burning rate constant	$\dot{m}''_0$	-0.002 to 0.0 kg/m^{2}s
fuel burning rate augmentation constant	C_s	1.8×10^{-7} to 4.3×10^{-7} kg/J
fuel fraction of heat released as radiation	χ	0.30
burner fuel heating value	H_f	5.05×10^7 J/kg
burner fuel specific burning rate	$\dot{m}''_0$	0.0694 kg/m^{2}s
burner fraction of heat released as radiation	χ	0.39
burner area	A_f	0.0025 m^2
combustion efficiency	η	0.90

Table 4.7 - Upward Flame Spread Velocity of Cable Tray Test

$\dot{m}''_0$ (kg/m²s)	C_S (kg/J)	$\bar{v}$(cm/s)
-0.002	1.8×10^{-7}	0.58
-0.0001	1.8×10^{-7}	0.54
0.00	4.3×10^{-7}	1.27
Experiment [52]		$0.08 < \bar{v} < 0.36$

Table 4.8 - Properties of Wood Crib in [53]

b (stick thickness)	5.1 cm
ℓ (stick length)	36 cm
n (no. of sticks per layer)	4 (top 6 layers)
	2 (bottom 2 layers)
N (no. of layers)	8
h (height of crib)	30 cm
s (spacing between sticks)	5.1 cm (top 6 layers)
M (mass of crib)	6.35 kg

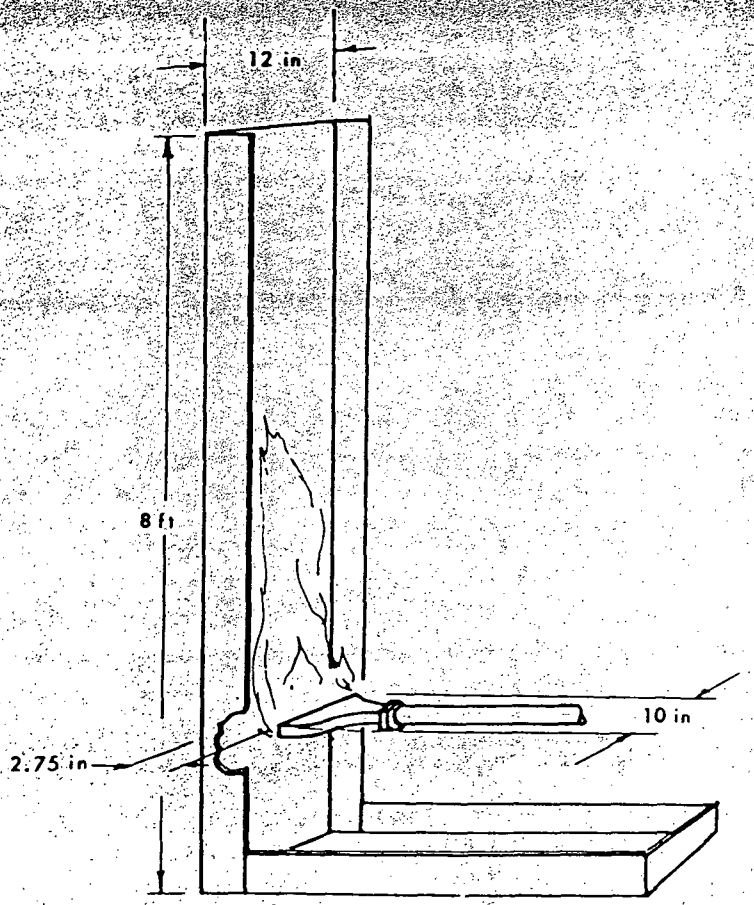

Fig. 4.14 - Cable Tray Experimental Set-up [52]

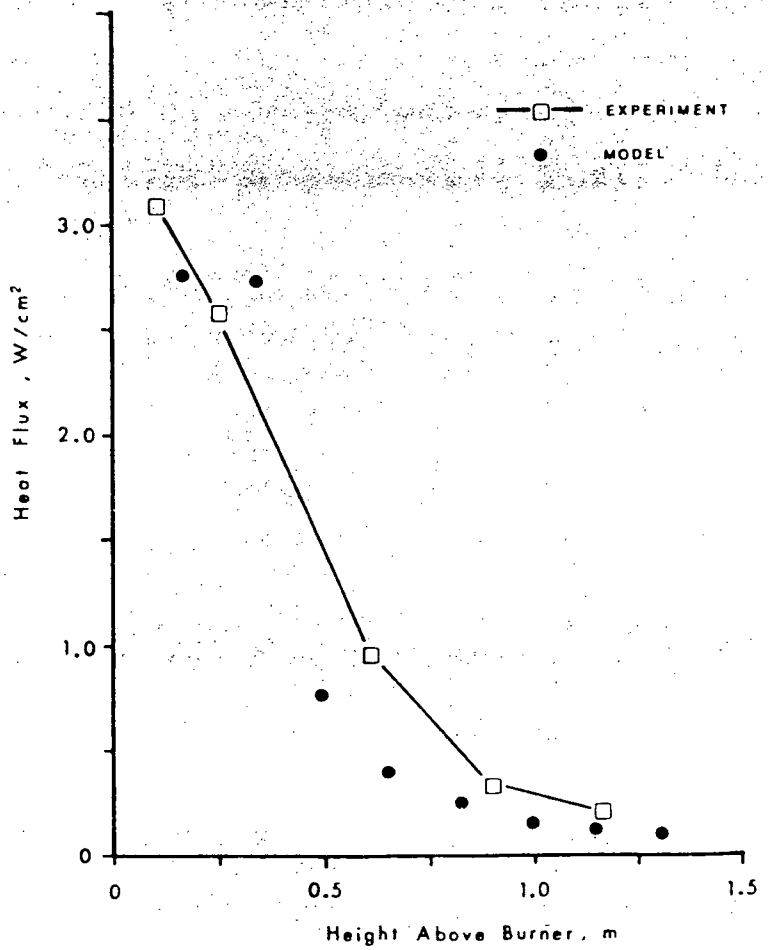

Fig. 4.15 - Comparison of Experimental and Predicted Burner Heat Fluxes Along Cable Tray [52]

the actual flames often stopped short of the tray top, and also proceeded more slowly up the tray. The conservatism of our model thus displayed is probably largely due to our neglect of heat loss mechanisms, especially insulation melting and dripping.

4.4.4 Compartment Fire Simulation

Our final simulation involves a small wood crib fire in an enclosure reported by Fang [53]. The experiment is one of a series of furniture and wood crib fires covered in that work, and the problem parameters of the particular experiment modeled are given in Table 4.8.

Fang reports an impressive amount of data from his experiments, including fuel mass burning rates, heat fluxes, and fire plume temperatures as functions of time. Our reference model predictions of these quantities are compared to the data in Figures 4.16, 4.17, and 4.18.

The observed differences in behavior of our reference model predictions and the experimental data can be largely attributed to the coarseness of the model used. Our model for the crib is a slab similar in type to the slab used in the simulation discussed in Section 4.4.1, i.e. it is composed of 25 fuel cells whose surface areas are enhanced by a porosity factor f_p, to account for the actual area available for burning. This discretization of the fuel bed is too coarse to allow the partial feedback modeling employed earlier, and so no feedback to the fuel bed is allowed. Consequently, our predicted burning rates and heat release rates are somewhat lower than expected. Another result of our use of relatively few fuel cells is that fuel burn-up can only be modeled rather crudely. We thus observe our model's prediction of a cons-

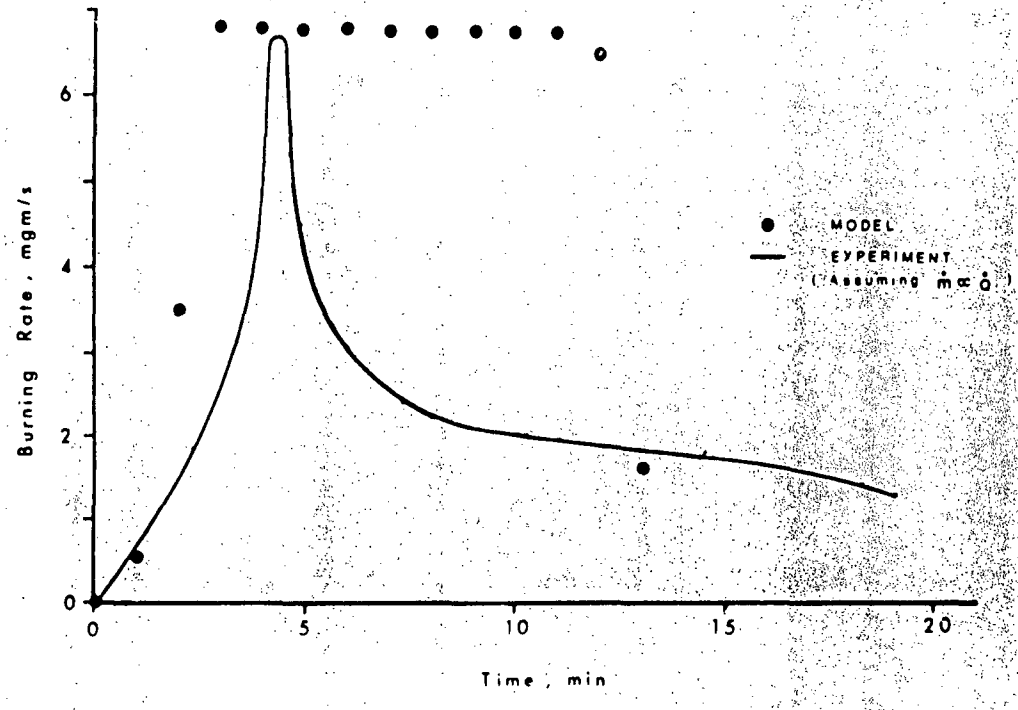

Fig. 4.16 - Experimental and Predicted Burning Rates [53]

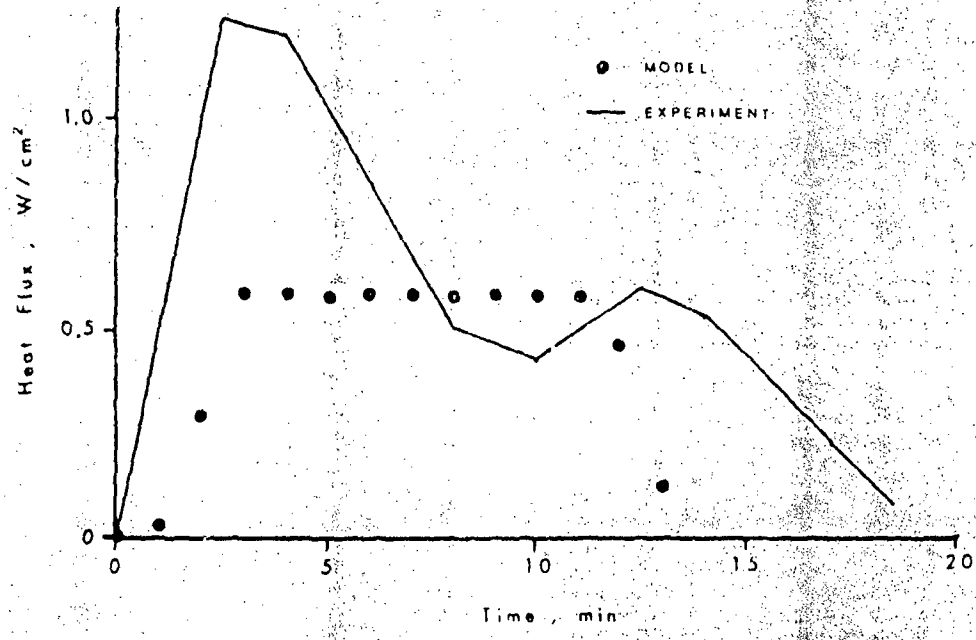

Fig. 4.17 - Experimental and Predicted Heat Fluxes [53]

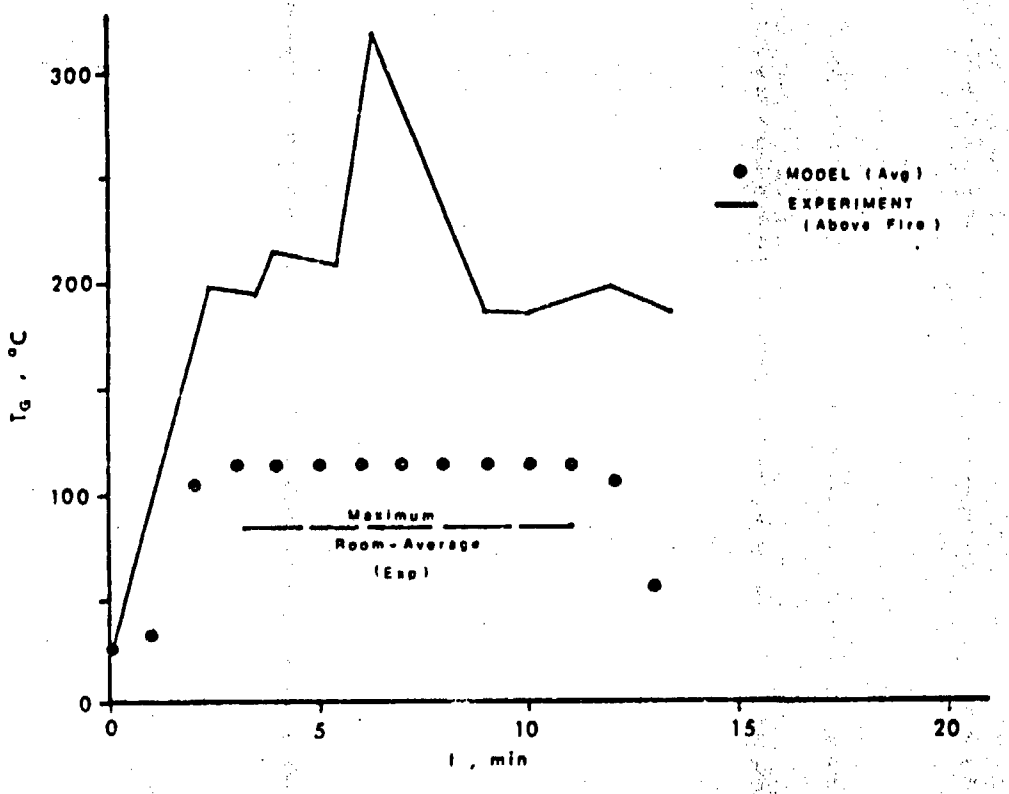

Fig. 4.18 - Experimental and Predicted Gas Temperatures [53]

tant fire behavior for a large part of the burning period, whereas the actual fire level rises to a peak and then gradually decays.

Despite these differences, our model once more performs adequately. We note that the heat flux data presented by Fang for this particular experiment actually seems somewhat anomalous when compared with results of his other experiments; his reported heat fluxes for large wood crib fires (measured by detectors much closer to the flames than those used in the small wood crib experiment) are not appreciably greater than those reported for the small wood crib case. We thus may have reason to believe that our reference model heat flux predictions are even better than shown in Figure 4.18.

Chapter 5

APPLICATION OF GROWTH PERIOD MODEL

In this chapter, we apply our model for the thermal hazards during the growth period to two fire scenarios of interest in our investigation of the risk to nuclear power plants due to fire. The first scenario concerns the exposure of an electrical cabinet to a fixed flame, while the second deals with fire spread between two vertically separated parallel cable trays.

5.1 ELECTRIC CABINET FIRE

Steel cabinets are often used in nuclear power plants to hold relays and logic circuits associated with plant control and instrumentation. These electrical components are generally quite sensitive to the temperature of the surrounding air; if the temperature rises more than a certain amount, e.g. 20°F or more, the components can be damaged and faulty signals may result. Thus, one question in a nuclear power plant risk analysis is what size fire is required to cause this temperature rise. In this section, we shall construct a crude physical model for the exposure fire and for the steel cabinet's thermal response. We cannot use our growth period reference model directly, since our concern lies primarily with determining a response to a thermal stress, rather than with the stress itself. However, the construction of the cabinet model will provide a simple illustration of the process used to construct the more

general growth model. Uncertainties shall not be incorporated into the analysis because we are looking for the broad characteristics of the critical exposure fire.

5.1.1 Exposure Fire Model

A fixed diameter pool of fuel is assumed to fire on the compartment floor a distance x_c away from one of the cabinet faces (see Figure 5.1). Since the aisle separating rows of these cabinets is typically 1 m wide, this is the maximum separation considered. The flame height of the fire is given by Equation (3.1),

$$Z_{fl} = 42\, D_f \left[\dot{m}''_0/\rho_A\sqrt{gD_f}\right]^{0.61} \tag{5.1}$$

where $\dot{m}''$ is replaced by $\dot{m}''_0$ since there are no other important heat sources in the scenario, and since the fire is assumed to be fuel surface controlled. We model the flame as a cylinder of diameter D_f and height Z_{fl}. The radiative heat flux at the flame boundary is then approximately given by

$$\dot{q}''_{fl} = \dot{m}''_0\, H_f\, (1 + 4Z_{fl}/D_f)^{-1} \tag{5.2}$$

and the heat flux impinging on the cabinet face is given by

$$\dot{q}''_{cab} = \varepsilon\, F_{cab\text{-}fl}\, \dot{q}''_{fl} \tag{5.3}$$

We conservatively assume that the heat flux received by a differential surface lying on the flame-cabinet axis and a distance Z_{fl} up from the floor is representative of the average heat flux received by the entire cabinet face, and so $F_{cab\text{-}fl}$ can be calculated using Equation (A.6).

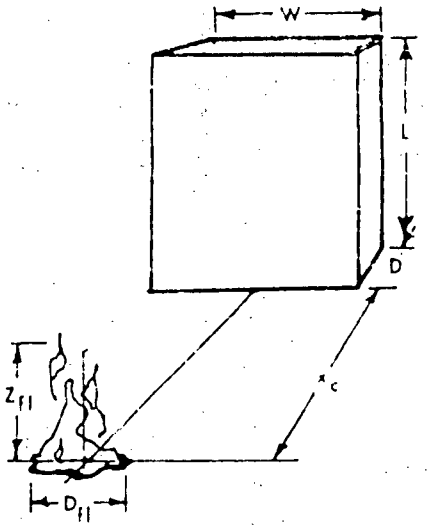

Fig. 5.1 - Exposure Fire for Cabinet

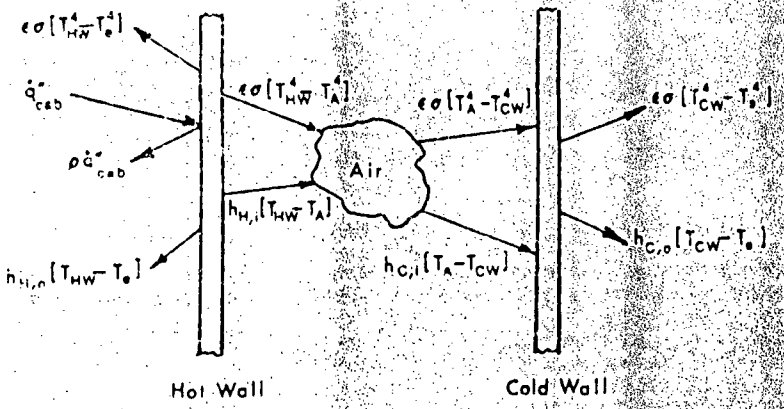

Fig. 5.2 - Heat Fluxes for Heat Balances at Each Node

The heat fluxes calculated for a number of fires at varying distances away from the cabinet are listed in Table 5.1.

5.1.2 Thermal Response Model

In order to calculate the air temperature within the cabinet, we represent the cabinet with a three node model. At each of the three nodes (corresponding to the "hot wall" facing the fire, the "cold wall" representing all the remaining cabinet faces, and the cabinet air itself), we perform a heat balance to obtain the governing equations.

Referring to Figure 5.2, there results,

a) Hot Wall:

$$\dot{q}''' = (1-\varepsilon)\dot{q}''_{cab} + h_{H,o}(T_{HW} - T_e) + \varepsilon\sigma(T^4_{HW} - T^4_e) + h_{H,i}(T_{HW} - T_A) + \varepsilon\sigma(T^4_{HW} - T^4_A) \quad (5.4)$$

b) Cold Wall:

$$h_{C,i}(T_A - T_{CW}) + \varepsilon\sigma(T^4_A - T^4_{CW}) = h_{C,o}(T_{CW} - T_e) + \varepsilon\sigma(T^4_{CW} - T^4_e) \quad (5.5)$$

c) Cabinet Air:

$$M_A c_p \frac{dT_A}{dt} = A_{HW}[h_{H,i}(T_{HW} - T_A) + \varepsilon\sigma(T^4_{HW} - T^4_A)] - A_{CW}[h_{C,i}(T_A - T_{CW}) + \varepsilon\sigma(T^4_A - T^4_{CW})] \quad (5.6)$$

The heat transfer coefficients can be calculated using standard natural convection correlations. For example, one formulation for a vertical wall of height L is [54]:

$$h = \frac{\bar{k}}{L}[49.7 + 0.0182a^{.4}(L - \frac{1585}{a^{.4}})] \quad (W/m^2{}^\circ K) \quad (5.7)$$

where

Table 5.1 - Exposure Heat Flux in W/cm^2

Separation Distance (m)	Exposure Fire * 1	2	3
0.25	0.23	0.67	1.60
0.50	0.095	0.32	0.81
0.75	0.048	0.20	0.53
1.00	0.028	0.14	0.39

* Exposure Fire 1: 15 cm radius paper fire
Exposure Fire 2: 7.5 cm radius oil fire
Exposure Fire 3: 15 cm radius oil fire

Table 5.2 - Cabinet Air Temperature (°F)

Exposure fire	Distance (m)	Time (sec) 0	20	40	60	80
1	1.0	100	100	99	99	99
2	1.0	100	111	115	118	119
3	1.0	100	141	156	162	165

$$a = g\Delta\rho/\bar{\rho}\bar{\nu}^2$$

and all barred quantities are evaluated at some reference temperature between the wall temperature and the air temperature.

Although these coefficients are temperature dependent (hence our distinction of cold and hot wall, outer and inner values), the dependence is fairly weak.

The unknowns to be solved for in Equations (5.4) through (5.6) are the hot wall temperature T_{HW}, the cold wall temperature T_{CW}, and the cabinet air temperature T_A. Note that Equations (5.4) and (5.5) do not contain time derivatives. This is due to the low mass and hence small thermal inertia of the cabinet walls. We have also neglected the temperature drop across the cabinet walls, since they are thin and their thermal conductivity is high.

A simple numerical scheme to solve this set of nonlinear equations begins by assuming an initial cabinet air temperature T_A, which is about 100°F. We solve for T_{HW} and T_{CW} in Equations (5.4) and (5.5), and use these new values to solve for an updated T_A in a finite difference formulation of Equation (5.6). The results of this solution scheme, when the exposure fires are those listed in Table 5.1, are given in Table 5.2. Some relevant problem parameters are given in Table 5.3.

It can be seen that in one calculation, the cabinet air temperature actually drops. This non-physical result is due to the neglect of the heat generated within the cabinet during normal operation, heat which causes the initial cabinet temperature to be 100°F. We note that calculations which roughly account for the heat sink effect of the components within the cabinet indicate that the components can usually be neglected.

Table 5.3 - Parameters for Cabinet Air Temperature Simulation

Parameter	Symbol	Value
cabinet length	L	2.0 m
cabinet width	W	1.0 m
cabinet depth	D	0.5 m
cabinet wall emissivity	ϵ	0.30
cabinet air volume	V	0.70 m^3
oil specific burning rate	$\dot{m}''_{O}$	0.061 kg/m^2s
oil heating value	H_f	4.67×10^7 J/kg
paper specific burning rate	$\dot{m}''_{O}$	0.0062 kg/m^2s
paper heating value	H_f	1.86×10^7 J/kg

5.2 CABLE TRAY FIRE

The power, control, and instrumentation signals for each safety division in a nuclear power plant are generally passed through electrical cables lying in cable trays dedicated to that division. The trays for each division are separated by a distance designed to prevent the spread of fire from one division to another; if a fire does spread between divisions, serious consequences may result.

5.2.1 The Deterministic Reference Model

A typical arrangement of cable trays within the cable spreading room is shown in Figure 5.3. The three cable trays in each horizontal layer carry the cables for one division; thus there are four divisions passing through this location (not all are safety-related). The trays are 12 inches wide, and are separated from their neighbors by 2 inches horizontally and 4 feet vertically. The trays are open and are presumed to be filled to capacity with cables.

Preliminary calculations indicate that the time for the fire to spread from the initially burning tray to the tray immediately above differs from the time to spread to a horizontally adjacent tray by a small amount. Further, once the fire has spread to another tray, the spread to the remaining trays is very rapid. We therefore concentrate on predicting the spread from the initiating tray to the next higher tray, where the lower tray is called tray 1 and the upper tray is called tray 2. We denote the characteristic time for fire spread between the trays by τ_G.

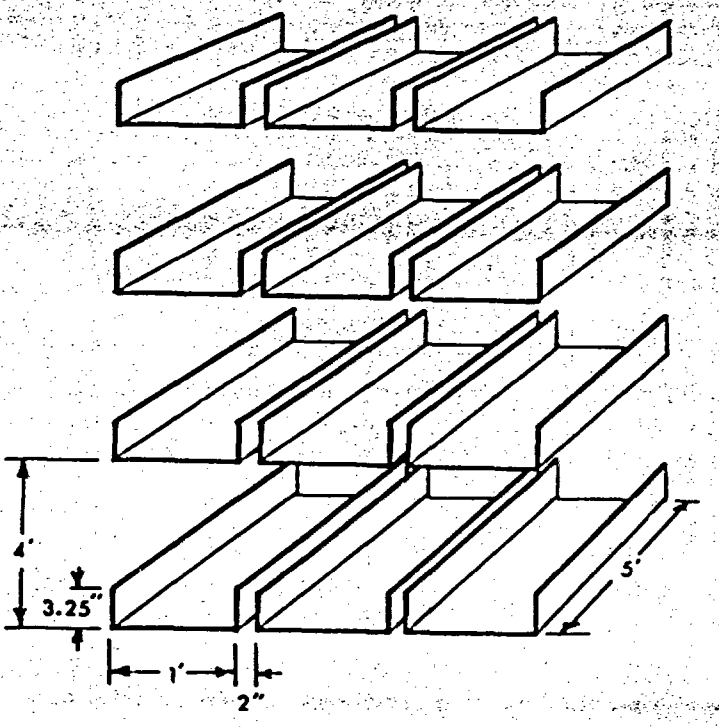

Fig. 5.3 - Cable Tray Fire Set-up

The deterministic reference model for this situation is the computer code COMPBRN described in Reference (1), with input suited to model the given fire. In Table 5.4, we list some important fixed parameters and their assigned values.

Some comments pertain to our modeling of the fire.

- The cable trays are 5 feet long, and are divided into 5 discrete fuel cells, each being 1 foot square.
- The fire starts on the middle fuel cell of tray 1, and additional piloting fuel (e.g. oil, trash) may be present in this cell. The pilot fuel is discussed in the next section. The remaining fuel is cable insulation (4.66 kg/tray).
- The porosity factor f_p for each tray is 3.14 (i.e. the actual surface area available for burning, per unit tray length, is 3.14 ft^2/ft).
- No credit is given to the shielding effect from the bottom of tray 2; the flames on tray 1 are assumed to transmit heat directly to the fuel in tray 2 with no attenuation by the intervening material. This, of course, is a conservative assumption.
- Enclosure effects are neglected. The fire is considered to be too small to cause a significant hot gas layer near the ceiling. We note that this neglect may be non-conservative when the trays are near the room walls, since reflection from the walls may be important.

Table 5.4 - Important Parameters for Cable Tray Simulation

Parameter	Value
number of cable trays	2
number of fuel cells per tray	5
cable tray length	1.52 m
cable tray width	0.30 m
mass of fuel per tray	4.66 kg
tray porosity factor (f_p)	3.14
elevation of tray 1	1.61 m
elevation of tray 2	2.83 m
room temperature	298°K
combustion efficiency	0.90
time increment	60 s
fuel density	1715 kg/m³
fuel specific heat	1045 J/kg°K
fuel thermal conductivity	0.092 W/m°K
fuel piloted ignition temperature	T_s - 40°K
fuel burning rate augmentation constant	1.86 x 10^{-7} kg/J
fraction of heat radiated	0.40

5.2.2 Parameter Uncertainties

The parameters which are varied in our calculation of τ_G are $\dot{m}''_0$, H_f, T^*_s, and the pilot fuel type. The first three parameters were discussed in Chapter 4. The pilot fuels are used to model the initial conditions of the fire, and require further explanation.

As has been noted previously, cable insulation is generally a difficult material to burn. The type and amount of pilot fuel involved in the initial fire is thus an important factor in determining the rate of fire growth. If there is a large amount of oil, rapid growth is nearly assured. If negligible amounts of additional fuel are present, fire growth may not occur at all. We model the pilot fuels with a single parameter Q_p, the amount of heat released when the pilot fuel is consumed:

$$Q_p = M_p H_{fp} \tag{5.8}$$

The use of this single parameter, while crude, is not entirely unreasonable, since the ignition of a fuel element is governed by the total amount of heat absorbed. A more sophisticated analysis may take the different burning rates of the pilot fuels into account, since the more intense fires, e.g. oil fires, have high flames, and thus transfer greater amounts of heat to the target cable.

Before we propagate the uncertainties in these parameters through the DRM to determine the resulting uncertainty in our prediction of τ_G, we construct a response surface for the DRM to lower computational costs.

The Latin Hypercube Sampling (LHS) method described in Appendix B requires us to first select upper and lower bounds for our continuous par-

ameters $\dot{m}''_0$, H_f, and T^*_s. These bounds are given in Table 5.5. We note that two sets of trials were used to construct the reponse surface. The second set of trials used tighter bounds on the parameters than the first, in order to more accurately represent the cable insulation properties actually expected. The bounds for $\dot{m}''_0$ are subjective estimates, while the bounds for H_f and T^*_s result from a synthesis of data for plastics and data from Reference (45). The pilot fuel variation requires a somewhat different treatment.

We choose 4 "pilot fuels", whose burning characteristics are given in Table 5.6. As seen in the last entry of Table 5.6, each "fuel" corresponds to a fixed amount of heat released when the pilot fuel is consumed. This quantity is the previously discussed Q_p; we use Q_p to define our pilot fuel. In our LHS simulations, therefore, we randomly assign one pilot fuel (one Q_p) to the input parameter vector which is then processed by the DRM.

To provide some physical basis for the choice of Q_p's, we note that 400 Btu from a 1 foot by 1 foot fuel packet roughly corresponds to cable insulation burning for one minute (i.e. no additional pilot fuel), 2,000 Btu roughly corresponds to wood chips or paper, 10,000 Btu can be associated with oily rags, and 40,000 Btu roughly corresponds to a quantity of oil (approximately one quart) burning for two minutes.

To correlate the COMPBRN predictions of τ_G, we can define a characteristic time before self-extinguishment τ_{se}, as

$$\tau_{se} = \frac{M_f}{\dot{m}''_0 A_f}$$

and a characteristic ignition time τ_i as (see Eq. 4.19)

Table 5.5 - LHS Bounds for $\dot{m}''_0$, H_f, T^*_s

Trial Set	Parameter	Lower Bound	Upper Bound
1	$\dot{m}''_0$ (kg/m²s)	0.0	0.0075
1	H_f (J/kg)	1.85×10^7	2.70×10^7
1	T^*_s (°K)	710	850
2	$\dot{m}''_0$ (kg/m²s)	1×10^{-5}	0.003
2	H_f (J/kg)	1.85×10^7	2.70×10^7
2	T^*_s (°K)	800	850

Note: 28 samples were selected from trial set 1, and 32 were selected from trial set 2.

Table 5.6 - Burning Parameters for Pilot Fuels

Pilot	$\dot{m}''_0$ (kg/m²s)	H_f (J/kg)	mass (kg)	Q_p (Btu)
1	0.001	2.32×10^7	0.02	400
2	0.0062	1.86×10^7	0.11	2,000
3	0.008	3.77×10^7	0.28	10,000
4	0.0231	4.67×10^7	0.81	40,000

$$\tau_1 = \frac{\pi}{4\alpha}\left[\frac{k(T_s^* - T_A)}{\gamma \dot{m}_O'' H_f / 7}\right]^2$$

where the denominator within the brackets represents a radiation heat flux to the target cable, when the shape factor from the cable to the flame is 1/7. The ratio of these two times yields a characteristic parameter θ, which upon substitution for constant values, is given by

$$\theta = \frac{3.96 \times 10^6}{\dot{m}_O''}\left[\frac{T_s^* - 298}{H_f}\right]^2$$

The results of our calculations then indicate that τ_G, the characteristic time for fire spread from tray 1 to tray 2, is well correlated by

$$\tau_G = A + B\theta \qquad (5.9)$$

where A and B are given in Table 5.7.

One difficulty with the above correlation is that occasionally, the DRM-predicted value of τ_G becomes infinite, even for relatively moderate values of θ. The physical situation is that the flames on tray 1 are moving to the ends of the tray as the fuel in the center of the tray is completely consumed. Occasionally, the middle fuel element in tray 2 (the portion closest to the initial fire location and the recipient of the greatest amount of heat) has not absorbed enough heat to ignite before the flames on tray 1 leave the center of that tray. As a result, the fire on tray 1 exhausts all its fuel and self-extinguishes before tray 2 can ignite.

We define a further parameter ψ;

$$\psi = \frac{c_p (T_s^* - T_A)}{\gamma H_f}$$

$$= 2610\left[\frac{T_s^* - 298}{H_f}\right]$$

Table 5.7 - Response Surface Coefficients (Eq. 5.9)

Pilot	A (min)	B (min)	Q_p (Btu)
1	0.3	19.8	400
2	1.1	14.7	2,000
3	1.5	8.0	10,000
4	2.0	0.0	40,000

Table 5.8 - Histogram for Vertical Spread Time

τ_G (min)	$Pr(\tau_G)$
10	0.26
30	0.21
50	0.12
70	0.08
90	0.04
110	0.03
> 120	0.26

and our response surface is Equation (5.9) with the following condition:

$$\tau_G \rightarrow \infty \text{ with a frequency of } 87.5\%$$

when

$Q_p = 400$ Btu, $\theta > 0.9$, and $\psi > 0.06$, or

$Q_p = 2{,}000$ Btu, $\theta > 1.9$, and $\psi > 0.06$.

It must be emphasized that this response surface is applicable only for the given problem; if the problem geometry is altered, the response surface coefficients will also change.

In order to propagate our state of knowledge uncertainties in $\dot{m}_0''$, H_f, T_s^*, and Q_p through the response surface, we must construct distributions for these parameters. We use the following subjective distributions:

$\dot{m}_0''$ = lognormally distributed with $\mu = -6.91$, $\sigma = 0.865$ (median = 0.001 kg/m^{2}s, error factor = 4)

H_f = uniformly distributed between 1.85×10^7 J/kg and 2.7×10^7 J/kg

T_s^* = uniformly distributed between 800°K and 850°K

and

$\Pr(Q_p = 400 \text{ Btu}) = 0.10$

$\Pr(Q_p = 2{,}000 \text{ Btu}) = 0.44$

$\Pr(Q_p = 10{,}000 \text{ Btu}) = 0.44$

$\Pr(Q_p = 40{,}000 \text{ Btu}) = 0.02$

The histogram for Q_p should be interpreted as follows. If we examine a large number of fires involving the configuration studied, we will reveal a frequency distribution for the heat released by the pilot fuel. We consider Q_p to be a characteristic parameter (e.g. the mean) of this frequency distribution and our uncertainty in the pilot fuel is modeled

by our uncertainty in this characteristic parameter of the unknown frequency distribution. Thus, our state of knowledge histogram says that we are 10% confident that the characteristic parameter is 400 Btu, 44% confident that it is 2,000 Btu, etc. This distribution quantifies our belief that the cable tray fire will probably involve additional fuel as well as the cable insulation.

Based on the above distributions, the probability histogram for τ_G reflecting our uncertainties due to parameter uncertainties is shown in Figure 5.4. This is a state-of-knowledge distribution for the variable τ_{DRM}. The large tail above 120 minutes is mainly due to our model's prediction of an infinite propagation time for certain values of θ. We choose to conservatively incorporate this information using a smooth, finite tail, noting that either treatment (i.e. incorporation or neglect) will make little difference when suppresion effects are included in the analysis.

5.2.3 Modeling Uncertainties

Our distribution for E_τ, the error factor for the spread time τ_G, is constructed not only from the qualitative information presented in Chapter 4 concerning the different sources of uncertainty in the DRM, but also from some rough comparisons of predicted flame spread velocities with published values.

There currently is no detailed data available for the fire spread times between non-contiguous cable trays. However, we do possess information on the average flame spread velocity $\bar{v}$ over a single cable tray. If we define τ to be a characteristic spread time, such that

$$\frac{\bar{v}_{experiment}}{\bar{v}_{DRM}} = \frac{\tau_{DRM}}{\tau_{experiment}} \sim \frac{1}{E_\tau}$$

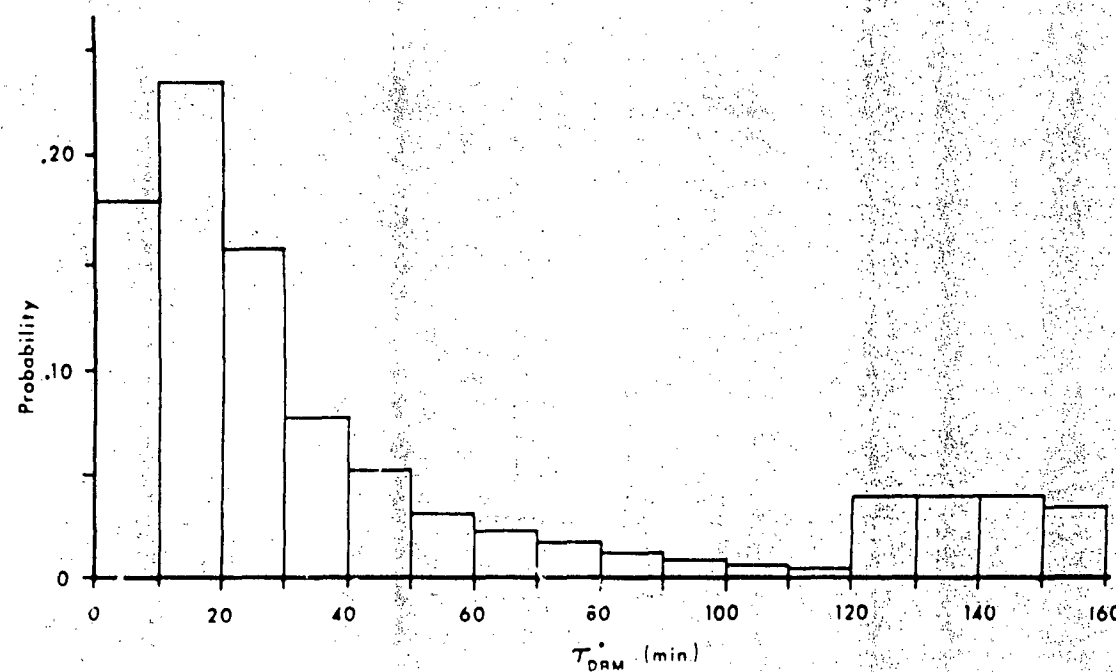

Fig. 5.4 - Distribution of Propagation Time, Due to Parameter Uncertainties

we can use our prediction of the average flame spread velocity to indicate the magnitude of E_τ.

In our modeling of Przybyla and Christian's vertical cable tray experiment in Chapter 4, we have shown that

$$0.08 < \bar{v}_{\text{experiment}} < 0.36 \text{ cm/s}$$

$$0.58 < \bar{v}_{\text{DRM}} < 1.27 \text{ cm/s}$$

and so

$$1.6 < E_\tau < 16$$

The conservatism of the DRM's prediction is expected for the vertical tray configuration, since fuel melting and dripping are ignored.

For horizontal tray fires, Pinkel quotes an "average propagation velocity" of one inch/minute, or 0.04 cm/s [3]. Calculation of the flame front velocity along tray 1 in our simulations, where no additional pilot fuel is added, indicates that

$$0.02 < \bar{v}_{\text{DRM}} < 0.14 \text{ cm/s}$$

where the variability is due to parameter uncertainties. The mean of this average velocity distribution is 0.06 cm/s, and the median is 0.04 cm/s.

If we use Pinkel's estimate as a reference point,

$$0.5 < E_\tau < 3.5$$

On the basis of this evidence, as well as our critical assessment of the conservatism of the various physical models used in our reference model code COMPBRN, we construct a lognormal distribution for E_τ with the fol-

lowing characteristics.

$$\mu = 0.582$$

$$\sigma = 0.489$$

$$\text{Mean} = 2.0$$

$$\text{Median} = 1.8$$

$$E_{\tau,.95} = 4.0$$

$$E_{\tau,.05} = 0.8$$

It is important to note that this quantification of our uncertainty in the predictions of the growth period DRM reduces the conservatism of our analysis.

5.2.4 Combined Probability Distribution for Spread Time

The average time required for fire spread from the initially burning tray to the tray immediately above, τ_G, is given by

$$\tau_G = E_\tau \tau_{DRM} \tag{5.10}$$

The first factor on the right-hand side is an error factor representing our modeling uncertainty, while the second factor is a prediction of our DRM which also incorporates input parameter uncertainties. Both factors have associated probability distributions.

In order to determine the distribution for τ_G, we choose to discretize the distribution for E_τ, and combine the two right-hand side distributions using the discrete probability distribution arithmetic described in Reference (55). In essence, if $E_{\tau,i}$ represents the ith block in the E_τ histogram (i=1,...,n), $\tau_{DRM,j}$ represents the jth block in the

τ_{DRM} histogram (j=1,...,m), and $\tau_{G,k}$ represents the kth block in the τ_G histogram (k=1,...,nm),

$$P(\tau_{G,k}) = P(E_{\tau,i})\, P(\tau_{DRM,j}=\tau_{G,k}/E_{\tau,i}) \qquad (5.11)$$

Although in general, the modeling accuracy is somewhat dependent on the problem parameters, this problem's parameters do not vary a great deal since we are looking at one particular type of fire, and so we have assumed independence between E_τ and τ_{DRM} in Equation (5.11).

A condensed histogram for τ_G is given in Table 5.8. We note that a significant fraction of fires takes longer than two hours to propagate to tray 2. This reflects our uncertainty that the cables are not flammable enough to allow such propagation.

5.3 FIRE SPREAD FREQUENCY INCLUDING SUPPRESSION

The distribution for τ_G derived in the last section is a probability distribution for the event "fire spreads to second division in t minutes, given an initial fire on tray 1 and ignoring suppression efforts." In order to compute the conditional frequency that two cable trays, each in a different division, are involved in a fire (given a fire in the cable spreading room), we must include a model for fire suppression.

Examination of the data reported by Fleming et al (23) leads to the following distribution for τ_S, the mean time between fire ignition and suppression. We note that the suppression times for fires occurring during plant construction have not been included in the distribution.

$$Pr(\tau_S = 5 \text{ min}) = 0.40$$

$$Pr(\tau_S = 15 \text{ min}) = 0.30$$

$$Pr(\tau_S = 30 \text{ min}) = 0.20$$

$$Pr(\tau_S = 60 \text{ min}) = 0.10$$

The justification for this distribution is as follows. The estimates reported in Reference (12) are the results of expert evaluation. There are 17 cable insulation-fueled fires studied which occurred during plant operation. The experts estimated that seven (~40%) of them were extinguished within 5 minutes. Four of the seventeen fires were estimated to have been extinguished between 5 and 25 minutes after initiation, and another group of four had extinguishment times between 30 and 35 minutes. Finally, there were two fires that were extinguished after 60 minutes (but before 85 minutes). Of course, these estimates are not statistical data; we judge that our discrete model is fairly consistent with the given information. Furthermore, it conforms with our belief that it is very likely that most of the fires in the cable spreading room will be extinguished fairly quickly by the personnel who started them. It is important to note that the distribution does not include the Browns Ferry cable spreading room fire as part of the data base. The seven hour duration of that fire was largely due to the hesitation of plant personnel to apply water to the flames, a procedure which has been much addressed since that incident. The neglect of this data point may be an important non-conservatism in the analysis.

Let us denote the conditional frequency of fire spread to a second tray, given a fire, by f_c. f_c is given by

$$f_c = \exp(-\tau_G/\tau_S) \qquad (5.12)$$

where we have assumed that the time to suppression is exponentially distributed with mean τ_S. We note that the frequency of fire spread by time t is also the frequency of non-suppression by that time. The distribution of f_c is given by

$$P(f_c) = P(\tau_G) P(\tau_S) \qquad (5.13)$$

where the distributions of τ_G and τ_S were given previously.

It should be noted that in this simple analysis, we ignore any dependence between τ_G and τ_S, although one certainly expects a correlation between the suppression time and the size of the fire (a large fire implying a large τ_S).

The distribution for f_c obtained is listed in Table 5.9.

5.4 COMMENTS ON ANALYSIS

Refinements of the proposed model are certainly possible and desirable. For example, it may be necessary to determine the distribution of the frequency of fire spread to trays other than the ones immediately adjacent to the initially burning tray, to give stronger information for the loss of two electrical divisions. Another concern is and the neglect of flame front slowing down caused by suppression efforts.

In our analysis of fire growth and suppression, no credit has been taken for the inhibiting effects suppression efforts have on the growth of fire. Agents such as Halon, CO_2, and water can markedly slow down the rate of growth. Indeed, the flame front speed during much of the Browns Ferry fire was relatively low [55]: rough modeling of the portion of the Browns Ferry fire in the Reactor Building indicates veloci

Table 5.9 - Histogram for the Conditional Frequency of Fire Spread to an Adjacent Tray, Given a Fire

Frequency	Probability
3.4×10^{-8}	0.16
3.8×10^{-8}	0.02
4.3×10^{-7}	0.03
4.9×10^{-6}	0.03
5.5×10^{-6}	0.06
6.2×10^{-4}	0.08
7.0×10^{-3}	0.12
4.4×10^{-2}	0.10
1.4×10^{-1}	0.10
3.0×10^{-1}	0.10
5.1×10^{-1}	0.10
6.9×10^{-1}	0.10

ties nearly an order of magnitude larger than those reported. Thus, the neglect of fire growth inhibition by suppression efforts adds strong conservatism to the analysis.

Finally, we comment on the problem of obtaining the unconditional frequency of fires which involve two cable trays. f_c is, as defined above, the conditional frequency of fires involving two trays in the cable spreading room of a hypothetical plant, given a fire. To make this frequency unconditional, we must incorporate the frequency of fires in that particular room. While Ref. (19) does provide a distribution for this quantity, some care must be exercised in using this information.

The initial fire assumed in this analysis is moderately sized (1 foot by 1 foot). Before we utilize any fire frequency distribution, we must decide if that distribution represents the frequency of fires which reach a comparable size (and thus are considered to be serious), or if it also includes the potentially large number of small fires which either self-extinguish or are put out immediately. We note that prior to the Browns Ferry fire, a number of small fires were initiated by the same leak test procedure which caused the large fire, but none of these were incorporated into the fire frequency data because they were small and were promptly extinguished [8].

Chapter 6

FULLY-DEVELOPED BURNING PERIOD MODEL DESCRIPTION

During the period of fully-developed burning, the spatial distribution of the compartment air temperature is assumed to be uniform, and so the thermal stress experienced by a component is independent of the component's position. The analysis of this period, which follows that of Kawagoe and Sekine [10], is therefore computationally much simpler than the period analysis.

It should be mentioned that the likelihood of fully-developed burning within most of the compartments in a nuclear power plant is considered to be small. One of the inhibiting factors is the large size of the average room, larger rooms being better heat sinks. Another factor is the low combustibility of cable insulation, which forms a major portion of the fuel bed in many rooms. The slow burning rate means a low rate of heat release into the compartment, a slow fire growth rate, and thus a higher likelihood of fire suppression before fully-developed burning occurs. Finally, we note the low overall amount of fuel in most compartments; even if suppression efforts are not initiated, the local fuel bed may be exhausted during the growth period, preventing further burning.

6.1 THE DETERMINISTIC REFERENCE MODEL

The compartment is modeled with two nodes: the compartment walls and the compartment air. Heat balances for each node yield the governing equations for the compartment air temperature.

a) Compartment Wall (of thickness L):

$$\frac{\partial T}{\partial t} = \alpha \frac{\partial^2 T}{\partial x^2} \tag{6.1}$$

Initial Condition: $T(x,0) = T_A$

Boundary Conditions:

$$\varepsilon\sigma[T_G^4(t) - T^4(0,t)] + h[T_G(t) - T(0,t)] = -k \frac{\partial T}{\partial x}\Big|_{x=0}$$

$$h[T(L,t) - T_A] = -k \frac{\partial T}{\partial x}\Big|_{x=L}$$

The radiative term in the boundary condition at x equals 0 is generally neglected in most analyses.

b) Compartment Air

$$\eta \dot{m} H_f = A_0\sigma[T_G(t)-T_A] + \dot{m}c_p[T_G(t)-T_A] + A_W\varepsilon\sigma[T_G^4(t)-T^4(0,t)] + hA_W[T_G(t)-T(0,t)] \tag{6.2}$$

As opposed to our cabinet air model, the time derivative term is carried in the compartment wall heat balance, rather than that for the air mass. This is because the concrete walls have large heat capacity and low thermal conductivity (i.e. a low thermal diffusivity), and so the thermal wave penetrates the wall very slowly. As a result, the wall's transient behavior is important. On the other hand, the temperature rise in the room is expected to be slow enough that the time derivative term can be neglected with respect to the other terms.

Equation (6.1) is simply the standard transient heat conduction equation for slab geometry, with appropriate heat balances at the boundaries. Examining Equation (6.2), the left-hand side represents the heat source, while the right-hand side represents the heat losses. The first term on the RHS represents radiative losses out of the room openings (windows or doors), while the second represents the gross movement of hot gases out of the openings. The third and fourth terms represent the radiative and convective losses, respectively, to the room walls.

To put the compartment air heat balance into a more conventional form, we divide both sides of Equation (6.2) by A_W. There results

$$(\eta H_f - c_p(T_G - T_A))\frac{\dot{m}}{A_W} = \frac{A_O}{A_W}\sigma(T_G^4 - T_A^4) + \varepsilon\,\sigma[T_G^4 - T^4(0,t)] + h[T_G - T(0,t)] \qquad (6.3)$$

As we saw in Chapter 4, the mass burning rate may be either fuel surface controlled or ventilation controlled. If we assume that the room ventilation is the limiting factor (as is usually the case), Equation (4.2) shows that

$$\dot{m} = C_V W_{in} \quad (kg/s) \qquad (6.4)$$

If there is no forced ventilation, Reference (11) states that

$$W_{in} = 0.145\,\rho_A\sqrt{g}\,A_O\sqrt{Z_O} \quad (kg/s) \qquad (6.5)$$
$$= 0.54\,A_O\sqrt{Z_O}$$

Thus,

$$\frac{\dot{m}}{A_W} = 0.54\,C_V\,(A_O\sqrt{Z_O}/A_W) \quad (kg/m^2s) \qquad (6.6)$$

and the geometry of the compartment is contained in the ratios $(\dot{m}/A_W)$ and (A_O/A_W). The grouping $(A_O\sqrt{Z_O}/A_W)$ is frequently called the ventila-

tion factor F_o. To account for forced ventilation, we define a modified ventilation factor F_o' such that

$$F_o' = F_o + \frac{W_{FV}}{.145\rho_A\sqrt{g}A_W} = F_o + 2.20\ (V_{FV}/A_W) \quad (m^{1/2}) \tag{6.7}$$

Thus, our general expression for $\dot{m}$ is given by

$$\frac{\dot{m}}{A_W} = 0.54\ C_V\ F_o' \tag{6.8}$$

Equations (6.1) and (6.3) form a relatively simple set of equations. One possible numerical solution scheme would be to solve Equation (6.3) for $T_G(t)$, with T(0,t) fixed at its initial value, use this new value of T_G to solve Equation (6.1) for T(x,t), increment time, and repeat this process until a set fraction of the fuel is consumed.

As discussed in Chapter 2, the results of these calculations are typically presented in the form of time-temperature curves. Since it turns out that varying the ratio (A_O/A_W) has little effect on the calculations, one curve is calculated for each value of F_o'.

6.2 PARAMETER UNCERTAINTIES

For a fire in a given nuclear power plant room, the only parameters possibly subject to significant variations are the combustion efficiency η, the fuel heating value H_f, and the burning rate constant C_V. The room geometry, the physical properties of the concrete walls, and the heat transfer coefficients are either known or, in the last case, can be calculated with reasonable accuracy.

The combustion efficiency is actually somewhat of an unknown for fully-developed compartment fires. Investigators often use this term as an

empirical adjustment factor to bring the results of calculations in better agreement with experimental data. Kawagoe and Sekine use an "effective heating value" for wood which is 60% of the nominal heating value for wood (i.e. $\eta = .60$) in deriving the theoretical time-temperature curves seen in Figure 2.2. One reason for the adjustment is that in some enclosure fires, combustion gases are burnt outside of the enclosure in flames which extend out of the compartment windows, and so some energy is lost from the room [11].

The heating value H_f is generally well-known for most fuels. As in the growth period modeling, our uncertainty in this factor arises primarily from our uncertainty in the actual mixture of fuel types within the room. Since η and H_f do not appear individually in Equation (6.3) but rather as a product, we choose to fix H_f at its nominal value for wood, i.e. 1.85×10^7 J/kg, and model our uncertainty in its value using a modified efficiency factor η', where

$$\eta' = \eta \frac{H_{f,wood}}{H_{f,fuel}} \tag{6.9}$$

As for C_V, we have presented a frequency distribution for this factor (derived from wood-fueled fire data) in Figure 4.7. We adopt this distribution directly as our probability distribution for C_V, because of the large amount of data used to construct the distribution and because best-estimates of C_V from other sources [10,11,57] are generally clustered around the mode, median, and mean of this distribution. However, we note that the experimentally derived frequency distribution and the identically shaped probability distribution for C_V represent two different notions. The first distribution presents the measured values of C_V

from a multitude of different experiments; the second represents our uncertainty in the value of C_v for a particular fire scenario.

6.3 MODELING UNCERTAINTIES

The two primary sources of uncertainties in our basic modeling are the assumption of spatial uniformity of thermal stresses and the burning rate relation Equation (6.4).

In computing the stress experienced by a component, it is assumed that the stress is only a function of time, that varying the location of the component will not vary the heat it absorbs. While the assumption of a uniform air temperature may be reasonable, the radiative heat flux will still vary with position, unless the fire's flames occupy the entire compartment. This latter condition will not hold if the fire is strongly limited by the available ventilation.

Somewhat more importantly, the direct proportionality of the burning rate $\dot{m}$ and the ventilation rate W_{in} in Equation (6.4) is an observed relationship for ventilation controlled fires burning in wood-fueled rooms with moderate ventilation. However, this proportionality may not hold for fires with very low levels of ventilation. If the amount of fresh air available is too low to support open combustion, smoldering of the fuel may occur instead, with the consequent release of toxic gases and unburnt fuel vapors. Thomas [13] notes sources which state that fires burning in compartments with very low levels of ventilation may oscillate in size and intensity (as opposed to the monotonically increasing fire severity predicted). One can even visualize explosions within the compartment resulting from the sudden availability of fresh air, perhaps

due to the opening of a door or breaking of a window, to a room filled with hot, combustible vapors.

Further uncertainties in the burning rate model arise if the fire is not wood-fueled. Although we extend this model to allow for non-cellulosic fuels in our analysis (see Equation (4.20)), such an extension is not necessarily a trivial matter; Harmathy states that fires burning liquid fuels and some plastics may involve rather different burning mechanisms.

6.4 REFERENCE MODEL VERIFICATION

The accuracy of the DRM approach was indicated earlier in Figure 2.2. However, the fires simulated in that figure are wood-fueled and are relatively well-ventilated, and thus are more representative of residential fires than they are of nuclear power plant fires.

The ventilation factor for a residential fire is typically about 0.1 $m^{1/2}$, while Figure 6.1 presents a histogram for F_o' for rooms in two nuclear power plants. It should be noted that these latter values are estimated on the basis of the rated volumetric flow rate of the forced ventilation systems for each room, that the effects of doors have not been accounted for.

To check the accuracy of the simple reference model approach used for fires with low ventilation levels, we consider Gross and Robertson's experiments on fires in scaled-down compartments. The time-averaged compartment air temperatures measured for a given value of F typically exhibit a fairly wide range of values. Figure 6.2 shows a plot of the upper and lower values measured for a ventilation factor of 0.0022 $m^{1/2}$,

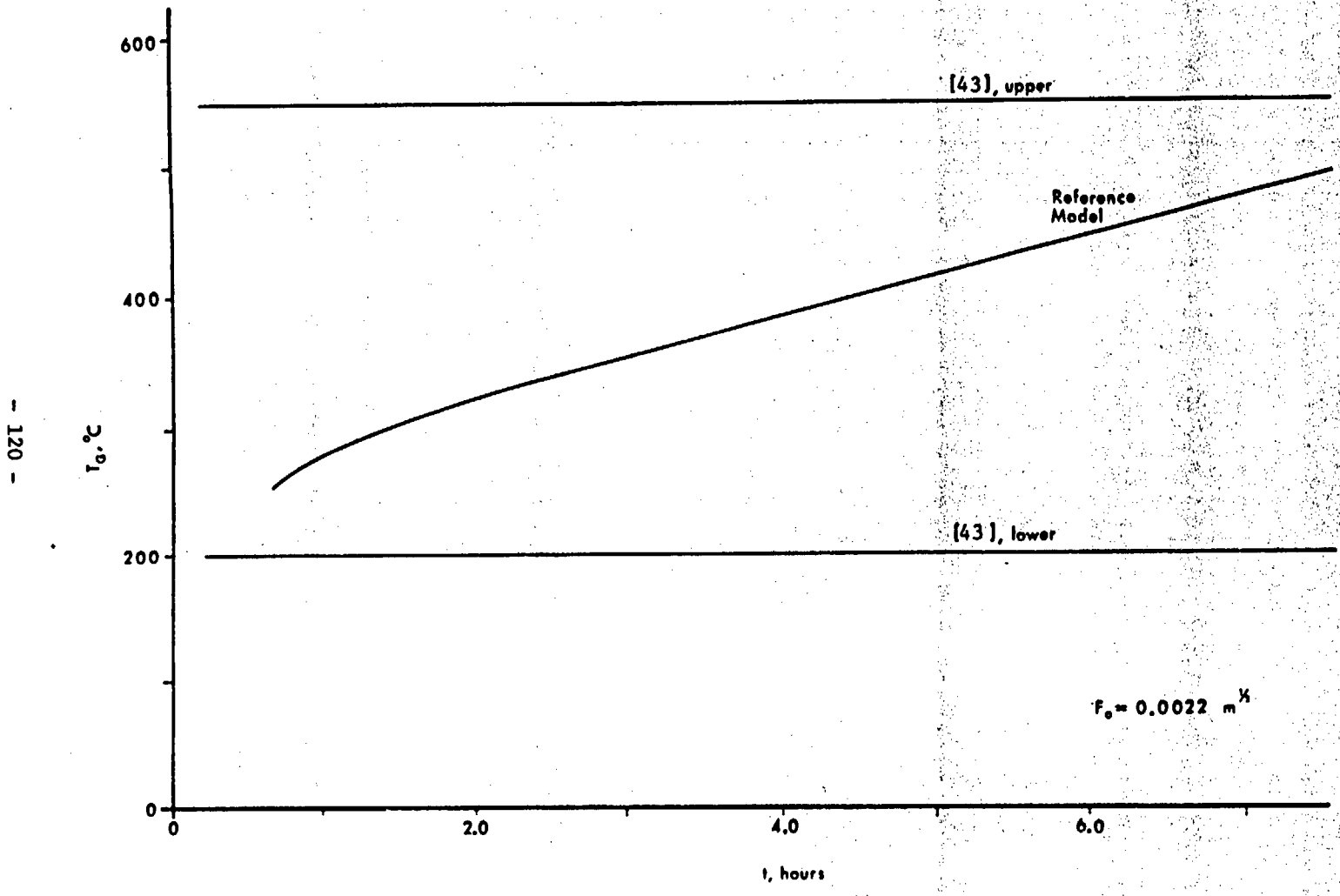

Fig. 6.1 - Comparison of DRM Prediction with Experimental Data from Ref. (43)

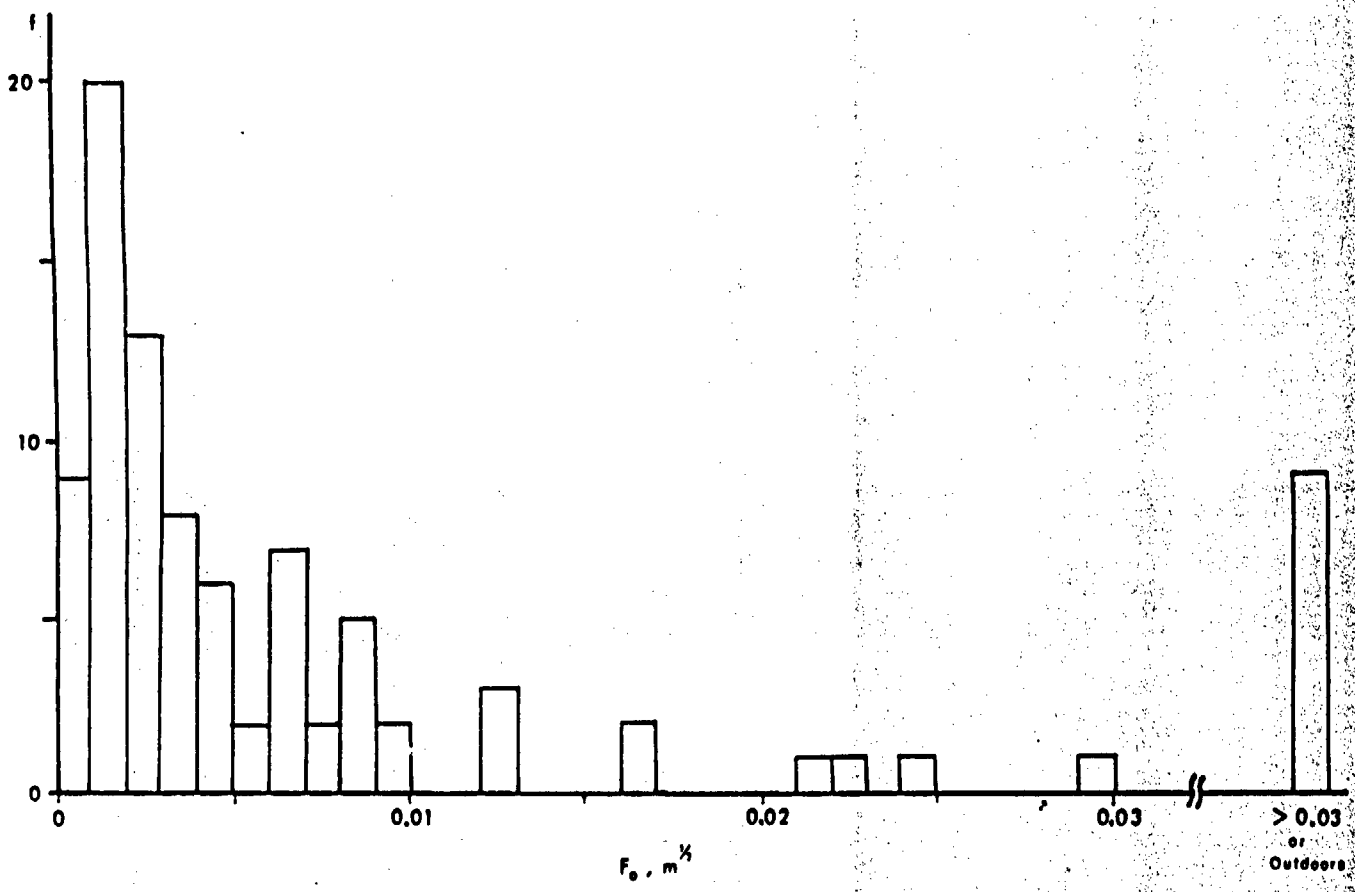

Fig. 6.2 - Distribution of the Ventilation Factor for Two Nuclear Power Plants [58,59]

as well as a time-temperature curve developed using the DRM. If we assume that the experimental fires have about the same duration, we can see that there is a considerable variation about the predicted time-temperature curve.

6.5 A SIMPLE APPLICATION

To illustrate the fully-developed burning period model, we consider a ventilation controlled fire in a room whose characteristics are given in Table 6.1. We note that the room is very large, has a fairly low ventilation factor (we assume that one of the doors leading into the room is open), and has a fuel loading consisting of cable insulation.

The two parameters varied because of state-of-knowledge uncertainties are C_V and η'. The distribution for C_V is as shown in Figure 4.7, i.e. C_V is lognormally distributed with $\mu = -2.12$ and $\sigma = 0.37$. We choose η' to be uniformly distributed between 1.0 and 1.46, which corresponds to a combustion efficiency of 100% and a heating value H_f ranging from 1.86×10^7 J/kg to 2.7×10^7 J/kg.

The response surface fitted to the time-temperature curves computed using the DRM in a 20 trial Latin Hypercube Sampling scheme is

$$T_{DRM}(t) = A + Bt \quad (°C) \tag{6.10}$$

where t is measured in minutes, and the coefficients are given by

$$A = 142 + 832C_V - 2290C_V^2 + 821\eta'C_V$$

$$B = 0.480 + 0.153C_V - 0.124C_V^2 + 0.0394\eta'C_V \tag{6.11}$$

The time-averaged temperature after one hour is given by

Table 6.1 - Fixed Parameters Used in Fully-Developed Fire Simulation

Parameter	Symbol	Value
ventilation factor	F_o	0.0083 $m^{1/2}$
door-to-wall area ratio*	A_O/A_W	0.0011
gas emissivity	ϵ_G	1.0
gas specific heat	c_p	6560 J/kg°K
ambient temperature	T_A	298°K
wall emissivity	ϵ	1.0
wall surface heat transfer coefficient	h	10 W/m²°K
wall thermal conductivity	k	1.16 W/m°K
wall mesh thickness	Δx	0.01 m
fuel heating value	H_f	1.86×10^7 J/kg

* does not include floor area

$$\bar{T}_{DRM} = 157 + 827C_V - 2300C_V^2 + 820\eta' C_V \quad (°C) \qquad (6.12)$$

We remark that this reponse surface's predictions vary from the solutions of Equations (6.1) and (6.3) only by a few degrees in most cases. The largest errors (typically around 10°C) occur at the beginning of the fire, when the fire is growing rapidly, and the assumption of fully-developed burning is not necessarily a good one.

Since the temperature rise is quite linear and fairly slow, we consider the average temperature predicted by the DRM, $\bar{T}_{DRM}$, as the representative measure of fire severity in this analysis.

The propagation of the uncertainties in C_V and η through the given response surface leads to the histogram in Figure 6.3. The lognormal distribution superimposed on this histogram has the following characteristics:

$$\mu = 5.81$$

$$\sigma = 0.157$$

$$\text{Mean} = 338\ °C$$

$$\text{Median} = 334\ °C$$

$$\bar{T}_{DRM,.95} = 432\ °C$$

$$\bar{T}_{DRM,.05} = 258\ °C$$

With regard to the modeling uncertainties in Equations (6.1) and (6.3), it is felt that the DRM is somewhat conservative in its neglect of heat transfer to the compartment floor and contents. Furthermore, conservative values were generally used for the constant input parameter values used in the response surface construction. On the other hand, Figure 6.2 seems to indicate that the DRM may be rather non-conserva-

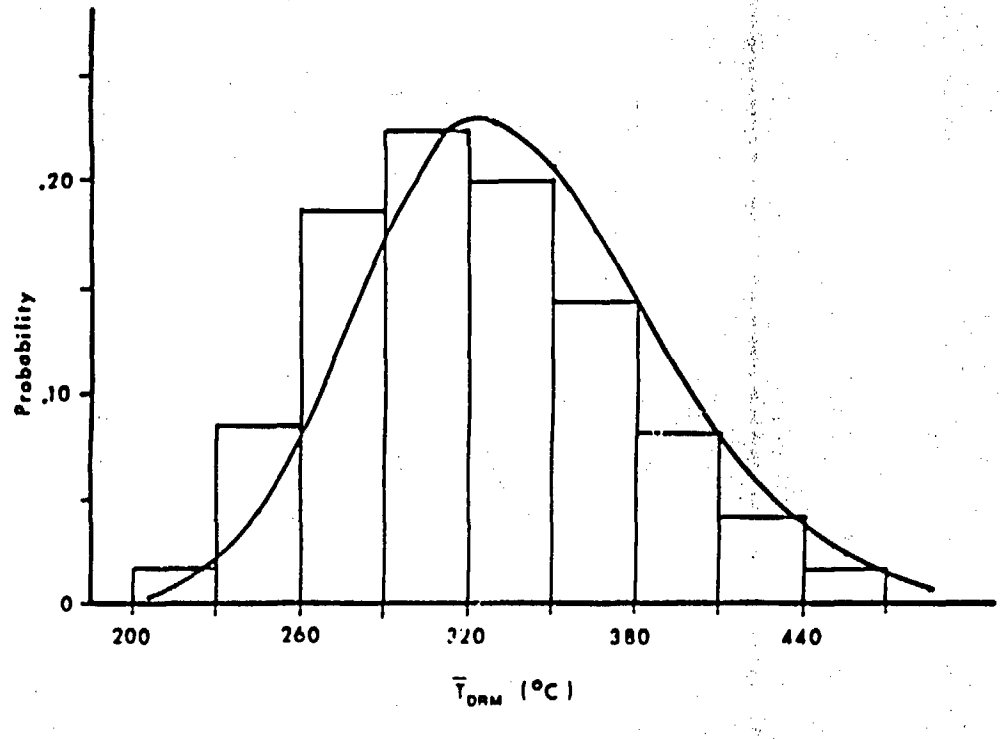

Fig. 6.3 - Distribution of the Average Compartment Temperature (Uncertainties Due to Input Parameter Uncertainties)

tive. While we do make use of this latter source of information, we do not give it overwhelming weight. Gross and Robertson's experiments were conducted in scaled-down compartments, where we intuitively expect the behavior of a fully-developed fire to differ from the behavior of a fully-developed fire within a real room. It is also well known that the scaling of a fire experiment is a difficult task, since many of the important physical phenomena do not follow the same scaling laws.

For the purposes of this analysis, our distribution for E_T, the error factor representing our uncertainty in the DRM's predictions, is adequately represented by a lognormal distribution with the following parameters:

$$\mu = -0.144$$

$$\sigma = 0.334$$

$$\text{Mean} = 0.92$$

$$\text{Median} = 0.87$$

$$E_{T,0.95} = 1.5$$

$$E_{T,0.05} = 0.5$$

The bulk of the distribution lies to the left of unity, indicating our belief in the conservatism of the model. However, a substantial tail lies to the right of this point, allowing for the possible non-conservatism seen in Figure 6.2.

Since both our distribution for $\bar{T}_{DRM}$ and our distribution for E_T are lognormal, our final state-of-knowledge distribution for $\bar{T}_1$, the average compartment air temperature after one hour's duration of fully-developed burning in the given room, is also lognormal, and has the following par-

ameters:

$$\mu = 5.67$$

$$\sigma = 0.369$$

Mean = 309 °C

Median = 289 °C

$$\bar{T}_{1,0.95} = 530\ ^\circ C$$

$$\bar{T}_{1,0.05} = 157\ ^\circ C$$

Chapter 7

REFERENCES

1. N. O. Siu, "COMPBRN - A Computer Code for Modeling Compartment Fires," UCLA-ENG-8113, June 1981.

2. S. Atallah and D. S. Allan, "Safe Separation Distances from Liquid Fuel Fires," Fire Technology, 7, 47-56 (1971).

3. I. I. Pinkel, Estimating Fire Hazards Within Enclosed Structures as Related to Nuclear Power Stations, BNL-23892, Brookhaven National Laboratory, Jan. 1978.

4. Plant Design Report, Offshore Power Systems, Appendix 2A, 73-104, May 1973.

5. E. M. Sparrow and R. D. Cess, Radiation Heat Transfer, McGraw-Hill, New York, 1978.

6. R. Siegel and J. R. Howell, Thermal Radiation Heat Transfer, McGraw-Hill, New York, 1972.

7. P. H. Thomas, "The Size of Flames from Natural Fires," Tenth Symposium (Intl.) on Combustion, 844-859 (1963).

8. M. Kazarians and G. Apostolakis, "On the Fire Hazard in Nuclear Power Plants," Nuclear Engineering and Design, 47, 157-168 (1978).

9. K. Odeen, "Theoretical Study of Fire Characteristics in Enclosed Spaces," Bulletin 10, Division of Building Construction, Royal Institute of Technology, Stockholm, 1963.

10. K. Kawagoe and T. Sekine, "Estimation of Fire Time-Temperature Curve in Buildings," B.R.I. Occasional Report No. 11, Building Research Institute, Ministry of Construction, Tokyo, April 1963.

11. T. Z. Harmathy, "A New Look at Compartment Fires, Parts I and II," Fire Technology, 8, 196-217, 326-351 (1972).

12. Y. Tsuchiya and K. Sumi, "Computation of the Behavior of Fire in an Enclosure," Combustion and Flame, 16, 131-139 (1971).

13. P. H. Thomas, "Some Problem Aspects of Fully-Developed Fires," Fire Standards and Safety, ASTM STP 614, A. F. Robertson, ed., American Society for Testing and Materials, 112-130 (1977).

14. J. Quintiere, "The Growth of Fire in Building Compartments," Fire Standards and Safety, ASTM STP 614, A. F. Robertson, ed., American Society for Testing and Materials, 131-167 (1977).

15. J. D. Rockett, "Fire Induced Gas Flow in an Enclosure," Combustion Science and Technology, 12, 165-175 (1976).

16. R. Pape, J. Mavec, D. Kalkbrenner, and T. Waterman, "Semi-stochastic Approach to Predicting the Development of a Fire in a Room from Ignition to Flashover; Program Documentation and Users Guide," NBS-GCR-77-111, U. S. Dept. of Commerce and U. S. Dept. of Health, Education, and Welfare, June 1976.

17. T. E. Waterman and R. Pape, "A Study of the Development of Room Fires," NBS-GCR-77-110, U. S. Dept. of Commerce and U. S. Dept. of Health, Education, and Welfare, Sept. 1976.

18. R. W. Fitzgerald, "Development of Engineering Models and Design Aids to Predict Flame Movement and Fire Severity Within a Room," NBS-GCR-119, U. S. Dept. of Commerce and U. S. Dept. of Health, Education, and Welfare, Dec. 1977.

19. G. Apostolakis and M. Kazarians, "The Frequency of Fires in Light Water Reactor Compartments," presented at the ANS/ENS Topical Meeting on Thermal Reactor Safety, Knoxville, Tennessee, April 6-9, 1980.

20. A. G. Sideris, R. W. Hockenbury, M. L, Yeater, and W. E. Vesely, "Nuclear Plant Fire Incident Data File," Nuclear Safety, 19, 305-315 (1978).

21. H. W. Emmons, "Fire and Fire Protection,"Scientific American, 231, 21-27 (1974).

22. G. W. Parry and P. W. Winter, "Characterization and Evaluation of Uncertainty in Probabilistic Risk Analysis", Nuclear Safety, 22, 28-41 (Jan.-Feb. 1981).

23. K. N. Fleming, W. T. Houghton, and F. P. Scaletta, "A Methodology for Risk Assessment of Major Fires and its Application to an HTGR Plant", GA-A15402, General Atomic Company, 1979.

24. S. Kaplan and B. J. Garrick, "On the Quantitative Definition of Risk," to appear in Risk Analysis, 1, 1981.

25. G. Apostolakis, "Bayesian Methods in Risk Assessment," to appear in Advances in Nuclear Science and Technology, J. Lewins and M. Becker, Eds., Plenum Press, 1981.

26. G. Apostolakis and A. Mosleh, "Expert Opinion and Statistical Evidence: An Application to Reactor Core Melt Frequency," Nuclear Science and Engineering, 70, 135-149 (1979).

27. G. Apostolakis, S. Kaplan, B. J. Garrick, and W. Dickter, "Assessment of the Frequency of Failure to Scram in Light Water Reactors," Nuclear Safety, 20, 690-705 (1979).

28. F. R. Steward, "Prediction of the ght of Turbulent Diffusion Buoyant Flames," Combustion Science and Technology, 2, 203-212 (1970).

29. Y. T. Lee and G. Apostolakis, "Methods for the Estimation of Confidence Bounds for the Top-Event Unavailability of Fault Trees," Nuclear Engineering and Design, 41, 411-419 (1977).

30. J. K. Vaurio, "Response Surface Techniques Developed for the Probabilistic Analysis of Accident Consequences," Proceedings of ANS/ENS Topical Meeting on Probabilistic Analysis of Nuclear Reactor Safety, Los Angeles, May 8-10, 1978.

31. R. L. Iman, J. C. Helton, and J. E. Campbell, "Risk Methodology for Geologic Disposal of Radioactive Waste: Sensitivity Analysis Techniques," NUREG/CR-0394, SAND78-0912, Oct. 1978. *

32. K. T. Yang, J. R. Lloyd, and M. L. Doria, "Fire and Smoke Spread," Semi-Annual Progress Report to the National Science Foundation on Grant AEN73-07749-A02, University of Notre Dame, ND-PR-07749-6, Mar. 1976.

33. National Fire Protection Association, NFPA Fire Protection Handbook, 14th Edition, Boston, 1976.

34. A. Tewarson and R. F. Pion, "Burning Intensity of Commercial Samples of Plastic," Fire Technology, 11, 274-281 (1975).

35. R. S. Magee and R. D. Reitz, "Extinguishment of Radiation Augmented Plastic Fires by Water Sprays," Fifteenth Symposium (Intl.) on Combustion, 1974.

36. D. Burgess and M. Hertzberg, "Radiation from Pool Flames," Heat Transfer in Flames, N. H. Afgan and J. M. Beer, eds., Scripta Book Co., Washington D.C., 413-430 (1974).

37. M. A. Delichatsios, "Fire Growth Rates in Wood Cribs," Combustion and Flame, 27, 267-278 (1976).

38. A. M. Kanury, "The Science and Engineering of Hostile Fires," Fire Research Abstracts and Reviews, 18, 72-96 (1976).

39. R. L. Alpert, "Calculations of Response Time of Ceiling Mounted Fire Detectors," Fire Technology, 8, 181-195 (1972).

40. A. T. Modak and P. A. Croce, "Plastic Pool Fires," Combustion and Flame, 30 251-265 (1977).

41. M. Sibulkin, "Estimates of the Effect of Flame Size on Radiation from Fires," Combustion Science and Technology, 7, 141-143 (1973).

42. A. M. Kanury, "Modeling of Pool Fires with a Variety of Polymers," Fifteenth Symposium (Intl.) on Combustion, 193-202 (1975).

43. D. Gross and A. F. Robertson, "Experimental Fires in Enclosures," Tenth Symposium (Intl.) on Combustion, 931-942 (1965).

44. W. Barnard, F. Ellenwood, and C. Hirshfeld, Heat-Power Engineering, Part II, 3rd Edition, Wiley, 1935.

45. Zion Station Fire Protection Report, Commonwealth Edison Company, April 30, 1980.

46. W. K. Smith and J. B. King, "Surface Temperature of Materials During Radiant Heating to Ignition," Journal of Fire and Flammability,

47. F. A. Williams, "Mechanisms of Fire Spread," Sixteenth Symposium (Intl.) on Combustion, 1978.

48. P. H. Thomas, "Fires in Enclosures," Heat Transfer in Flames: Thermophysics, Social Aspects, and Economic Impact, P. L. Blackshear, ed., Scripta Book Co., 73-89 (1974).

49. R. F. Lindemann, "Fire Retardation of Polystyrene and Related Thermoplastics," Flame Retardancy of Polymeric Materials, Vol. 2, W. C. Kuryla and A. J. Papa, eds., Marcel Dekker Inc., New York, 1973.

50. H. S. Carslaw and J. C. Jaeger, Conduction of Heat in Solids, 2nd Ed., Oxford (England) Clarendon Press, 1959.

51. L. Orloff, J. deRis, and G. H. Markstein, "Upward Turbulent Fire Spread and Burning of Fuel Surface," Fifteenth Symposium (Intl.) on Combustion, 183-192 (1974).

52. L. Przybyla and W. J. Christian, "Development and Verification of Fire Tests for Cable Systems and System Components, Quarterly Reports 2 and 3, Sept. 1, 1977 - Feb. 28, 1978," NUREG/CR-0152, Underwriters Laboratories, Inc., June 1978. *

53. J. Fang, "Measurements of the Behavior of Incidental Fires in a Compartment," Journal of Fire and Flammability, 7, 368-386 (1976).

54. D. K. Edwards, V. E. Denny, and A. F. Mills, Transfer Processes, McGraw-Hill, 1976.

55. S. Kaplan, "On the Method of Discrete Probability Distributions in Risk and Reliability Calculations," to appear in Risk Analysis, 1, 1981.

56. R. L. Scott, "Browns Ferry Nuclear Power-Plant Fire on Mar. 22, 1975," Nuclear Safety, 17, 592-611 (Sept.-Oct. 1976).

57. A. J. M. Helselden, P. H. Thomas, and M. Law, "The Burning Rate of Ventilation Controlled Fires in Compartments," Fire Technology, 6, 123-125 (1970).

58. San Onofre Nuclear Generating Station Units 2 and 3 Fire Hazards Analysis, Southern California Edison Co., Oct. 1977.

59. Waterford Steam Electric System Unit 3 Fire Protection Program Re-Evaluation, Louisiana Power and Light Company, June 1977.

60. D. T. Neill, J. R. Welker, and C. M. Sliepcevich, "Direct Contact Heat Transfer from Buoyant Diffusion Flames," Journal of Fire and Flammability, 1, 239-301 (1970).

61. C. C. Veldman, T. Kubota, and E. E. Zukoski, "An Experimental Investigation of the Heat Transfer from a Buoyant Gas Plume to a Horizontal Ceiling, Part I," NBS-GCR-77-97, June 1975.

62. K. G. Huffman, J. R. Welker, and C. M. Sliepcevich, "Interaction Effects of Multiple Pool Fires," Fire Technology, 5, 225-232 (1969).

63. L. Orloff, A. T. Modak, and R. L. Alpert, "Burning of Large-Scale Vertical Surfaces," Sixteenth Symposium (Intl.) on Combustion, 1345-1354 (1976).

*Available for purchase from GPO Sales Program, Division of Technical Information and Document Control, U.S. Nuclear Regulatory Commission, Washington, D.C. 20555 and/or the National Technical Information Service, Springfield, VA 22161.

Appendix A

SHAPE FACTORS

In general, the radiative heat transfer from a source to a receiver can be separated into two factors: one represents the strength of the source and the other represents the fraction of the source output intercepted by the reciever. This last fraction is called the shape factor from the source to the receiver. Thus, if the source strength is $\dot{Q}_S$ watts, the receiver sees $\dot{Q}_R$ watts, where

$$\dot{Q}_R = F_{S-R}\,\dot{Q}_S \quad (W) \tag{A.1}$$

If we define an average source heat flux $\dot{q}''_S$ as

$$\dot{q}''_S = \dot{Q}_S/A_S \quad (W/m^2) \tag{A.2}$$

and an average receiver heat flux $\dot{q}''_R$ in a similar manner, then

$$A_R\dot{q}''_R = A_S F_{S-R}\dot{q}''_S ,$$

or

$$\dot{q}''_R = (A_S F_{S-R}/A_R)\,\dot{q}''_S \quad (W/m^2) \tag{A.3}$$

This is the basic equation needed to calculate the heat flux impinging on an object's surface, given a heat flux source of strength $\dot{q}''_S$. We see that the modification term is purely geometry dependent (we are neglecting any attenuation of the radiation between the source and the receiver).

In order to compute F_{S-R}, we first look at the shape factor for exchange between differential surface elements. Given the situation shown in Figure A.1, it can be shown that

$$dA_1 F_{dS_1-dS_2} = \frac{\cos\phi_1 \cos\phi_2 \, dA_1 \, dA_2}{\pi r^2}$$

Clearly, if we wish to compute the shape factor between arbitrarily shaped and oriented surfaces, we must perform a quadruple integration, i.e.

$$F_{1-2} = \frac{1}{A_1} \int_{A_1} dA_1 \int_{A_2} dA_2 \frac{\cos\phi_1 \cos\phi_2}{\pi r^2} \qquad (A.4)$$

Analytical solutions of the above integral are few. Moreover, in the context of our problem, we rarely deal with transfer between exactly defined surfaces. In order to reduce the complexity of our problem, we assume that our receiver can be adequately characterized by a strategically located differential surface element, that the heat flux received by this element is the average heat flux received by the receiver over its entire surface. We now have

$$\dot{q}''_R = (A_S F_{S-R}/dA_R) \, \dot{q}''_S.$$

Employing the reciprocity theorem for shape factors,

$$A_i F_{i-j} = A_j F_{j-i} \qquad (A.5)$$

we obtain

$$\dot{q}''_R = (dA_R F_{dR-S}/dA_R) \, \dot{q}''_S$$
$$= F_{dR-S} \, \dot{q}''_S$$

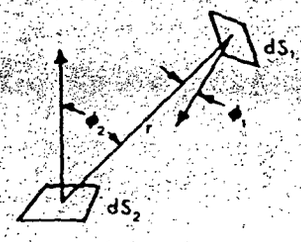

Fig. A.1 - Transfer Between Two Differential Surfaces

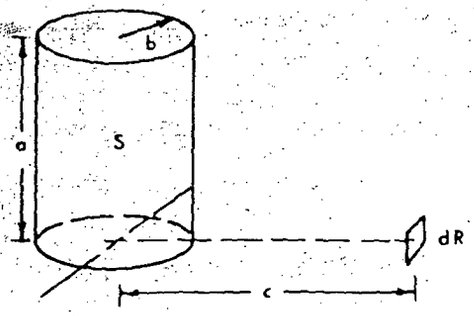

Fig. A.2 - Transfer Between a Cylinder and a Parallel Surface

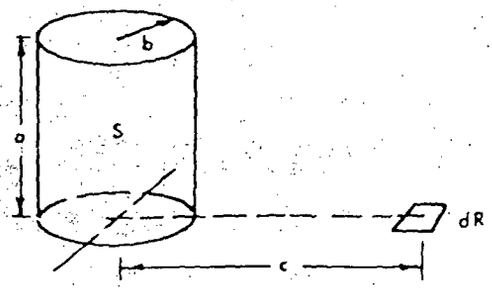

Fig. A.3 - Transfer Between a Cylinder and a Perpendicular Surface

Since the evaluation of F_{dR-S} only requires a double integration, many more analytical solutions are available than for the earlier case of two finite surfaces. Some representative formulae for transfer from a cylinder to a surface element and transfer from a rectangle to a surface element are as follows [5,6].

1. Transfer from a cylinder to a surface element parallel to the cylinder axis (see Fig. A.2):

$$F_{dR-S} = \frac{1}{\pi Y} \tan^{-1}\left(\frac{X}{\sqrt{Y^2-1}}\right) + \frac{X}{\pi}\left[\frac{A-2Y}{Y\sqrt{AB}} \tan^{-1}\sqrt{\frac{A(Y-1)}{B(Y+1)}} - \frac{1}{Y}\tan^{-1}\sqrt{\frac{Y-1}{Y+1}}\right] \quad (A.6)$$

where

$X = a/b$

$Y = c/b$

$A = (1+Y)^2 + X^2$

$B = (1-Y)^2 + X^2$

2. Transfer from a cylinder to a surface element perpendicular to the cylinder axis (see Fig. A.3):

$$F_{dR-S} = \frac{1}{\pi}\left[\tan^{-1}\sqrt{\frac{X+R}{X-R}} - \frac{A}{B}\tan^{-1}\sqrt{\frac{X-R}{X+R}}\right] \quad (A.7)$$

where

$X = c/a$

$R = b/a$

$A = 1 + X^2 - R^2$

$B = 1 + X^2 + R^2$

3. Transfer from a rectangle to a surface element parallel to the plane of the rectangle (see Fig. A.4):

$$F_{dS-R} = \frac{1}{2\pi}\left[\frac{X}{A}\tan^{-1}(Y/A) + \frac{Y}{B}\tan^{-1}(X/B)\right] \qquad (A.8)$$

where

$$X = a/c$$

$$Y = b/c$$

$$A = \sqrt{1 + X^2}$$

$$B = \sqrt{1 + Y^2}$$

4. Transfer from a rectangle to a surface element perpendicular to the plane of the rectangle (see Fig. A.5):

$$F_{dS-R} = \frac{1}{2\pi}\left[\tan^{-1}(1/Y) - AY\tan^{-1}(A)\right] \qquad (A.9)$$

where

$$X = a/c$$

$$Y = c/b$$

$$A = 1/\sqrt{X^2 + Y^2}$$

If the receiving object is not conveniently aligned as in the figures, we apply another shape factor relation (derivable from the defining integrals):

$$A_i F_{i-j} = \sum_{k \in i} (A_k F_{k-j}) \qquad (A.10)$$

For example, if we have the situation shown in Figure A.6,

$$A_{(1+1')} F_{(1+1')-2} = A_1 F_{1-2} + A_{1'} F_{1'-2}$$

and so

$$A_1 F_{1-2} = A_{(1+1')} F_{(1+1')-2} - A_{1'} F_{1'-2}$$

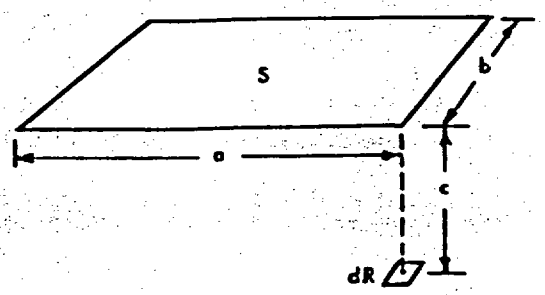

Fig. A.4 - Transfer Between a Rectangle and a Parallel Surface

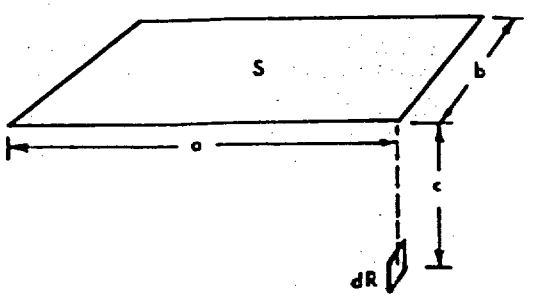

Fig. A.5 - Transfer Between a Rectangle and a Perpendicular Surface

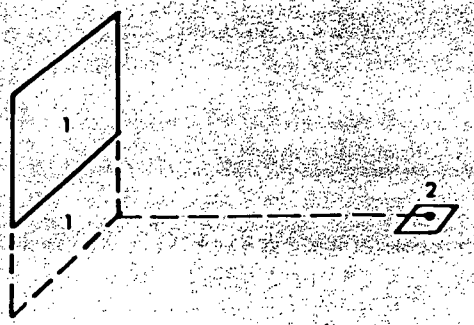

Fig. A.6 - Transfer Between Combinations of Surfaces

Since we know how to find both terms on the right-hand side, we can find R_{1-2}, our desired quantity.

Appendix B

LATIN HYPERCUBE SAMPLING

The success of a response surface simulation depends strongly on the accuracy of the function (response surface) used to approximate the actual physical model in question. Since the response surface is based on the physical model's predictions for a limited number of points, the physical model's input parameter vectors required in the calculation of these points must be carefully chosen. One successful scheme for selecting input vectors is the Latin Hypercube Sampling (LHS) technique, described in Reference (31).

To illustrate the LHS approach, we consider a simple example. Let us assume that our physical model only requires three input parameters, i.e.

$$\bar{X} = (X_1, X_2, X_3),$$

and that we wish to construct our response surface from only five data points. In order to select the data points, we proceed as follows (see Figure B.1).

1. Define the highest and lowest values of each parameter expected in the problem, i.e. find x_i° and x_i^* such that

$$x_i^\circ < X_i < x_i^* \quad , \qquad i=1,2,3 \tag{B.1}$$

2. Divide each of the parameter ranges so defined into five sections (since we desire five data points). The widths of the intervals need not be equal, but often are.

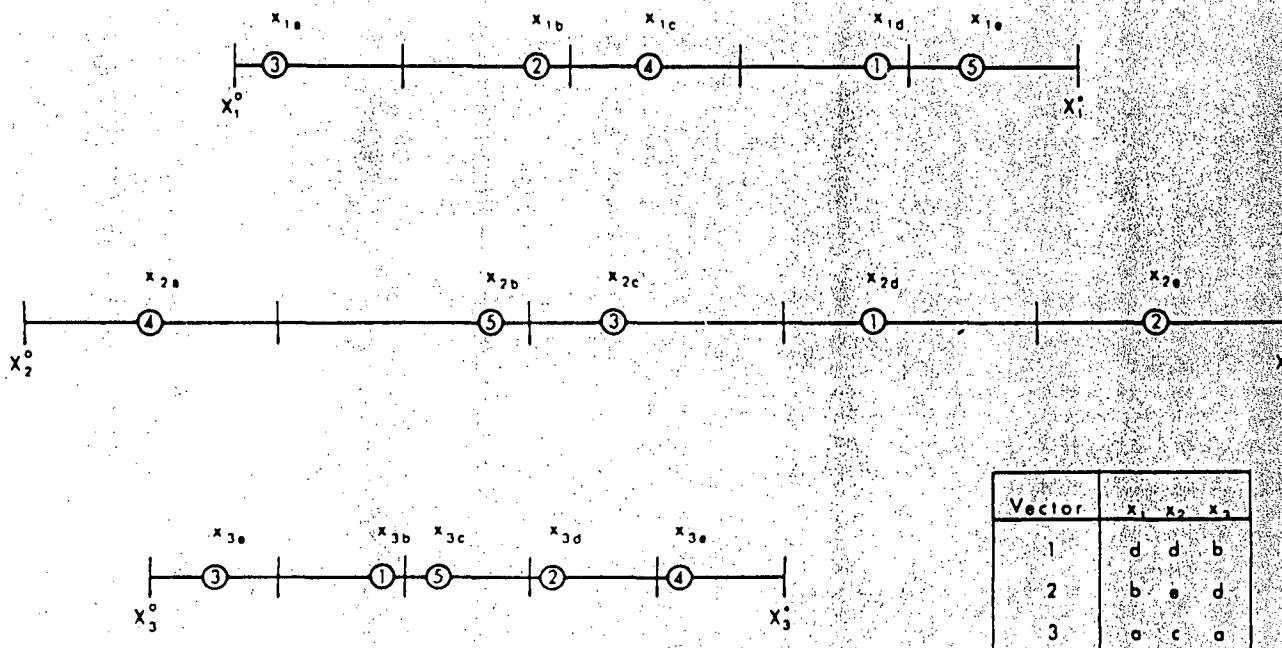

Vector	x_1	x_2	x_3
1	d	d	b
2	b	e	d
3	a	c	a
4	c	a	e
5	e	b	c

Fig. B.1 - Illustration of Example Latin Hypercube Sampling Scheme

3. Randomly select one of the five intervals from the range of parameter 1. Assign this interval a rank of one. In Figure B.1, this is the interval with a circled one. Randomly select one of the remaining intervals and assign to it a rank of two. Continue in a similar manner until all five of the intervals have an associated ranking. Repeat the entire process for parameters 2 and 3.

4. Randomly select a point within the first interval of parameter 1. This point, labeled x_{1d}, will represent the range of values within this interval when we construct a response surface. We note that the selection process need not be based on a uniform distribution over the interval. Repeat the process for the remaining intervals of parameter 1, and for all of the intervals of parameters 2 and 3. By following this procedure, we generate five values of each parameter which represent the entire range of values for that parameter. Moreover, each of the five values has an associated ranking, derived in step 3 above. Thus, x_{1a} has a rank of three, x_{3e} has a rank of four, etc.

5. Form the first input vector by grouping the value of parameter 1 whose rank is one with the values of parameters 2 and 3 whose ranks also are one. In Figure B.1, this vector is the triplet (x_{1d}, x_{2d}, x_{3b}). Next, form the second input vector from the parameter values whose ranks are two, and so forth. The inset table in Figure B.1 shows the five input vectors generated in this simple example.

Among the many advantages of the LHS, one of the most important ones is that the full range of each parameter is represented in the sample, and so extrapolation of the response surface constructed from the sample is not necessary. This can be contrasted with an ordinary random sampling technique where sample parameter values are randomly selected from the entire parameter range, and so certain ranges of the parameter values may be over-represented, while others may be under-represented in the construction of the response surface.

Once the input vectors have been selected, we can calculate the response of the physical model to these inputs. We next fit an appropriate approximating function to the results of these calculations, typically using least-squares regression, and our response surface is complete.

Conceptually, the above procedure is not difficult. In practice, however, the situation may be different, since the determination of an appropriate functional form for the response surface's dependence on the input parameters is often a non-trivial problem.

Appendix C

CONVECTIVE HEAT TRANSFER DURING FIRE GROWTH

The convective heat fluxes to an object during the period of fire growth are assumed to be non-zero only when the object is within the fire's flames, the hot buoyant plume above the flames, or when the object is within the layer of hot gases accumulating near the ceiling. Heat transfer within the flames is treated in Chapter 4. In the remaining two cases, we need models for the temperature of the hot gases and for the heat transfer coefficient between the gases and the object's surface, since

$$\dot{q}''_{o,c} = h [T_e - T_o] \quad (W/m^2) \tag{C.1}$$

C.1 HOT GAS TEMPERATURE

A number of researchers have studied the characteristics of the plume caused by turbulent flames, and have arrived at similar correlations for the temperature profile. The correlation we shall use is reported by Alpert [39]:

$$T_{pl} - T_A = \begin{cases} 0.0538 \dfrac{(\dot{Q}_c/r)^{2/3}}{z} & {}^{o}C, \quad r > .18z \\ 0.169 \dfrac{\dot{Q}_c^{2/3}}{z^{5/3}} & {}^{o}C, \quad r < .18z \end{cases} \tag{C.2}$$

where

$\dot{Q}_c = (1 - \chi)\dot{Q}$ (W)

z = axial distance from flame base (m)

r = radial distance from plume centerline (m)

Note that $r = 0.18z$ can be taken to define an effective radius of the buoyant plume.

Strictly speaking, the above correlation is good only when the fire is small compared to the room dimensions and is far away from any walls. However, if the fire is very close to a wall or is in a corner of the room, Alpert claims that the correlation also works well if $\dot{Q}_c$ is doubled or quadrupled, respectively.

As for the temperature within the ceiling hot gas layer, Section 4.1.2 describes a simple model for this quantity. If a small fire under a high ceiling is considered, Equation (C.2) can also be used, where z is replaced by the height of the ceiling above the flame base.

C.2 HEAT TRANSFER COEFFICIENTS

The convective heat transfer also depends on the surface heat transfer coefficient h. For object surfaces parallel to the plume flow, this parameter does not vary strongly. Experimentally derived values for heat transfer within a flame are of the order of 23 $W/m^2{}^\circ K$ [60], and this value can be used conservatively for transfer within the buoyant plume and in the ceiling gas layer.

When the object is perpendicular to the plume flow and is large with respect to the plume radius, Veldman et al. [61] give

$$0.01(r/z)^{-0.6} < h' < 0.02(r/z)^{-0.7}, \quad (r/z) > 0.1 \qquad (C.3)$$

where

h' = non-dimensionalized heat transfer coefficient

$= h/[\rho_A c_p \sqrt{gz}\dot{Q}^{*1/3}]$

$\dot{Q}^*$ = non-dimensionalized heat production rate

$= \dot{Q}/[\rho_A c_p \sqrt{gz} z^2 T_A]$

If R is the object's effective radius, we compute the average heat transfer coefficient to be

$$\bar{h} = \frac{\int_0^R h(r)\,[T_{pl}(r) - T_A]\,r\,dr}{\int_0^R [T_{pl}(r) - T_A]\,r\,dr}$$

or

$$\bar{h} = \begin{cases} 0.64\ (\dot{Q}_c/z) & W/m^{2\,o}K, \quad (R/z) > .18 \\ 2.06\ (\dot{Q}_c/z) & W/m^{2\,o}K, \quad (R/z) < .18 \end{cases} \qquad (C.4)$$

if Equation (C.2) is used for $T_{pl}(r)$.

Appendix D

HEAT FLUX FROM CEILING GAS LAYER

In the following derivation of the expression for the heat flux from the ceiling gas layer (Eq. 4.15), we follow a more general and detailed description found in Ref. (5).

Let us assume that the gas layer can be modeled as an infinite slab of thickness D, with an isotropically reflecting and emitting boundary at z = 0 and a vaccum boundary at z = D (see Fig. D.1).

Consider a slice of the gas layer of thickness dz. The wavelength dependent emission of the slab per unit solid angle per unit surface area is

$$\frac{a_\lambda e_{b\lambda}(z)dz}{\pi}$$

a_λ = absorption coefficient

$e_{b\lambda}$ = blackbody emissive power

The subscript λ denotes the wavelength dependencies of the quantities. The emission per unit solid angle per unit surface area in the direction of the angle dependent flux is

$$\frac{a_\lambda e_{b\lambda}(z)dz}{\pi \cos\theta}$$

The attenuation of the rays passing through the element is

$$\frac{\beta_\lambda \tau_\lambda(z)dz}{\cos\theta}$$

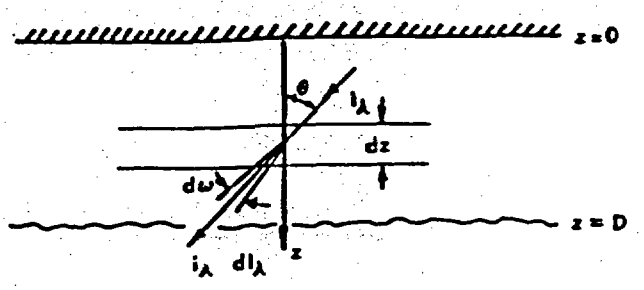

Fig. D.1 - Model of Ceiling Hot Gas Layer

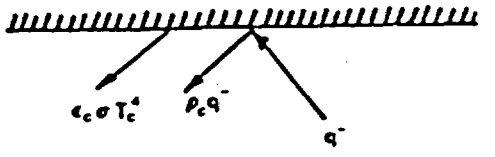

Fig. D.2 - Model of Ceiling

$$\beta_\lambda = a_\lambda + \gamma_\lambda$$

γ_λ = scatte ing coefficient

If we assume that our gas is a pure absorber, $\gamma_\lambda = 0.0$. We further assume that our absorption coefficient is wavelength independent, i.e. $a_\lambda = a$. This is known as the "gray approximation." Defining

$$\tau = \int_0^z a\, dz,\ \tau_D = \tau(D),\ \text{and}\ \mu = \cos\theta,$$

$$\mu \frac{dI_\lambda}{d\tau} + I_\lambda(\tau,\mu) = \frac{1}{\pi} e_{b\lambda}(\tau)$$

or

$$I_\lambda(\tau,\mu) = \begin{cases} I_\lambda(0,\mu)e^{-\tau/\mu} + \frac{1}{\pi}\int_0^\tau e_{b\lambda}(t)e^{-(t-\tau)/\mu}\frac{dt}{\mu}, & 0 < \mu < 1 \\ I_\lambda(\tau_D,\mu)e^{-(\tau_D-\tau)/\mu} + \frac{1}{\pi}\int_\tau^{\tau_D} e_{b\lambda}(t)e^{-(t-\tau)/\mu}\frac{dt}{\mu}, & -1 < \mu < 0 \end{cases}$$

Integrating over all λ, and noting that

$$\int_0^\infty e_{b\lambda} d\lambda = \sigma T^4 \text{ and } \int_0^\infty I_\lambda d\lambda = I,$$

$$I(\tau,\mu) = \begin{cases} I(0,\mu)e^{-\tau/\mu} + \frac{1}{\pi}\int_0^\tau \sigma T^4(t)e^{-(\tau-t)/\mu}\frac{dt}{\mu}, & 0 < \mu < 1 \\ I(\tau_D,\mu)e^{-(\tau_D-\tau)/\mu} + \frac{1}{\pi}\int_\tau^{\tau_D} \sigma T^4(t)e^{-(t-\tau)/\mu}\frac{dt}{\mu}, & -1 < \mu < 0 \end{cases}$$

Integrating over the ranges $0 < \mu < 1$ and $-1 < \mu < 0$, and defining

$$q^+ = 2\pi\int_0^1 I(\tau,\mu)\mu d\mu \text{ and } q^- = 2\pi\int_0^{-1} I(\tau,\mu)\mu d\mu ,$$

there obtains

$$q^+(\tau) = 2\pi\int_0^1 I(0,\mu)e^{-\tau/\mu}\mu d\mu + 2\int_0^\tau \sigma T^4(t)E_2(\tau-t)dt \ , \ 0 < \mu < 1$$

and

$$q^-(\tau) = 2\pi\int_0^{-1} I(\tau_D,\mu)e^{-(\tau_D-\tau)/\mu}\mu d\mu + 2\int_\tau^{\tau_D} \sigma T^4(t)E_2(t-\tau)dt, \ -1 < \mu < 0$$

To find $I(0,\mu)$, $0 < \mu < 1$, we assume that the ceiling is an isotropic reflector and emitter of radiation. Thus, as shown in Fig. D.2,

$$I(0,\mu) = [\varepsilon_C \sigma T_C^4 + \rho_C q^-(0)]/\pi \qquad 0 < \mu < 1$$

where

ε_C = ceiling emissivity

ρ_C = ceiling reflectivity

T_C = ceiling surface temperature.

To find $I(\tau_D,\mu)$, $-1 < \mu < 0$, we further assume that any incoming radiation at the vacuum boundary is isotropic, i.e.

$$I(\tau_D,\mu) = q_D/\pi \qquad -1 < \mu < 0$$

Thus

$$2\pi\int_0^1 I(0,\mu)e^{-\tau/\mu}\mu d\mu = 2[\varepsilon_C \sigma T_C^4 + \rho_C q^-(0)]E_3(\tau)$$

and

$$2\pi\int_0^{-1} I(\tau_D,\mu)e^{-(\tau_D-\tau)/\mu}\mu d\mu = 2q_D E_3(\tau_D-\tau) \ ,$$

where

$$E_3(x) = \int_0^1 e^{-x/\mu}\,\mu d\mu$$

Evaluating $q^-(\tau)$ at $\tau = 0$, we obtain

$$q^-(0) = 2q_D E_3(\tau_D) + 2\int_0^{\tau_D} \sigma T^4(t) E_2(t)dt$$

and so

$$q^+(\tau_D) = 2E_3(\tau_D)[\varepsilon_C \sigma T_C^4 + 2\rho_C q_D E_3(\tau_D) + 2\rho_C \int_0^{\tau_D} \sigma T^4(t) E_2(t)dt] + 2\int_0^{\tau_D} \sigma T^4(t) E_2(\tau_D - t)dt$$

If the gas temperature is uniform and equal to T_G throughout the entire slab, and if the absorption coefficient is independent of z ($\tau = aD$),

$$q^+(aD) = 2\varepsilon_C \sigma T^4 E_3(aD) + [2E_3(aD)]^2 \rho_C q_D + 2\sigma T_G^4[2\rho_C E_3(aD)\int_0^{aD} E_2(t)dt + \int_0^{aD} E_2(aD-t)dt]$$

We now approximate the exponential integrals $E_3(t)$ and $E_2(t)$ by equating the zeroth and first central moments with those of the function $A \exp(-Bt)$ (a good approximation in most cases), and it turns out that

$$E_3(t) \doteq 0.50 \exp(-1.5t)$$

$$E_2(t) \doteq 0.75 \exp(-1.5t)$$

Finally, the outgoing heat flux at the vacuum boundary is

$$\dot{q}''_{ceil} = q^+(aD)$$

$$= \varepsilon_C \sigma T_C^4 X + \rho_C q_D X^2 + \sigma T_G^4 (1-X)(1+\rho_C X)$$

where

$$X = \exp(-1.5aD)$$

Appendix E

VERIFICATION OF EQUATION (4.3)

The equation for the fuel-surface controlled burning rate per unit area, Eq. (4.3), introduces positive feedback to our burning rate model. Because this represents an important factor in predicting the acceleration of fire growth, we simulate two experiments in order to check the validity of the equation.

The first experiment, reported by Huffman et al. [62], investigates the burning rate of cyclohexane in pans arranged in a hexagon surrounding a central pan of cyclohexane (also burning) as a function of pan diameter and separation (see Fig. E.1). The fuel parameter values assumed in our simulation are given in Table E.1.

If the feedback to the fuel from the flames were not important, we would expect to see little change in $\dot{m}''$ with changes in pan separation. As seen in Fig. E.2 however, there are dramatic changes as the pans are brought closer together.

Our reference model predictions are also shown in Fig. E.2. While the agreement with experimental data is not outstanding, especially for the smaller separation distances (where flame interaction effects such as mergin become important), nevertheless the predictions are reasonably close in magnitude, considering the simple nature of the model.

The second simulation is of Orloff, Modak, and Alpert's experiment, where a 3.56 x 0.914 x 0.064 m slab of polymethylmethacrylate (PMMA) was

Table E.1 - Parameters Used in Cyclohexane Simulation

$\dot{m}''_0$	0.0231 kg/m²s
C_S	2.56×10^{-6} kg/J
H_f	4.67×10^{7} J/kg
γ	0.35
η	1.00

Table E.2 - Parameters Used in PMMA Simulation

ρ	1190 kg/m³
c_p	2090 J/kg°K
k	0.27 W/m°K
H_f	2.67×10^{7} J/kg
T^*_p	636°K
T^*_s	743°K
$\dot{m}''_0$	0.006 kg/m²s
C_S	6.21×10^{-7} kg/J
γ	0.39
η	0.90

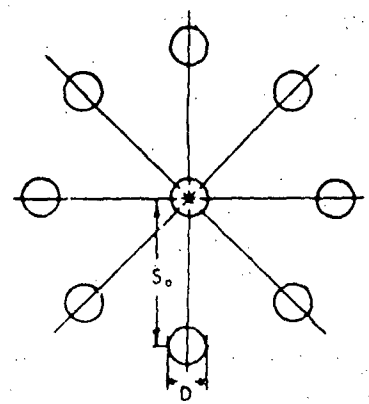

Fig. E.1 - Model of Experiment [62]

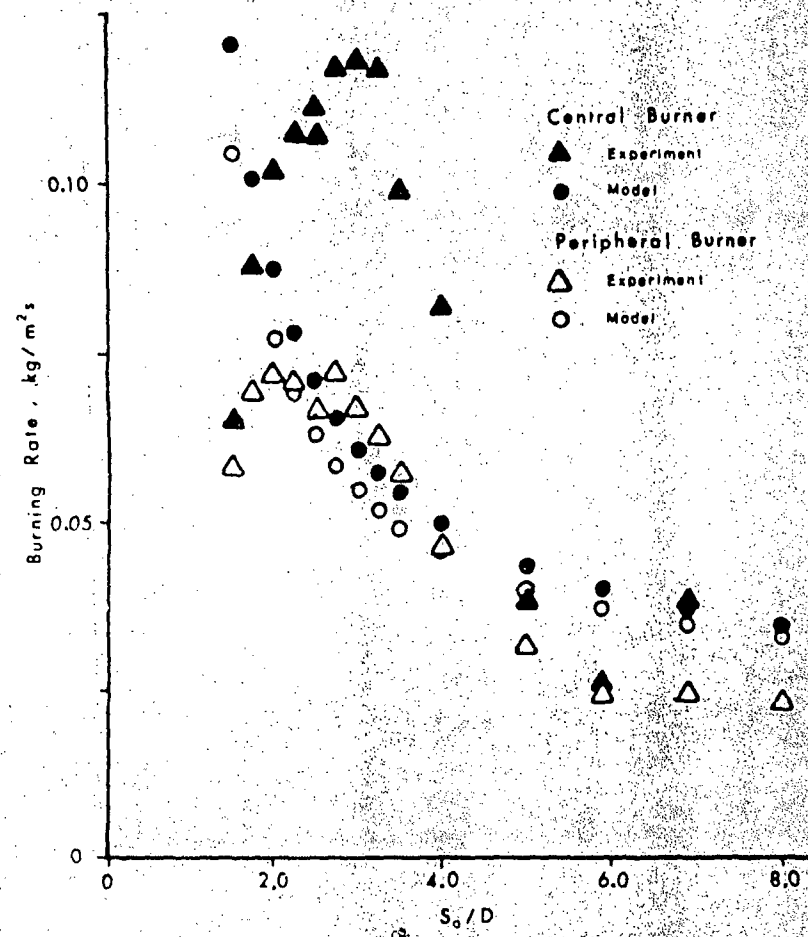

Fig. E.2 - Comparison of Predicted Results With Experimental Data [62]

burned [63]. Some pertinent physical properties of the slab are given in Table E.2.

Since the hot gases from the fire on the lower portions of the slab will pass through the upper burning zones, causing the flames to grow in thickness and intensity, we expect the increasing heat fluxes from the flames to the burning fuel bed to cause an increase in the local burning rate with height, thus providing a good test for Eq. (4.3). We note that although the flux to the fuel bed is not an external heat flux as we have defined earlier, we model it as such for convenience.

Referring to Figure E.3, it is assumed that the flame height Z_{fl} is much greater than the flame width W. In order to determine the heat flux from the flame to a particular differential element at height Z on the fuel bed, we model the flame as a rectangular slab of height $Z_{fl}+\ell$, width W, and thickness d. The flame height Z_{fl} is given by Thomas' correlation for a line source fire [7]:

$$Z_{fl} = C_{fl}(\dot{m}') \qquad \text{(E.1)}$$

where

$\dot{m}'$ = burning rate per unit length of line source (kg/m s)

$$= \int_0^z \dot{m}''(z')dz'$$

C_{fl} = 29.7 $m^{5/3}s^{2/3}/kg^{2/3}$ for flames adjacent to walls.

For our problem, we assume that $\dot{m}''$ is roughly constant, and so

$$\dot{m}' \doteq z\dot{m}''(z) \quad (kg/m\ s) \ .$$

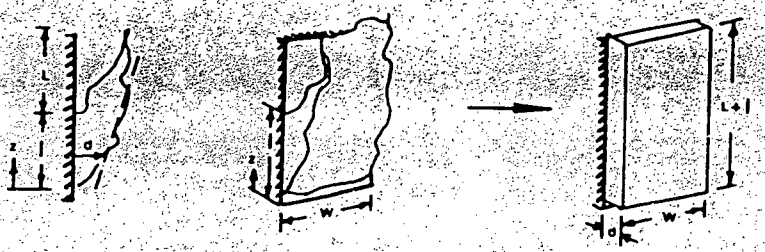

Fig. E.3 - Model of Experiment [63]

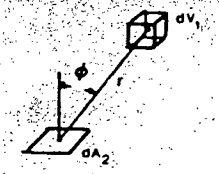

Fig. E.4 - Transfer Between a Differential Volume and a Differential Surface

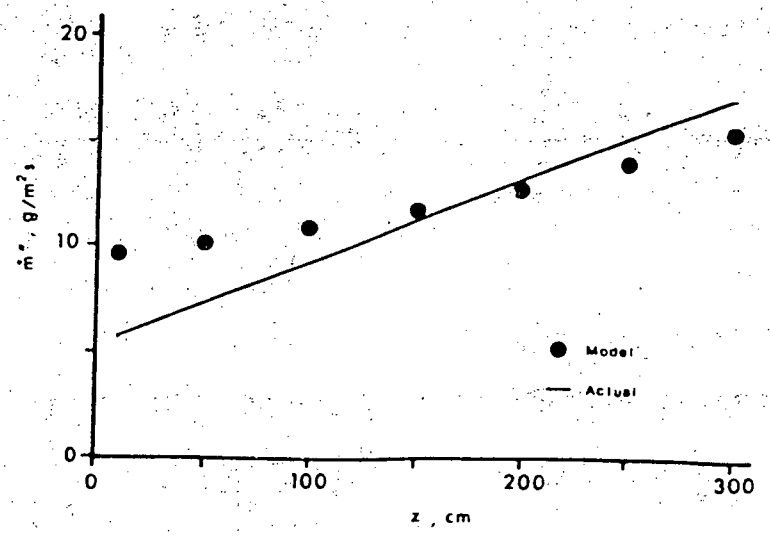

Fig. E.5 - Comparison of Predicted Results With Experimental Data [63]

As for the flame thickness, Orloff et al. use experimental evidence to show that $d(z) = z/16$.

Although the heat flux to the fuel bed has both convective and radiative components, we assume that the radiative component dominates. It is hoped that the resulting model will reasonably predict the desired burning rate, even when this assumption is not good.

The heat flux received by a differential surface element is (assuming 100% combustion efficiency)

$$\dot{q}''_{dS} = F_{dS-fl}\ \dot{q}''_{fl}$$

For the problem at hand, where the radiative exchange is between a differential gas volume and a surface (see Fig. E.4),

$$F_{dS-fl} = \int_{V_{fl}} dV[a \cos\phi\ \tau(r)/\pi r^2] \qquad (E.2)$$

where

$\tau(r)$ = transmissivity of gas

= $\exp(-ar)$ for constant property gas.

a = attenuation constant for flame gases (m^{-1}).

If the differential surface is located along the centerline of the flame $(W/2,y,0)$, it turns out that

$$F_{dS-fl} = 1 - 2E_3(aD) - \frac{2}{\pi}\sum_i \int_{\theta_i}^{\theta_{i+1}} d\theta[E_3(a\rho_i) - E_3(a\sqrt{d^2+\rho_i^2})]$$

where

$\rho_1 = Z_o/\cos(\pi/2 + \theta)$ $\qquad$ $\theta_1 = -\pi/2$

$\rho_2 = W/2\cos\theta$ $\qquad$ $\theta_2 = \tan^{-1}(-2Z_o/W)$

$\rho_3 = (L+Z_{fl}-Z_o)/\cos(\pi/2 - \theta)$ $\qquad$ $\theta_3 = \tan^{-1}[2(L+Z_{fl}-Z_o)/W]$

$\theta_4 = \pi/2$

Now since

$$\dot{q}''_e = \frac{F_{dS-f1}}{A_{f1}} \dot{Q}_{f1} \doteq \frac{F_{dS-f1}}{2(L+Z_{f1})} (\gamma \dot{m}'' Z_{f1} W\ell) \qquad (E.3)$$

and

$$\dot{m}'' = \dot{m}''_0 + C_S \dot{q}''_e ,$$

$$\dot{m}'' = \left[\frac{\dot{m}''_0}{1 - \frac{C_S F_{dS-f1} \gamma H_f \ell}{2(L+Z_{f1})}} \right]$$

Assuming $\gamma = 0.39$ [40] and $\dot{m}''_0 = 0.006$ kg/m²s [35], the predictions of this model are compared with the experimental results in Fig. E.5. Again, the predictions are reasonably close in magnitude to the experimental data.

LIST OF VARIABLES

Variable	Definition
A	Area (m^2)
C	Surface controlled burning rate constant (kg/J)
C	Ventilation controlled burning rate constant
F	Shape factor from object to flame
H	Heating value of fuel (J/kg)
Q	Rate of heat production (W)
Q	Rate heat is radiated away from fire (W)
T	Temperature (°K)
T*	Ignition temperature (°K)
W	Rate of air flow into compartment (kg/s)
Z	Height (m)
c	Specific heat (J/kg°K)
h	Heat transfer coefficient ($W/m^2°K$)
k	Thermal conductivity (W/m°K)
m	Burning rate of fuel (kg/s)
m''	Specific burning rate constant (kg/m^2s)
q''	Heat flux (W/m^2)
t	Time (s)
t*	Time to ignition (s)
α	Thermal diffusivity (m^2/s)
ε	Emissivity
γ	Fraction of Q radiated away from fire
η	Combustion efficiency
σ	Stefan-Boltzmann constant (5.6697×10^{8} $W/m^2°K^4$)

elected Subscripts	Definition
e	Environment
ext	External to fuel bed
fl	Flame
f	Fuel
G	Gas
O	Opening (e.g. window)
o	Object
W	Wall

NRC FORM 335 (7-77) U.S. NUCLEAR REGULATORY COMMISSION

BIBLIOGRAPHIC DATA SHEET

1. REPORT NUMBER (Assigned by DDC): NUREG/CR-2269

2. (Leave blank)

3. RECIPIENT'S ACCESSION NO.

4. TITLE AND SUBTITLE (Add Volume No., if appropriate)
Probabilistic Models for the Behavior of Compartment Fires

5. DATE REPORT COMPLETED
MONTH: November YEAR: 1980

7. AUTHOR(S)
Nathan O. Siu

9. PERFORMING ORGANIZATION NAME AND MAILING ADDRESS (Include Zip Code)
UCLA
Los Angeles, California 90024
School of Engineering and Applied Science

DATE REPORT ISSUED
MONTH: August YEAR: 1980

6. (Leave blank)

8. (Leave blank)

12. SPONSORING ORGANIZATION NAME AND MAILING ADDRESS (Include Zip Code)
U. S. Nuclear Regulatory Commission
Office of Nuclear Regulatory Research
Division of Risk Analysis
Risk Methodology and Data Branch
Washington, D.C. 20555

10. PROJECT/TASK/WORK UNIT NO.

11. CONTRACT NO.
NRC FIN B6284

13. TYPE OF REPORT
Technical

PERIOD COVERED (Inclusive dates)
10/78 - 11/80

15. SUPPLEMENTARY NOTES

14. (Leave blank)

16. ABSTRACT (200 words or less)

Physical models which predict the thermal hazards (including temperatures and heat fluxes) during a compartment fire as functions of space and time are developed. Since large uncertainties are inherent to the analysis, the models are probabilistic.

General models are constructed for the periods of fire growth and fully-developed burning. These models are used in sample analyses to estimate the fire hazard in particular compartments.

The overall methodology requires the synthesis of a deterministic physical model from information available in the literature. Uncertainties in the input parameters required by the deterministic model are addressed and are incorporated with the uncertainties in the model itself, to form state of knowledge distributions for the thermal hazards.

17. KEY WORDS AND DOCUMENT ANALYSIS

17a. DESCRIPTORS

Fires
Thermal Hazards
Fire Growth Model
Heat Flux

17b. IDENTIFIERS/OPEN-ENDED TERMS

18. AVAILABILITY STATEMENT
Unlimited

19. SECURITY CLASS (This report): Unclassified

21. NO. OF PAGES

20. SECURITY CLASS (This page): Unclassified

22. PRICE: $

NRC FORM 335 (7-77)